CrystEngComm

Accepted Manuscript

ROYAL SOCIETY OF CHEMISTRY

www.rsc.org/crystengcomm

A table of contents entry

Recent developments of transition-metal oxides nanostructures with designed shape and dimensionality, including various synthesis methods and applications, are presented.

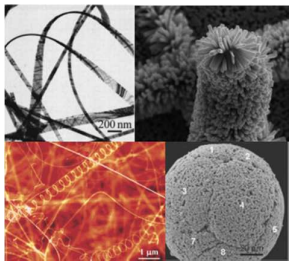

A Comprehensive Review on Synthesis Methods for Transition–Metal Oxides Nanostructures

Ting Guo,[1)] Ming–Shui Yao,[2)] Yuan–Hua Lin*,[1)] Ce–Wen Nan[1)]

1 State Key Lab of New Ceramics and Fine Processing, School of Materials Science and Engineering, Tsinghua University, Beijing 100084, P. R. China

2 State Key Laboratory of Structural Chemistry, Fujian Institute of Research on the Structure of Matter, Chinese Academy of Sciences, 155 Yangqiao Road west, Fuzhou, 350002, P. R. China

1. Introduction

Over the past few decades, transition–metal oxides nanostructures (MONSs), which have great potential in magnetic, electronic, and optical applications, have been widely studied. MONSs have been integrated into a variety of devices to achieve unprecedented excellent performances, such as enhanced gas sensing, efficient photocatalysis.[1,2] In transition–metal oxides, although the s–shells of positive metallic ions are always fully filled by electrons, the d–shells of them may be not completely filled. This characteristic brings them various unique properties, which involve reactive electronic transitions,[3, 4] high dielectric constants,[5, 6] wide bandgaps,[7, 8] good electrical characteristics[9,10] and so on. Meanwhile, transition–metal oxides possess various states, such as ferromagnetic state, ferrimagnetic state and semiconductive state. Therefore, transition–metal oxides are considered to be one of the most fascinating functional materials.

Currently, the studies of nanostructures have greatly promoted the development of electron devices. Nanostructures are defined as the materials with at least one dimension between 1 and 100 nm. In general, nanostructures possess three different morphologies: zero–dimensional (0D), one–dimensional (1D), and two–dimensional (2D) nanostructures. It has been well–known that with the size and dimension reduced, the electronic structures of the nanostructures can be tuned, which lead to a variety of changes in both chemical and physical properties.[11,12] For example, magnetic property of MONSs can transform from ferro / ferrimagnetic to superparamagnetic with their size reduced. Thus nanoscale design and process of synthesis can be used to tune the properties of nanostructures.

Up to now, the control of the size, shape and structure of MONCs have been achieved by various synthetic methods. Vapor phase growth is always carried out in a thermal furnace. In the course, it is necessary to regulate the reaction between oxygen gas and metal vapor source. In order to achieve it, various methods have been developed to control the aspect ratio, diameter and specific surface area of the product. It mainly involves thermal chemical vapor deposition (CVD) and metal–organic chemical vapor deposition (MOCVD), *etc*.[13, 14] Meanwhile, the mechanism could be classified as vapor–solid (VS) and vapor–liquid–solid (VLS). Back in 1964, Wagner and Ellis first presented VLS mechanism to describe the growth of Si whisker.[15, 16] Generally, metal nanoparticles are used as the nucleation seeds, which have essential influences on the growth direction and diameter of products in VLS process. In the

beginning, catalysts are molten into liquid alloy droplets which also contain source metal. When the alloy droplets achieve supersaturated, source metal start to precipitate and form metal oxide under the oxygen flow. In general, the as–synthesized metal oxides preferentially grow along particular orientation, which lead to the formation of 1D nanostructures. So far, the preparation of metal oxide nanowires, such as ZnO,[17] CdO,[18] In_2O_3,[19] SnO_2[20] and TiO_2,[21] have been achieved by means of VLS mechanism. From what have been discussed above, VLS process belongs to catalyst–assisted growth, while VS process belongs to catalyst–free growth.[22,23] In the course of VS process, the reactants are first heated to form vapor under high temperature and directly condensed on the substrate, on which seed crystals will take shape and be served as the nucleation sites located. Facilitate directional growth followed will minimize the surface energy of product.

Electrochemical deposition has been successfully applied to fabricate metal oxide nanostructures. It exhibits many advantages during synthesis process. Take the preparation of ZnO[24] for example, making use of appropriate electrolyte, ZnO have been successfully prepared. Meanwhile, researchers also try to introduce the template into electrochemical deposition method. A gel comprising of sol particles is essential for sol–gel process. Firstly, precursor molecules, which compose the sol particles, are used to synthesize colloidal suspension. Then a template will be introduced into the suspension, and the particles will aggregate on the surface of the template. After sol particles fill the channels of the template, the structure with predesigned morphology will be formed. Using thermal treatment process to remove the residual gel, final product will be achieved.

Back in the 1970s, hydrothermal process was firstly employed to synthesize crystalline structures. The reactants are placed in a closed vessel with water as a reaction medium. The reaction is conducted under high temperature and pressure conditions. Hydrothermal process can accelerate the reactions between ions and promote the hydrolysis reaction. Ultimately, the growth and self–assembly of crystals will be achieved in solution. The advantages of the method involve low cost, mild reaction conditions and controlling the device easily. By changing the experimental parameters (temperature, pressure, time, the reaction medium, *etc.*), the morphology, structure and properties of the product can be well regulated. In order to improve the hydrothermal process, surfactants are introduced to the system. Surfactant–promoted process has been demonstrated to be an effective method to fabricate metal oxide with

a variety of morphologies. The system is always composed of three phases: oil phase, surfactant phase and aqueous phase. In the course of process, surfactants can confine the growth of product. Meanwhile, temperature, pH value and concentration of the reactants also have an essential influence on the morphology, structure and properties of the product.

In this review, recent developments of MONCs, including fabrication of representative of MONCs with designed shape and dimensionality and their important technological applications in various fields have been presented. Due to rich morphologies and structures, various synthetic methods, wide applications and excellent properties, a comprehensive review of syntheses and applications of a variety of MONCs (*e.g.* nickel oxide, tungsten oxides, zinc oxides, vanadium oxides, iron oxides, *etc.*) was presented. The applications involve gas sensors, electrochromic devices, LEDs, field emitters and so on. Finally, the outlook of the MONSs is given.

2. WO_x

It is well known that nanostructures with specific exposed facets and hierarchical structures usually exhibit unique physical and chemical properties.[25–27] Among various transition metal oxides, tungsten oxides (WO_x, $2 \leq x \leq 3$) attracted great interest and have been extensively investigated due to their outstanding performances in applications such as photo−catalysis,[27–29] gas sensors,[30–34] anode materials of Li−ion batteries,[35] supercapacitors,[36,37] field emitters[38], electrochromic (EC) devices[39–42]and so on.

Besides stoichiometric WO_3,[27,32,33] and WO_2,[38,43] non−stoichiometric $WO_{3-\delta}$ ($0 < \delta < 1$) were synthesized, for example $WO_{2.9}$,[44] W_5O_{14} ($WO_{2.8}$),[45,46] $W_{18}O_{49}$ ($WO_{2.72}$),[47–49] W_2O_5,[50] and W_3O_8.[51] It should be noted that many types of stoichiometric WO_3 crystals have been found, which makes it more difficult to be understood. Generally, WO_3 crystals are formed by corner and edge sharing of WO_6 octahedra. Based on the tilting angles and rotation direction of WO_6 octahedra with reference to the "ideal" cubic structure (ReO_3 type), the corner sharing phases can be classified as follows: monoclinic II (ε−WO_3), triclinic (δ−−WO_3), monoclinic I(γ−WO_3), orthorhombic (β−WO_3), tetragonal (α−WO_3), and cubic WO_3.[52,53] In addition, hexagonal phase (h−WO_3) with the form of three and six−membered rings of WO_6 octahedra in the ab−plane was observed.[54–58]

For the purpose of obtaining nanostructures with specific exposed facets and hierarchical structures, tungsten oxides can be synthesized using varying techniques

to form 0D,[30,55,59–61] 1D,[33,43,62–65] 2D[34,66–69] and 0[70] / 1[71] / 2D–based[32,72,73] hierarchical structures. In this section, we present a general review on shape–controlled syntheses of WO_x nanostructures. Because of more interest have been attracted than other WO_x nanostructures due to their structural stability and excellent properties, various nanostructured forms of WO_3 and $W_{18}O_{49}$ have been presented emphatically in the literature to date. We also summarize methods for syntheses of nanostructured WO_x based on two major categories: vapor phase and liquid phase.

2.1 0D WOx nanostructures

In this paper, 0D nanostructures only refer to quantum dots (QDs) and nanoparticles with specific exposed facets.

0D QDs now attract much attention because their energy levels can be designed by controlling their particle size due to the strong quantum–size (Q–size) effects.[74,75] Among various liquid phase methods for syntheses of WO_x QDs, template directed synthesis is usually used. For example, Watanabe *et al.*[76] successfully prepared WO_3 QDs (~1.0 nm, Fig. 1a) with the help of a new template called as super–microporous silicas (SMPSs). In contrast, liquid phase template–free synthesis of WO_x QDs is rather difficult, and structure–tailoring agents usually lead to 1D[47,77] / 2D[78] morphologies due to the unequal growth rate in the plane and normal to the plane direction.[134,79] In this case, vapor / liquid phase method based on the decomposition of precursor and proper structure–tailoring agents will be a good choice. Cong *et al.*[75] synthesized tungsten aryloxide ($W(OC_6H_5)_6$) precursor firstly, then reacted it with octylamine at 180°C under N_2 flow to obtain γ–WO_3 QDs (~1.6 nm, Fig. 1b, γ phase was re–indexed by us mainly according to Raman peaks at ~270, 310, 700 and 805 cm^{-1},[80,81] together with its size, colour[82] and XRD pattern[82]). By exchanging surface ligands, γ–WO_3 QDs stabilized with pyridine brings about excellent hydrophilicity and conductivity, which exhibited excellent electrochromic performance with coloration / bleaching time within 1 s (> 50 s for bulk sample, Fig. 1c and d) and coloration efficiency up to 154 $cm^2\ C^{-1}$, which is much superior to inorganic analogues and even competitive to organic related materials.[75]

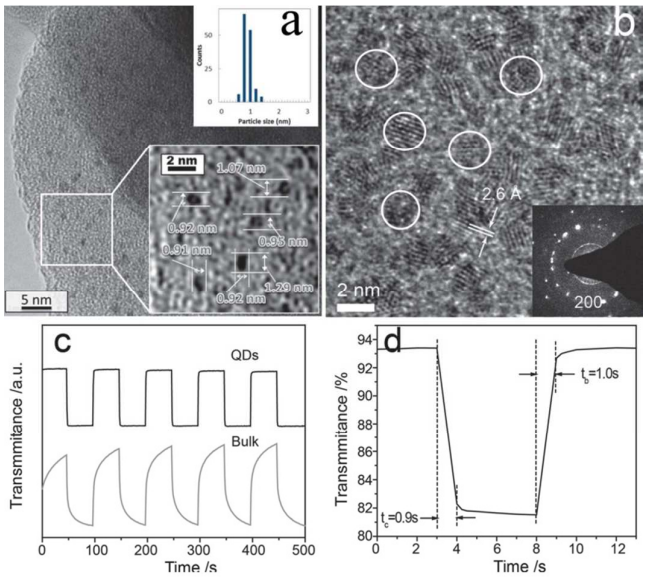

Fig. 1 (a) TEM images and size distribution of WO_3 particles synthesized in super–microporous silicas (SMPSs). Reproduce with permission.[76] Copyright 2013, The Royal Society of Chemistry. (b) High–resolution TEM images of as–prepared γ–WO_3 QDs with average sizes of 1.6 nm (the inset is the SAED pattern composed of individual reflected spots supporting the single crystalline nature of the QDs), (c) transmittance switching for bulk and QDs WO_3 and (d) enlarged in situ transmittance variation curve between the colored and bleached states for WO_3 QDs. Reproduce with permission.[75] Copyright 2014, Wiley–VCH.

Vapor phase methods for syntheses of uniform and undoped WO_x QDs were rarely reported, which might due to wide range of temperature (wide particle size distribution) and difficulty on collecting QDs. However, vapor phase method is suitable for 0D nanostructures with specific exposed facets. For instance, Guo *et al.*[61] prepared α–WO_3 octahedra bounded by eight {101} exposed facets via a DC thermal plasma system (Fig. 2a and b). Similarly, Zhang *et al.*[30] reported the synthesis of uniform γ–WO_3 octahedra enclosed by eight {111} exposed facets via a RF thermal plasma system (Fig. 2c). Both of α–WO_3 (stable at temperature > 740°C) and γ–WO_3 (stable at 17 – 330°C)[83,84] octahedra are equilibrium forms that determined by the corner sharing of WO_6 octahedra at different temperature regions. The mainly reason why WO_3 octahedra bound by {111} facets performed good gas sensing properties (Fig. 2d) can be attributed to dangling bonds of W^- or O^- on the surface (highly active crystal surface).

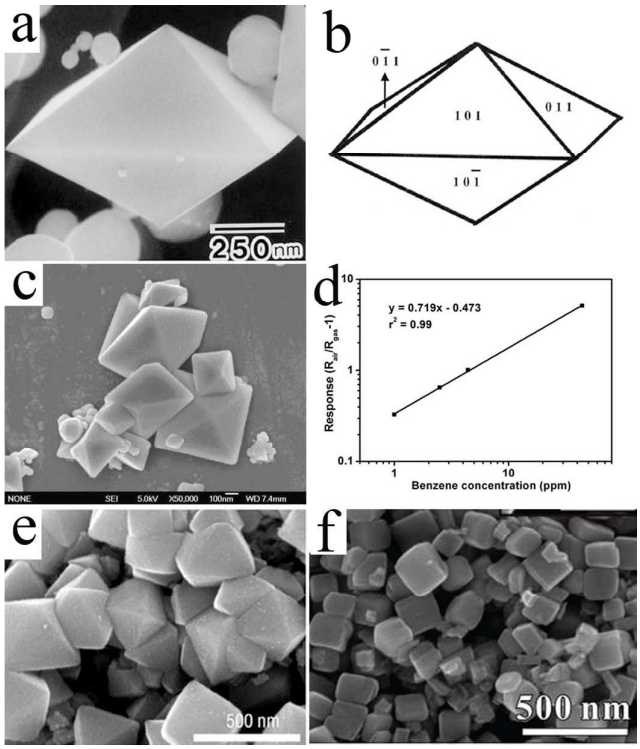

Fig. 2 (a) The SEM image of α–WO_3 octahedron and (b) its illustration with tetragonal structure bounded by eight {101}. Reproduce with permission.[61] Copyright 2005, Springer. (c) The SEM image of γ–WO_3 octahedra and (d) the corresponding linear fitting of gas sensing responses to benzene with different concentrations at 400°C. Reproduce with permission.[30] Copyright 2013, The Royal Society of Chemistry. (e) The SEM image of γ–WO_3 octahedra. Reproduce with permission.[60] Copyright 2010, The Royal Society of Chemistry. (f) The SEM image of δ–WO_3 cuboid. Reproduce with permission.[59] Copyright 2012, The Centre National de la Recherche Scientifique (CNRS) and The Royal Society of Chemistry.

0D nanostructures with specific exposed facets can also be prepared by liquid phase method, of which hydro / solvothermal reaction assisted by directed / capping agents were usually used. Directed / capping agents can control growth rates along specific direction by changing the free energies of different crystal facets. For example, via a simple solvothermal route with the assistance of urea, γ–WO_3 octahedra with eight {111} facets can be obtained (Fig. 2e).[60] In contrast, growth rates along [001], [010] and [100] can be controlled to the slowest directions (Fig. 2f).[59] The crystal phase can be tuned by changing the reaction temperature. By increasing the temperature to 180°C, more stable phase β–WO_3 cuboids were obtained.

2.2 1D WOx nanostructures

The width and thickess of 1D nanostructure are confined to the nanoscale range

between 1 and 100 nm, while the length can be hunderds of nanometers or more. The length scale allows the 1D nanostructuresto contact the macroscopic world. It should be noted that although lengths (width) of some nanostructures described in this section are less (larger) than 100 nm, which should be 0D (2D) nanostructures according to general definition of 0D (2D) nanomaterials, we classified them as 1D nanostructures for their significant aspect ratios.

Enormous efforts have so far been made to synthesize and characterize 1D metal–oxide nanostructures in the forms of rods,[35,40,41,55,57,85] wires / fibers,[33,62,63,86,87] needles / tips,[33,64] tubes,[65,88] hemitubes[89] and belts.[58,63,71]

For vapor phase method, the growth mechanism can be simply summarized as VS,[22] and VLS.[15] And morphologies of products can be contorlled by changing parameters such as depositing temperature,[33,62] asisisting electric filed,[64] catalyst,[38] substrate,[62] pre–treament,[40] *etc.*

With rich oxygen atmosphere, we can find that vapor phase methods usually obtained WO_3 1D nanostructures with high aspect ratios (*e.g.* nanowires / fibers, nanoneedles, *etc.*, Fig. 3a), which exhibited excellent performaces in various application such as a field emission display (FED, Fig.3b), gas sensors, photodectors and so on.[33,62–64,90–94] In most cases, it is easy to understand the formation of monoclinic γ–WO_3 phase (stable at 17 – 330°C)[83,84] by cosidering that each growth temperature was lower than 1000°C, the phase transitions of WO_3 is partially reversible[52] and that γ–WO_3 has been reported as the most stable phase at room temperature.[83] 1D nanostructures always grew on heterogenious substrates.[33, 38, 62–64, 92] Affected by the surface of the substrate, most of them showed [001] growth direction along the length (Fig. 3c), while nanowires on Si wafer[63] or Si+W supported Au film[38] exibited [100] / [010] or [010] growth direction (Fig. 3d and e). By replacing the substrate with Si+W supported Ni film, WO_2 nanowires were synthesized due to the lack of oxygen gas caused by oxidation of Ni (Fig. 3f).[38]

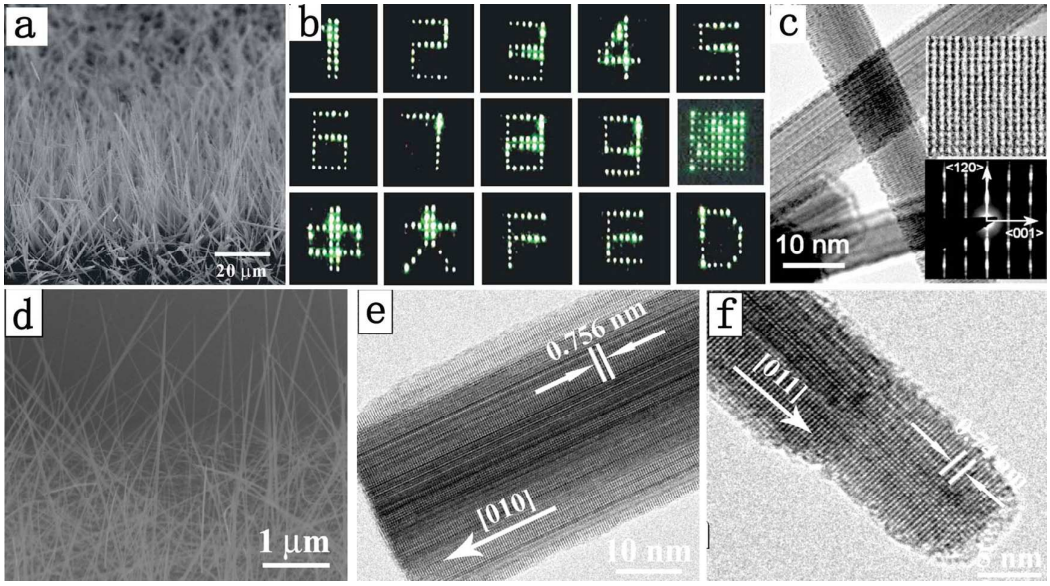

Fig. 3 (a) The cross–sectional SEM image of as–prepared WO_3 nanowires, and (b) Arabic numerals and Chinese characters displayed by the double–gated FED. Reproduce with permission.[93] Copyright 2007, American Institute of Physics. (c) TEM micrographs showing the lattice fringes and the diffraction pattern (insets) of individual tungsten oxide nanowires. Reproduce with permission.[62] Copyright 2005, American Chemical Society. (d) The SEM image of γ–WO_3 nanowires, (e) typical HRTEM images of γ–WO_3 nanowire and (f) WO_2 nanowire, respectively. Reproduce with permission.[38] Copyright 2010, American Chemical Society.

With poor oxygen atmosphere, $WO_{3-\delta}$ ($0 < \delta < 1$) 1D nanostructures (especially $W_{18}O_{29}$) can be fabricated via vapor phase method (reacted with leaking / poor oxygen or gas like CO_2).[48,95–98] Because the close–packed planes are {010}, $W_{18}O_{29}$ 1D nanostructures (nanowire,[48,96] nanotip,[97] nanoneedles,[98] *etc.*, depending on substrates) usually showed monoclinic phase with selective growth along [010] direction (Fig. 4).

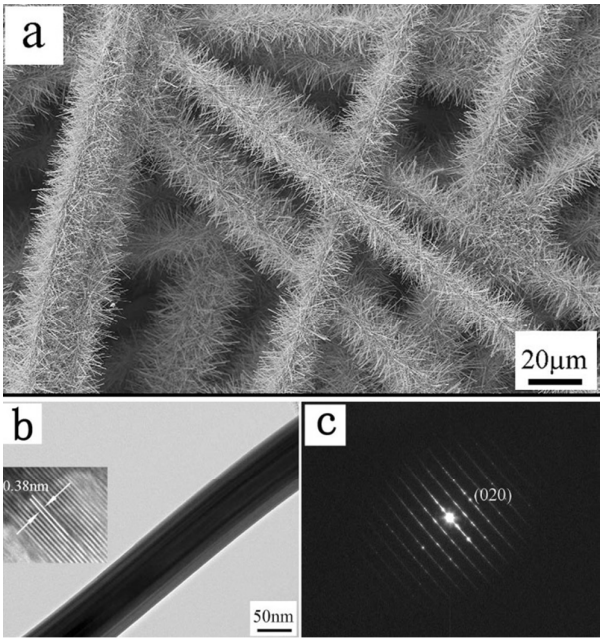

Fig. 4 (a) SEM images of three–dimensionally aligned $W_{18}O_{49}$ nanowires on carbon microfibers, (b) a typical TEM image of a single $W_{18}O_{49}$ nanowire (the inset ishigh resolution image of the nanowire), and (c) selected area electron diffraction (SAED) pattern of the nanowire. Reproduce with permission.[96] Copyright 2009, American Institute of Physics.

As for liquid phase methods, more abundant morphologies and crystal phase of WO_x 1D nanostructures were observed than vapor phase methods. In spite of different reactants ($WO_3 \cdot nH_2O$,[57,58] Na_2WO_4,[35,49,41,54,55,85,88] Li_2WO_4,[56] *etc.*) and directed / capping / accelerating agents (Li_2SO_4,[56,57] NaCl & HCl,[85] Na_2SO_4 & $H_2C_2O_4$,[94] *etc.*) were used, final products of hydrothermal reaction at 140–180°C (pH: 1.0–2.0) usually obtained h–WO_3 1D nanostructures with [001] direction along the length (Fig. 5a and b). Among these works, stabilizing cations (*e.g.* Na^+, NH_4^+, Li^+, *etc.*) and directing anions (*e.g.* SO_4^{2-}, Cl^-, $C_2O_4^{2-}$, *etc.*) were reported as the key factor to deteminate the crystal phase and morphologies of final products, respectively (Fig. 5c–e).[99] As a typical example for structure directing works, hydrothermal system of Na_2WO_4, $H_2C_2O_4$ and Rb_2SO_4 (0.3 g) at 180°C reported by Gu *et al.*[71] is worth of studying. During the growth stage, SO_4^{2-} may act as capping agent to preferentially adsorb on the faces parallel to the c axis of the h–WO_3 nanocrystal, leading to the formation of c–axis oriented nanorods and finally urchin–like spheres (Fig. 5g). The high concentration of sulfate (1.0 g Rb_2SO_4) tends to induce the oriented aggregation of the nanorods, thus nanoplates were observed (Fig. 5h). Similarly, h–WO_3

nanowires (Fig. 5i) and nanobelts growing along [001] direction (Fig. 5j and k) can be observed when 0.3 g and 1.0 g K_2SO_4 were used instead of Rb_2SO_4, respectively. In addition, the pH value was reported as an essential factor to affect the crystal phase (Fig. 5f).[35]

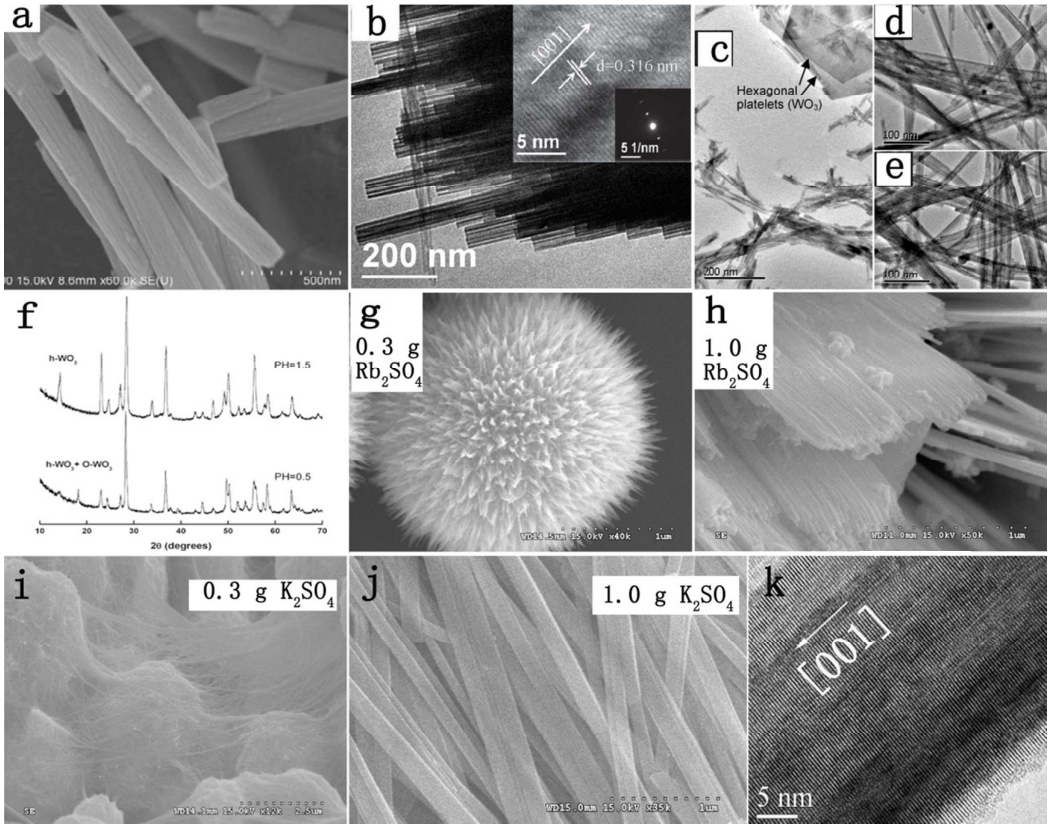

Fig. 5 (a) The SEM image and (b) TEM image of WO_3 nanotube bundleswith the diameter of about 70 nm, (the inset is HRTEM and SAED images of the WO_3 nanotube wall). Reproduce with permission.[88] Copyright 2013, The Royal Society of Chemistry. $W_{18}O_{49}$ nanorods synthesized at 180°C for 16 h with different amounts of Na_2SO_4 salt: (c) 2.5 g, (d) 5 g, and (e) 10 g. Reproduce with permission.[99] Copyright 2003, American Chemical Society. (f) XRD patterns of products at different pH values. Reproduce with permission.[35] Copyright 2008, IOP Publishing Ltd. SEM images of h–WO_3 products prepared by adding (g) 0.3 g of Rb_2SO_4 (urchin–like spheres), (h) 1.0 g of Rb_2SO_4 (nanoplates), (i) 0.3 g of K_2SO_4 (nanowires), (j) 1.0 g of K_2SO_4 (nanobelts), and the corresponding (k) HRTEM image. Reproduce with permission.[71] Copyright 2006, American Chemical Society.

Without using any ions mentioned above, $W_{18}O_{49}$ nanowires were obtained by solvothermal reaction of WCl_4 and ethanol.[47,100] By changing systematically changing the kind and concentration of the alcohols and W–source raw materials, $W_{18}O_{49}$

nanostructures with interesting morphologies were obtained, including nanorods, nanofibers, nanospheres, nanoparticles, and even nanoassembles.[49]

Other types of liquid phase methods (*e.g.* template directed synthesis, precursor based method, electron beam irradiation, *etc.*) were utilized to synthesize WO_x 1D nanostructures. Take carbon nanotubes (CNTs), SBA−15, polymeric fiber, the porous anodic alumina (PAA) as templates, 1D nanostructures such as nanowires[86, 87, 101] and hemitubes (γ−WO_3,[89] Fig. 6a and b) can be obtained. Zhao *et al.*[65] synthesized tungsticacid hydrate ($H_2W_{1.5}O_{5.5}\cdot H_2O$) nanotube precursor via solvothermal reaction firstly, then calcinated it at 450°C to obtain porous δ−WO_3 nanotube (Fig. 6c−f). Besides, β−WO_3 nanorods with [100] direction along the length were synthesized by electron beam irradiation in aqueous solution contain WO_3 particles and triethylamine.[102]

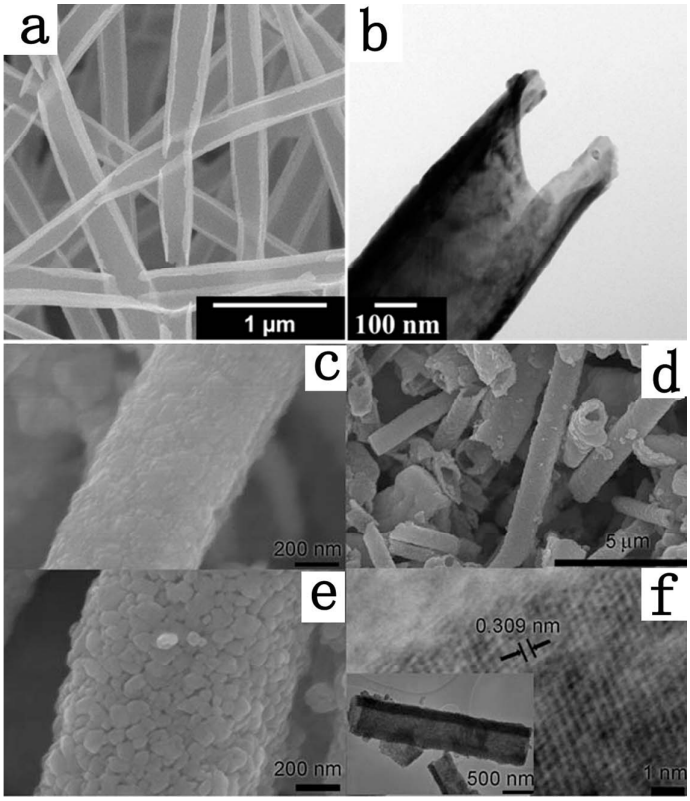

Fig. 6 (a) The SEM image and (b) TEM image of WO_3 hemitubes. Reproduce with permission.[89] Copyright 2012, American Chemical Society. SEM images of NTs (c) before and (d,e) after annealing, (f) high−magnification TEM image (the inset shows the TEM image of a single NT after annealing). Reproduce with permission.[65] Copyright 2008, Wiley.

2. 3 2D WOx nanostructures

2D WO_x nanostructures usually obtained via liquid phase methods.

By changing the stabilizing caions and structure directing agents (p–aminobenzoic acid,[103] tartaric acid,[59] HBF_4,[68] *etc.*), nanoplates can be synthesized via hydrothermal reactions (Fig. 7a).

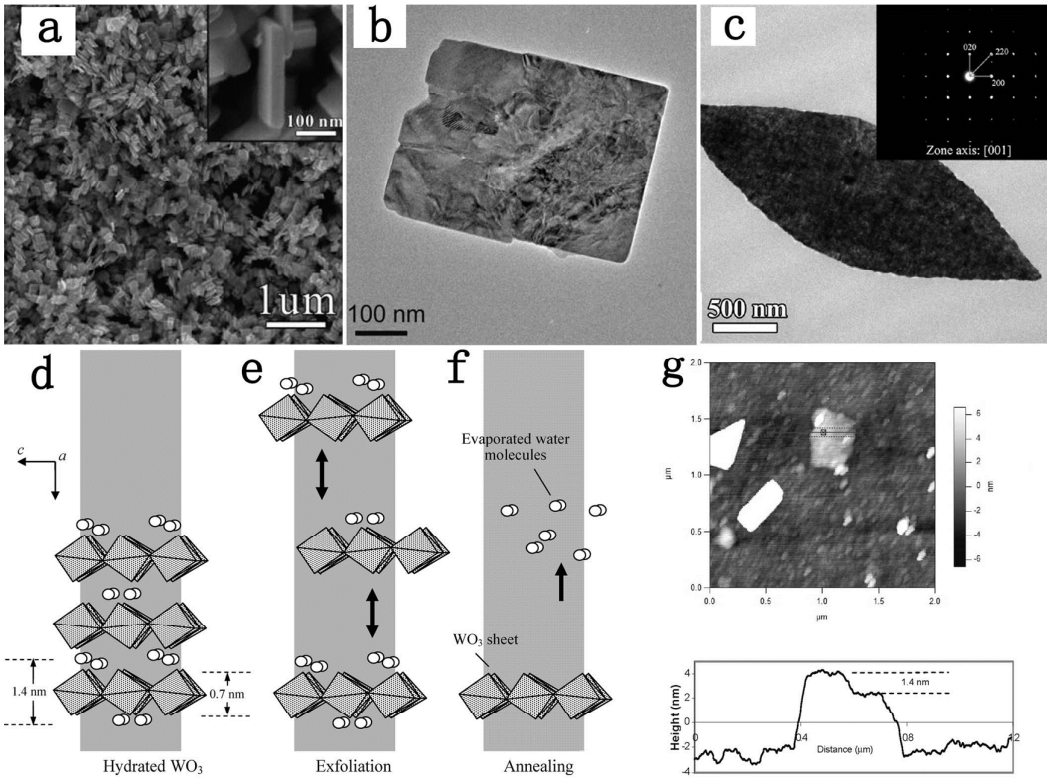

Fig. 7 (a) The SEM image of δ–WO_3 nanoplatesusing 0.11 mol L^{-1} tartaric acid. Reproduce with permission.[59] Copyright 2012, The Centre National de la Recherche Scientifique (CNRS) and The Royal Society of Chemistry. (b) The TEM image of 2D H_2WO_4 precursor. Reproduce with permission.[66] Copyright 2008, Wiley. (c) The HRTEM image of an isolated γ–WO_3 leaf (the inset shows the corresponding SAED pattern of the isolated nanoplatelet). Reproduce with permission.[69] Copyright 2012, American Chemical Society. Schematic of the formation of single layer of monoclinic WO_3 from layered hydrated WO_3 via an exfoliation process: (d) hydrated WO_3, (e)mechanical exfoliation separate layers at their weakest bonds into 1.4 nm sheets, and (f) water molecules are evaporated and WO_3 layers of multiples of 0.7 nm thickness are formed. (g) Typical AFM image and profiles of hydratedWO_3 sheets. Reproduce with permission.[82] Copyright 2010, American Chemical Society.

Assited by agents[66–68] or not[69], 2D H_2WO_4 precursors (Fig. 7b) were fabricated, which can be transformed into δ–WO_3[68] or γ–WO_3[34,66,67,69] nanoplates or nanoleaves

(Fig. 7c). Kalantar–zadeh *et al.*[82] develop a three–step method (Fig.7d–f) based on $WO_3 \cdot 2H_2O$ precursor to obtain atomically thin γ–WO_3 quantum sheets. The minimum resolvable thickness of the hydrated flakes to be ~1.4 nm (Fig. 7g).

2. 4 0 / 1 / 2D–based WOx hierarchical nanostructures

Numerous hierarchical structures based on 0 / 1 / 2D units possessing enhanced physical and chemical properties than the pristine structures have been introduced to nano–structure based devices for a given application.

For vapor phase method, substratesare often required for the growth of WO_x hierarchical structures such as forest (Fig. 8a),[105] hierarchical arrays,[92,95,106,107] 3D networks (Fig. 8b and c),[106] and so on.

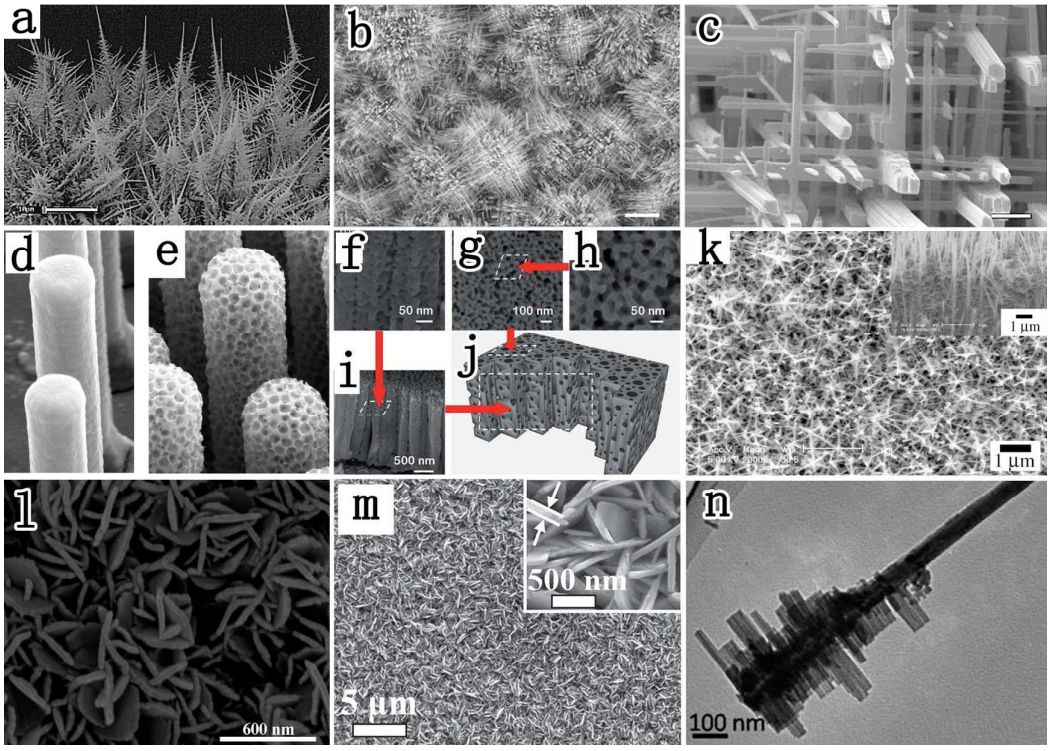

Fig. 8 (a) The SEM image of WO_3 nanoforests. Reproduce with permission.[105] Copyright 1999, Elsevier. (b, c) SEM images of tungsten oxide networks (scale bar: 3 μm for (b) and 200 nm for (c)). Reproduce with permission.[108] Copyright 2005, Wiley. SEM images of (d) Si nanorod arrays and (e) mesoporous WO_3 thin film based on Si nanorod arrays. Reproduce with permission.[109] Copyright 2014, American Chemical Society. SEM images of (f–h) the top view and (i, j) cross–sectional view of an annealed 3D WO_3 nanoporous network. Reproduce with permission.[111] Copyright 2012, The Royal Society of Chemistry. (k) The SEM image of WO_3 nanoforests. Reproduce with permission.[36] Copyright 2009, Elsevier. (l) The SEM image of W foil anodized for 60 min (calcined at 400°C for 4 h). Reproduce with permission.[112]

Copyright 2010, American Chemical Society. (m) The SEM image of nanosheets arrays (the inset is the corresponding high–manification SEM image). Reproduce with permission.[27] Copyright 2014, Elsevier. (n) The TEM image of a single nanobrush. Reproduce with permission.[113] Copyright 2011, The Royal Society of Chemistry.

Liquid phase method is an effective way to fabricate 0 / 1 / 2D based hierarchical structures. For 0D based hierarchical structures, mesoporous hollow spheres[70] and mesoporous thin film (Fig. 8d and e)[109,110] can be fabricated via removal of the template. In addtion, Ou *et al.*[111] reported that they prepared a 3D WO_3 nanoporousnetwork at room temperature by the electrochemical anodization of a RF sputteredtungsten film deposited on a FTO glass (Fig. 8f–j).

Various 1D based hierarchical structures (urchin–like spheres,[71,113] nanoforests (Fig. 8k)[95,114] *etc.*) can be obtained by solvo / hydrothermal reaction[36,71,113,114] and precursor based method.[115] Similarly, 2D based hierarchical structures (*e.g.* flower (Fig. 8l),[112] array (Fig. 8m),[27,116] brush–like (Fig. 8n),[113] *etc.*) can be synthesized by solvo / hydrothermal reaction[113,117] and precursor based method.[27,73,112,116]

3 FeO_x

Iron oxides represent the most common iron compounds found in nature. Up to present, apart from amorphous iron (III) oxide, six crystalline nonhydrated iron oxides have been recognized.[118,119] *i.e.* Fe_3O_4 (magnetite); four polymorphs of Fe_2O_3, labeled as α–Fe_2O_3 (hematite, rhombohedrally centered hexagonal structure of the corundum type, space group $R\bar{3}c$), β–Fe_2O_3 (body–centered cubic "bixbyite" structure, space group $Ia\bar{3}$), γ–Fe_2O_3 (maghemite, cubic crystal structure of an inverse spinel type, at least three different crystal symmetries), and ε–Fe_2O_3 (orthorhombic structure, space group $Pna2_1$); and FeO phase (wüstite). Highly crystalline α–Fe_2O_3 and γ–Fe_2O_3 occur in nature, while β–Fe_2O_3 and ε–Fe_2O_3 are generally synthesized in the laboratory.[120] Researches also indicated that the following sequence of polymorphous transformations may occured with increasing temperature and particle size: γ–Fe_2O_3 → ε–Fe_2O_3 → β–Fe_2O_3 → α–Fe_2O_3.[121,122]

Iron oxide nanostructures have attracted great attention from many research fields due to their low–cost, corrosion–resistant and environmental–friendly features. Iron oxides can be synthesized using varying techniques to form 0D,[123–125] 1D,[126–129] 2D[130–133] and 0[134,135] / 1[136–139] / 2D[140,141]–based hierarchical structures. They have been found highly applicable and versatile in lithium ion batteries,[129,142–146] supercapacitors, catalysis (including photocatalysis),[124,136,140,147,148] gas sensors,[124,132,137,149]

field–emitter,[141] removal of heavy metal ions,[150] antimicrobial applications,[126] diagnostic magnetic resonance imaging (MRI),[123,151,152] thermal therapy,[153] drug delivery,[154] *etc.* In this section, a general review on shape–controlled syntheses of iron oxide nanostructures (especially for Fe_3O_4 α–Fe_2O_3 and γ–Fe_2O_3) is present based on two major categories of synthetic methods: vapor phase and liquid phase.

3.1 0D iron oxide nanostructures

Iron oxide QDs are usually prepared by liquid phase methods. Park *et al.*[155] successfully prepared mono–disperse Fe_3O_4 (5–12 nm, Fig. 9a) based on the thermal decomposition of the iron–oleate precursors in high boiling solvent. Similarly, Kim *et al.*[123] synthesized γ–Fe_2O_3 QDs (ESION) of < 4 nm by controlled thermal decomposition of iron–oleate complex in the presence of oleyl alcohol via heat–up process (Fig. 9b). The size of the QDs could be reduced by increasing the ratio of oleyl alcohol to oleic acid or decreasing the reaction temperature. The low toxicity, high r_1 relaxivity, long blood half–life, and low synthetic cost enable ESIONs to be competent T_1 MRI contrast agents for various clinical applications (Fig. 9b). The solvothermal reaction is an effective approach to prepare iron oxide QDs, too. Tian *et al.*[156] synthesized ultra–small monodisperse Fe_3O_4 QDs (4–6 nm) via solvothermal reaction. In addition, a template directed method was used for the synthesis of semiconductor–magnetic hybrid nanocrystals (HNCs) with selectable heterodimer topologies and tunable geometric parameters (Fig. 9c–e).

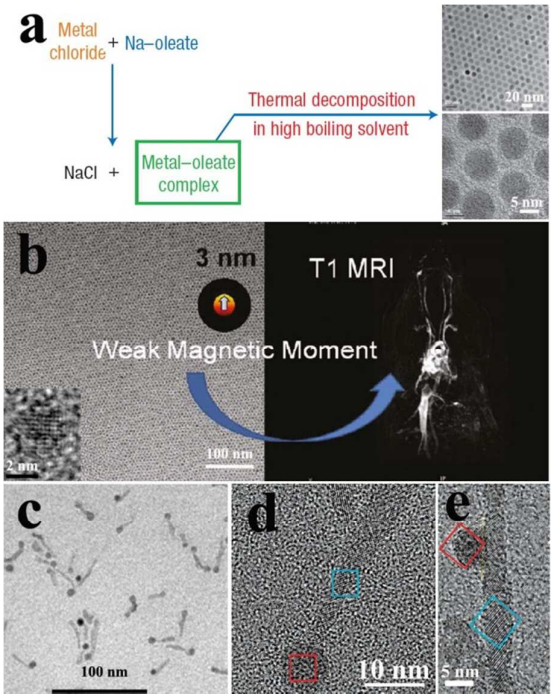

Fig. 9 (a) The overall scheme for the ultra–large–scale synthesis of monodisperse Fe_3O_4 QDs. Reproduce with permission.[155] Copyright 2004, Nature Publishing Group. (b) The TEM image of 3 nm–sized iron oxide nanoparticles (ESION, the inset is the HRTEM image of a single QD) and the corresponding ESION–enhanced high–resolution blood pool MR images obtained using 3d–FLASH sequence. Reproduce with permission.[123] Copyright 2005, American Chemical Society. Representative (c) low– and (d) high–magnification TEM images of asymmetrically Fe_xO_y–tipped TiO_2 nanorods; (e) HRTEM image of TiO_2 nanorods decorated with Fe_xO_y domains on their longitudinal sidewalls. Reproduce with permission.[157] Copyright 2010, American Chemical Society.

Vapor phase methods for preparing nanomaterials always involve thermal decomposition (pyrolysis), reduction, hydrolysis, disproportionation, oxidation, or other reactions to precipitate solid products from the vapor phase.[158,159] Normally, vapor phase methods are used for preparations of iron oxide continuous thin film[160,161] or 1D[162,163] / 2D[146] nano–arrays.

For syntheses of 0D Fe_3O_4 nanostructures with specific exposed facets, liquid phase methods will be good choices. Through a solvothermal approach, Wang *et al.*[125] synthesized magnetite with different morphology and size by using ferrocene as a single precursor and isopropanol (IPA) or an isopropanol–water mixture as solvent (Fig. 10a). Without any additive agents, it is most likely that the growth rate of (100) is much faster than that of (111) of the formed primary Fe_3O_4 seeds, which leads to the formation of star–shaped hexapods. By varying the ratio of IPA to water and the reaction temperature, octahedrons or star–shaped hexapods of opposite vertexes with the difference of six arms changing from spindle to round can be prepared. Due to adsorption and etching effect of SDBS, concave octahedrons formed at an appropriate concentration of SDBS, and octahedral frameworks become dominant at a high input of SDBS (SDBS / Fe at 2:1). Similar to the report of Wang *et al.*,[135] uniform Fe_3O_4 octahedra could be synthesized with the help of the nonionic surfactant Triton X100 (Fig. 10b and c).[164]

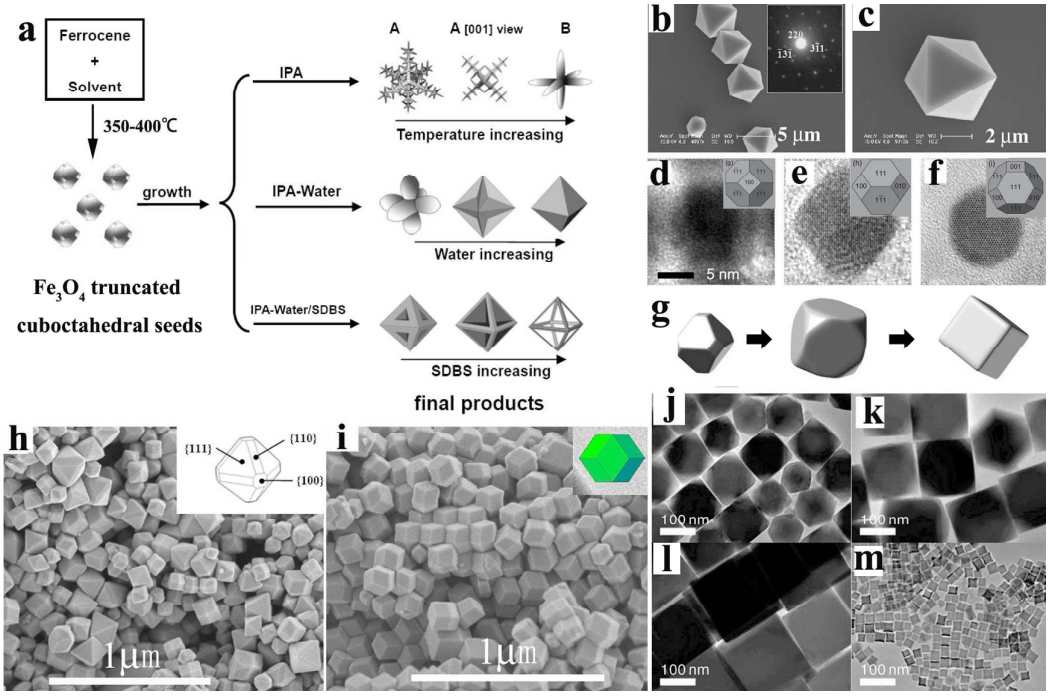

Fig. 10 (a) Schematic illustration for the formation of the Fe_3O_4 crystals with different morphologies. Reproduce with permission.[125] Copyright 2010, American Chemical Society. FESEM images of Fe_3O_4 octahedra: (b) low magnification; (c) high magnification. Reproduce with permission.[164] Copyright 2009, Elsevier. (d–f) The HRTEM images of [001]–, [101]–, and [111]–oriented truncated octahedra. Reproduce with permission.[165] Copyright 2009, Wiley–VCH. (g) Schematics showing the shape evolution of the Fe_3O_4 nanoparticles from truncated octahedron to cube; TEM images of (j) mixture of truncated cubic and truncated octahedral nanoparticles with an average dimension of 110 nm; (k) 150–nm–sized truncated nanocubes; (l) 160– and (m) 22–nm–sized nanocubes. Reproduce with permission.[166] Copyright 2008, American Chemical Society. FESEM images of the products prepared with different $Fe(acac)_3$ concentrations: (h) 0.01 (a mixture of octahedra, truncated cuboctahedra and rhombic dodecahedra, the inset is an ideal geometrical model of a truncated cuboctahedra) and (i) 0.025 (rhombic dodecahedra, the inset is an ideal geometrical model of rhombic dodecahedra viewed along the [110] direction). Reproduce with permission.[167] Copyright 2014, American Chemical Society.

For a face–centered cubic (fcc) crystal, the surface energies corresponding to different crystallographic facets are in the order of {111} < {100} ≪ {110},[168] which could explain why most of Fe_3O_4 crystals synthesized without capping / directing agents performed a octahedral shape bounded by {111} facets. With addition of

capping / directing agents, Fe_3O_4 crystals with different morphologies formed starting from the Fe_3O_4 truncated cuboctahedral seeds. One way is to minimize the growth speed along [100] direction to form truncated cuboctahedra (seeds), truncated octahedra (Fig. 10d–f),[165] truncated cubes () and cubes ();[166] the other is to minimize the growth speed along [110] direction to form rhombic dodecahedra (RD, Fig. 10h and i).[167]

Capping / directing agents assisted liquid phase method is also applicable to controlled syntheses of α–Fe_2O_3 crystals with specific exposed facets. It is reported that without the addition of sodium carboxymethyl cellulose (CMC) and N_2H_4 molecules, the crystal growth along six crystallographically equivalent directions of the hematite crystalline structure resulted in the dendritic shape (Fig. 11a and b); while in contrast,α–Fe_2O_3 spheres (Fig. 11a and c) and truncated hexagonal bipyramid (Fig. 11a and d) were obtained.[169] In the same way, α–Fe_2O_3 rhombohedra with nearly 100% exposed {104} facets could be obtained via a solvothermal reacion by simply tailoring the ratio of water and 1–propanol, of which the solvent play the role of the capping / directing agents (Fig. 11e and f).[170]

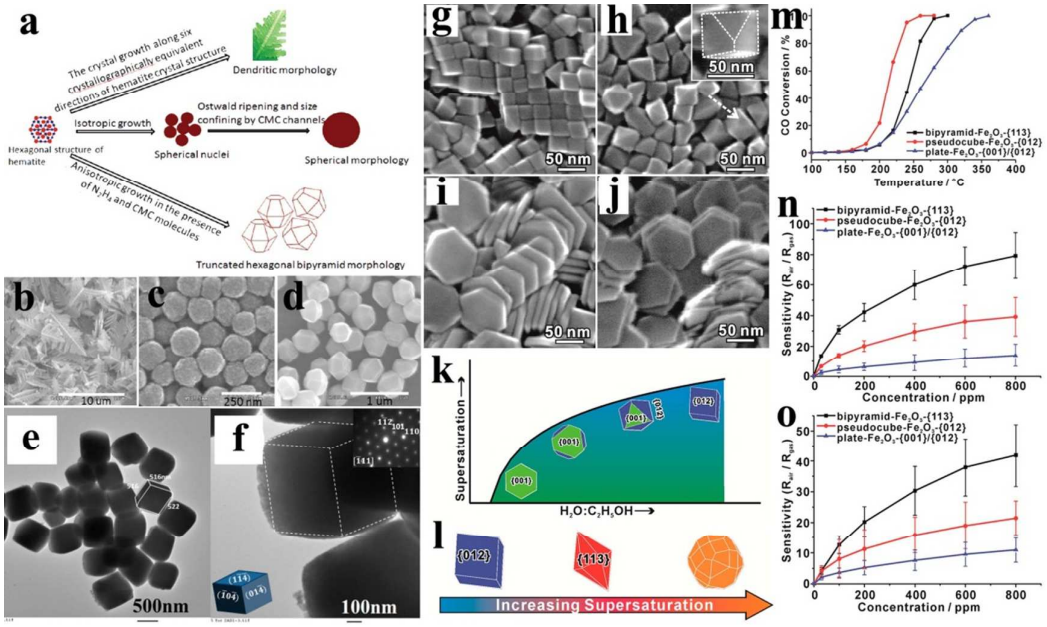

Fig. 11 (a) Schematic illustration for formation process of the hematite morphologies, and morphologies of the final α–Fe_2O_3 product obtained with various reactants under hydrothermal reaction conditions at 160°C for 8 h: (b) the dendritic shape, (c) spheres and (d) truncated hexagonal bipyramids. Reproduce with permission.[169] Copyright 2012, American Chemical Society. (e and f) TEM images of α–Fe_2O_3 rhombohedra. The insets are the SAED pattern and the schematic illustration

of the rhombohedra structure. Reproduce with permission.[170] Copyright 2014, American Chemical Society. SEM images of α–Fe_2O_3 nanocrystals synthesized with different ratios of water to ethanol: (g) 1:1, (h) 1:10, (i) 3:100, and (j) 1:100; (k) schematic illustration of the supersaturation–controlled morphology evolution of α–Fe_2O_3 nanocrystals as a function of solubility in mixed solvents; (l) schematic illustration of the supersaturation controlled morphology evolution of α–Fe_2O_3 nanocrystals, which was activated by changing concentrations of Fe^{3+} source; (m) CO conversion curves of α–Fe_2O_3 nanocrystals with different shapes as a function of temperature; concentration–dependent sensing curves of the α–Fe_2O_3 nanocrystals with different shapes: (n) acetone and (o) methanol. Reproduce with permission.[124] Copyright 2014, American Chemical Society.

Furthermore, the exposed facets of α–Fe_2O_3 crystals could be tailored by the supersaturation without using any capping / directing agents (Fig. 11g–l).[124] The higher ratio of water to ethanol (higher supersaturation) led to a smaller ratio of {001} to the total surface, which result in the morphology evolution as follow: thin nanoplates → thick nanoplates → truncated pseudocube → pseudocube (Fig. 11g–k). Further increasing the supersaturation by adding more $Fe(acac)_3$ will be conductive to the formation of exposed facets with higher surface energy, which result in the formation of hexagonal bipyramidal nanocrystals exposed with {113} facets (2 mmol) and nearly spherical nanocrystals bounded by multiple groups of uncertain high–index facets (> 3 mmol). The catalytic activity of facets in CO oxidation was demonstrated to follow the order of {012} > {113} > {001} (Fig. 11m), while the sensing ability followed the order of {113} > {012} > {001} (Fig. 11n and o). The distinct catalytic and sensing performances were ascribed to high chemisorption amounts of CO on {012} facets and high percentage of O_V and O_C of bipyramid–Fe_2O_3–{113}

3.2 1D iron oxide nanostructures

Morphologies of 1D nanostructures can be contorlled to be forms such as rods,[126,163] wires / fibers,[171] columns,[126] belts, tubes, *etc.* Using a pulsed laser deposition (PLD) method (Fig. 12a) with Au catalyst, aligned α–Fe_2O_3 (along [110] direction) and Fe_3O_4 (along [111] direction) 1D nanostructures can be obtained on alumina substrates (Fig. 12b).[172] Using CuO as the catalyst, cubic Fe_3O_4 nanowires grow along the [110] direction can be synthesized (Fig. 12c–f).[171] Without the catalyst and with rich oxysen atmosphere, α–Fe_2O_3 nanowires (800°C) and nanobelts (700°C)

growing along the [110] direction can be obtained by direct oxidation of Fe substrate (Fig. 12g–i).[173] In a plasma enhanced chemical vapor deposition (PECVD) system, the temperature for the formation of α–Fe_2O_3 nanowires (570°C) was lower than nanobelts (680°C) due to highly reactive oxygen plasma.[162] By applying a potential difference of 2.7–7.8 V to 5.8–15.0 cm long Fe wires in air, α–Fe_2O_3 nanowires (700°C) growing along the [110] direction was observed.[174]

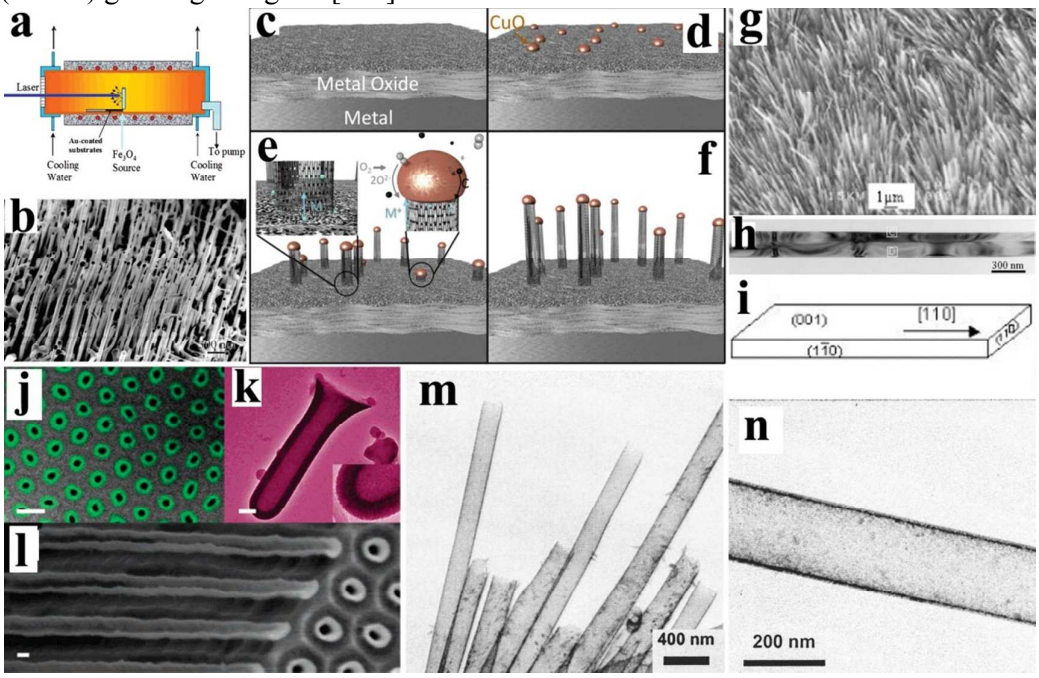

Fig. 12 (a) Schematic illustration showing PLD synthesis apparatus. Laser energy is directed through a treated glass window to a pressed magnetite target. Vapors are released and re–condensed as 1D nanostructures nucleated on gold catalyst particles. (b) SEM image of aligned iron oxide nanowires doped with Mg showing local alignment along alumina crystallites. Reproduce with permission.[172] Copyright 2006, American Chemical Society. Schematic representation of the catalyzed oxidation for nanowire growth process (c)–(f), where a metal catalyzes oxygen reduction, rapid cation diffusion occurs through the oxide scale and along the nanowire, and the two species meet at the base of the catalyst. Reproduce with permission.[171] Copyright 2014, IOP Publishing Ltd. (g) Typical SEM, (h) bright–field TEM images, and (i) a structural model of the α–Fe_2O_3 nanobelt array in the 700°C temperature zone. Reproduce with permission.[173] Copyright 2005, American Chemical Society. Electron micrographs of the iron oxide tubes. Scale bars: 100 nm. (j) SEM image of an array of narrow tubes (11 ± 2 nm Fe_2O_3, green circles) embedded in the alumina template. (k) TEM image of a single thick and short tube (42 ± 4 nm

Fe_3O_4) isolated by dissolution of the template; the inset zooms in on the very smooth wall. (l) SEM image of an array of thick ZrO_2 / Fe_2O_3 / ZrO_2 tubes embedded in the template: edge view at a crack, with tubes broken in their length and emerging on the top side of the membrane. Reproduce with permission.[175] Copyright 2007, American Chemical Society. TEM images of the magnetic nanotubes: (m) a bundle of Fe_3O_4 nanotubes, and (n) one Fe_3O_4 nanotube released from the matrix. Reproduce with permission.[176] Copyright 2004, American Institute of Physics.

With a porous anodic alumina membrane (AAM) as the substrate and template, Bachmann *et al.*[175] prepared Fe_2O_3 nanotubes with tunable size and variable layers by atomic layer deposition (Fig. 12j–l). Similar results can be obtained by simply decomposing Fe nitrate that precoated into AAM in air at 400°C.[177] Using the same template, Fe_3O_4 tubes can be obtained by first thermally decomposed Fe nitrate solution at 250°C in nanochannels of AAM, and then reduced it in hydrogen for 2.5 h at 560°C (Fig. 12m and n).[176]

Iron oxide 1D nanostructures fabricated by liquid phase methods (*e.g.* sonochemistry driven synthesis,[178] laser–induced (Fig. 13a and b) / asisted (Fig. 13c and d) reaction,[179,180] sonoelectrochemical anodization (Fig. 13e),[181] hydrothermal reaction (Fig. 13f–l),[182] co–precipitation,[183] *etc*.) perform various morphologies such as rods,[182] wires / fibers, necklaces,[184] belts,[180] tubes,[185] multi–tubes,[151] urchin–like nanostructures,[186,187] *etc*.

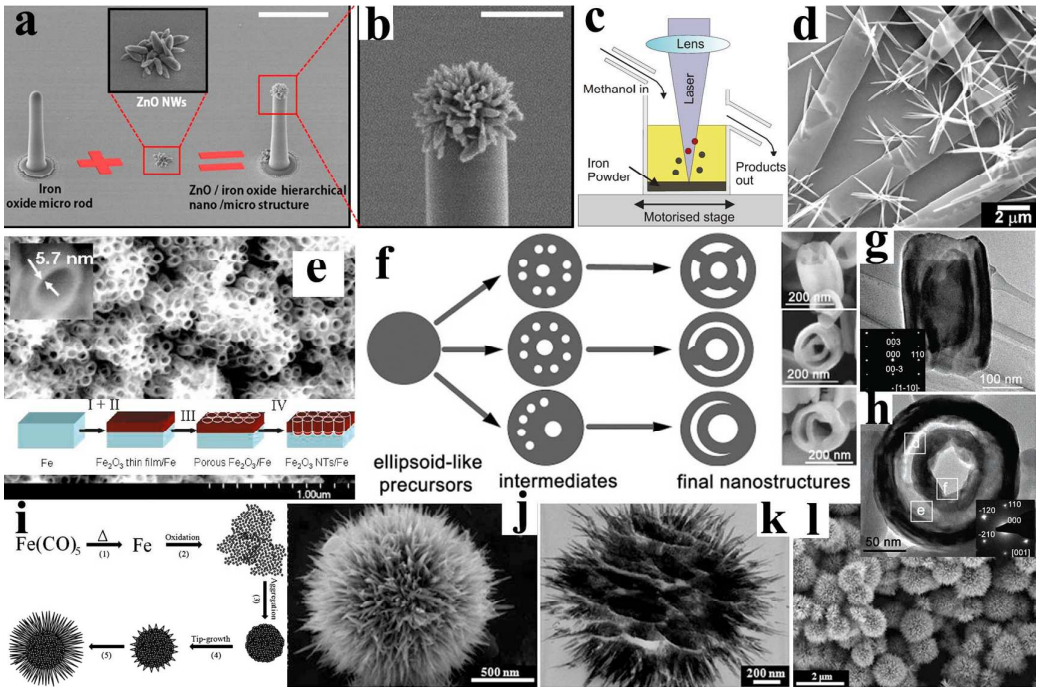

Fig. 13 (a) Tilted SEM image of the iron oxide microrod by photothermal chemical liquid growth (PCLG), ZnO NW by LIHG, and ZnO / iron oxide hierarchical nano– / microstructure, respectively. (b) Magnified SEM image of the ZnO/iron oxide hierarchical nano– / microstructure. Scale bars are 20 μm in (a) and 5 μm in (b). Reproduce with permission.[179] Copyright 2014, American Chemical Society. (c) Schematic diagram of the experimental set–up, and (d) a SEM image of iron oxide nanobelts and nanowires obtained after 5 min of laser irradiation just before starting the methanol flow. Reproduce with permission.[180] Copyright 2008, IOP Publishing Ltd. (e) As–anodized α–Fe_2O_3 nanotubes and nanoporous materials on Fe foil prepared at 50 V using 3 vol.%water for 13 min. Reproduce with permission.[181] Copyright 2009, American Chemical Society. (f) Schematic illustrations (top view) of the formation process of hematite tube–in–tube nanostructures with diversity, (g) side–view and (h) top–view TEM image of a single tube–in–tube nanostructure and the SAED pattern. Reproduce with permission.[127] Copyright 2007, American Chemical Society. (i) A schematic illustration of the formation process of the Fe_2O_3 urchin–like nanostructures and the corresponding (j–l) SEM and TEM images. Reproduce with permission.[187] Copyright 2011, The Royal Society of Chemistry.

In addition, precursor based / template directed methods with subsequent pyrolysis at high temperature are usually used for syntheses of α–Fe_2O_3[188] / Fe_3O_4[189] nanorods, Fe_2O_3 hollow fibers,[190] α–Fe_2O_3 / Fe_3O_4 nanotubes,[191–193] γ–Fe_2O_3 tube in tube (Fig. 13f–h),[127, 194] and so on.

3.3 2D iron oxide nanostructures

2D FeO_x nanostructures synthesized by liquid phase methods showed richer morphologies (*e.g.* hexagonal nanoplates,[190] nanodisks,[195] nanorings,[191] graphene–like nanofilms,[209] quantum sheets,[189] *etc.*, Fig. 14) and phases (*e.g.* α–Fe_2O_3,[131] Fe_3O_4,[196] γ–Fe_2O_3, *etc.*) than those of vapor phase methods.[146,197] In these works, the basal surfaces of 2D nanostructures are usually (0001) for α–Fe_2O_3 and (111) for Fe_3O_4 and γ–Fe_2O_3; and thicknesses of 2D FeO_x nanostructures are usually tailored by change the amounts and types of directing / capping agents from solutes[255] or solvents.[190] Latest studies indicated that template directed methods might be effective ways to obtain ultra–shin 2D FeO_x nanosheets (Fig. 14h–j).[130,143] As shown in Fig. 14i, Cheng *et al.*[130] synthesized atomically thin α–Fe_2O_3 quantum sheets via an CuO–template–assisted oriented growth strategy. After calcination, the obtained

α–Fe_2O_3 quantum sheets with half–unit–cell thickness robust intrinsic ferromagnetism of 0.6 μ_B / atom at 100 K and remain ferromagnetic at room temperature.

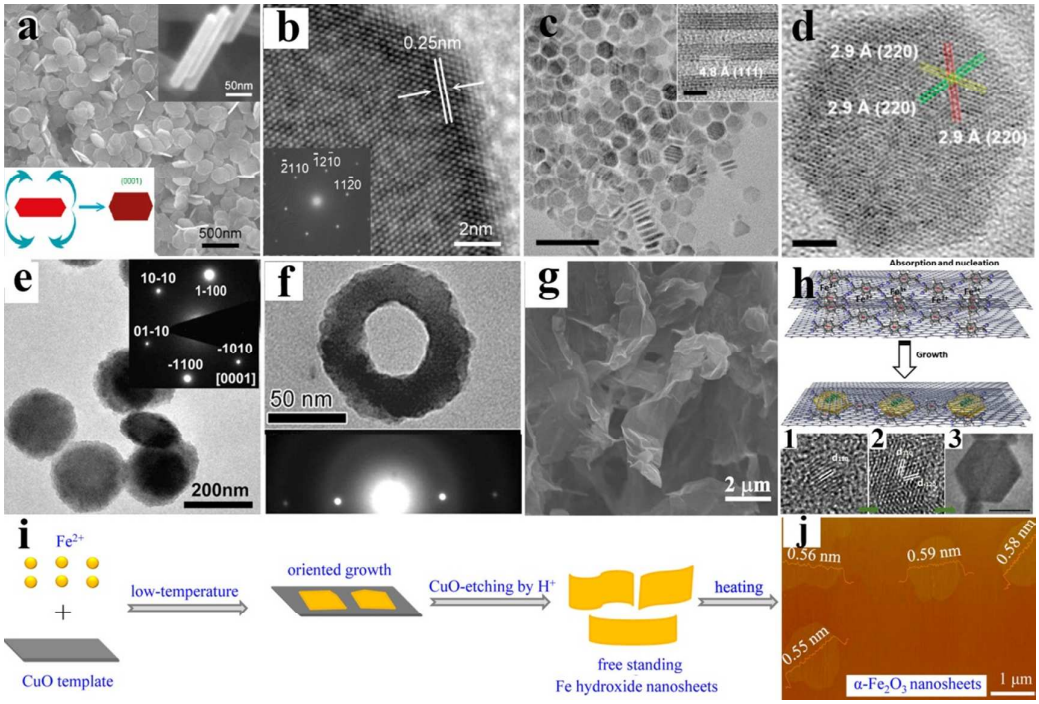

Fig. 14 (a) A SEM image of uniform α–Fe_2O_3 nanoplates with up–right inset showing the free–standing side surfaces and down–left inset showing thickness evolution when ethanol was replaced by water, and (b) HRTEMimage and its relatedFFT pattern from the white square along the [0001] zone axis. Reproduce with permission.[131] Copyright 2010, American Chemical Society. (c and d) Representative TEM and HRTEM images of 2.8 nm thick nanoplates. Reproduce with permission.[196] Copyright 2014, American Chemical Society. (e) TEM image (inset: SAED pattern) of the as–prepared α–Fe_2O_3 nanodisks. Reproduce with permission.[195] Copyright 2013, Wiley. (f) High–magnification TEM image and SAED pattern of a single nanoring. Reproduce with permission.[132] Copyright 2007,Wiley. (g) A SEM image of graphene–like nanofilms. Reproduce with permission.[150] Copyright 2013, The Royal Society of Chemistry. (h) Schematic illustration of the formation process of α–Fe_2O_3 hexagonal nanoplatelets sandwiched between graphene sheets (HP–Fe–G); time–dependent shape evolution of α–Fe_2O_3 nanocrystals: (1) 3min, (2) 10min, (3) 2h; Scalebar: 50nm. Reproduce with permission.[143] Copyright 2012, Elsevier Ltd. (i) Schematic of synthesis strategy and (j) AFM image of α–Fe_2O_3 nanosheets. Reproduce with permission.[130] Copyright 2014, American Chemical Society.

3.4 0 / 1 / 2D–based iron oxide hierarchical nanostructures

For vapor phase method, substrates are usually used for the growth of hierarchical structures. As shown in Fig. 15a–d, on the surface of Si substrate with a monolayer of polystyrene (PS) spheres, 0D– and 2D–based α–Fe_2O_3 hierarchical structures can be obtained by PLD–CVD at the oxygen pressure of 60 Pa and 6 Pa, respectively.[141] Since O atoms are rich and Fe atoms are deficient in the (110) plane, it can be considered to be the driving force for the preferential growth along the [110] direction. By pyrolysis of ferrocene in supercritical CO_2 at 450 °C, Cao *et al.*[198] successfully synthesized 1D–based 3D Fe_3O_4 networks on the inside wall of the autoclave (Fig. 15e and f). Decrease of the amout of CO_2 resulted in the reduction of the length of nanorods, while increase of the amount of Fe sources led to the formation of 2D nanosheets. In a PECVD system at room temperature, well defined α–Fe_2O_3 nanoplatelet arrays can be obtained on the FTO substrate (Fig. 15g–i), the thickness of which increased with increasing amount of Fe sources.[140]

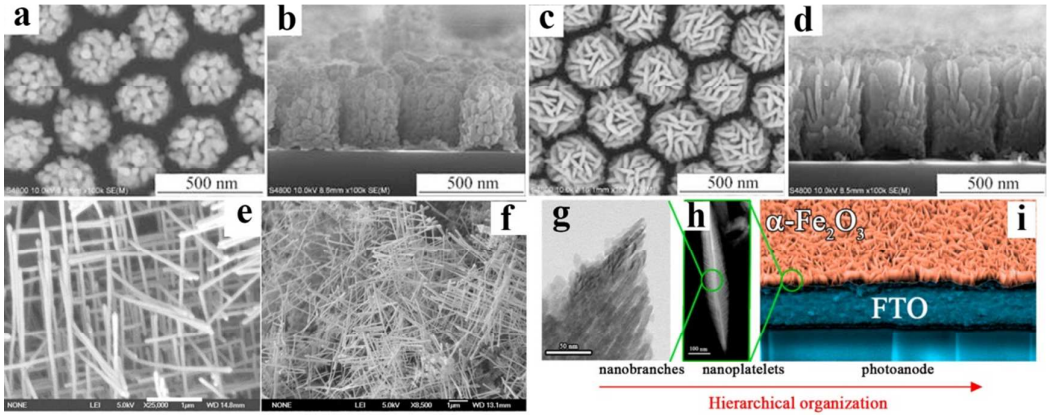

Fig. 15 (a) SEM images of as–deposited samples at the oxygen pressure of 6 Pa (0D based, a and b) and 60 Pa (2D based, c and d). (a), (c) top surface; (b), (d) cross–section. Reproduce with permission.[141] Copyright 2010, The Royal Society of Chemistry. (e and f) Typical FESEM images of 3D Fe_3O_4 networks. The length of the bars is 1 μm. Reproduce with permission.[198] Copyright 2008, American Chemical Society. (g) HRTEM image and (h) HAADF–STEM micrograph representing the hierarchical morphology of the hematite platelets; (i) a cross sectional SEM image of hematite nanoplatelet arrays. Reproduce with permission.[140] Copyright 2014, American Chemical Society.

For liquid phase methods, various FeOx hierarchical nanostructures can be synthesized by simply solution method, solvo / hydrothermal reaction, template–directed and precursor based method. 0D based FeOx hierarchical structures

(meso–porous particles such as super–structures,[199,200] spheres,[144] hollow spheres[201,202] / bowls,[203] cubes,[135,204] *etc.*, Fig. 16a–c) are usually prepared by solvo– / hydrothermal reaction[152,202] and precursor based methods.[135,144,204] As a new type of precursors, metal–organic frameworks (MOFs) with controllable size, shape, composition, and shell / internal structure have received great attention for MOX hierarchical nanostructures. For example, Lou *et al.*[204] synthesized Fe_2O_3 microboxes with various shell structures (Fig. 16e–j) based on controlled annealing of preformed Prussian blue (PB) microcubes (Fig. 16d). When evaluated as potential anode materials for lithium ion batteries, the as–prepared Fe_2O_3 microboxes with unique shell structures exhibited high lithium storage capacities and excellent cycling performance. Furthermore, since well defined hollow interiors can be created inside PB nanoparticles through controlled chemical etching in the presence of poly(vinylpyrrolidone),[205] nanoporous iron oxide nanostructures with hollow interiors and various phases can be synthesized by controlled calcination of these PB nanoparticles as starting precursors.[135]

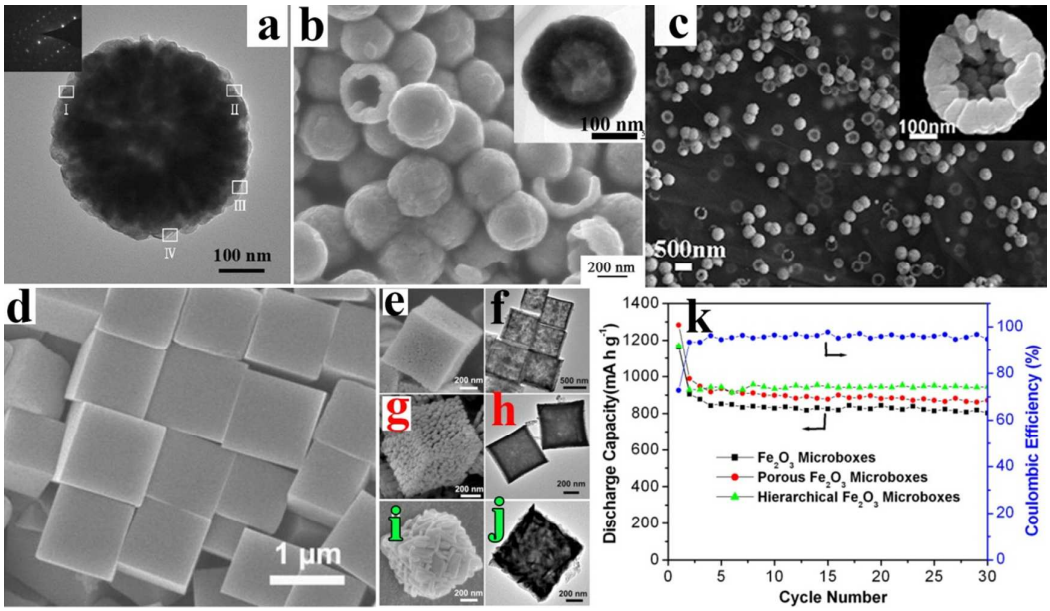

Fig. 16 (a) A TEM image of a single Fe_3O_4 microsphere, with a corresponding SAED pattern (inset). Reproduce with permission.[144] Copyright 2012, American Chemical Society. (b) A SEM image of Fe_3O_4 hollow microspheres (the inset is the corresponding TEM image). Reproduce with permission.[201] Copyright 2009, American Chemical Society. (c) SEM images of the bowl–like hollow Fe_3O_4 / r–GO composites. Reproduce with permission.[203] Copyright 2012, American Institute of Physics. (d) A FESEM images of PB microcubes; (e, g, i) FESEM and (f, h, j) TEM

images of hollow Fe_2O_3 microboxes obtained at (e, f) 350°C, (g, h) 550°C, and (i, j) 650°C; cycling performance (three types of Fe_2O_3 microboxes) and coulombic efficiency (porous microboxes (550°C) over the voltage range 0.01−3.0 V vs Li / Li^+ at the same current density of 200 mA g^{-1}). Reproduce with permission.[204] Copyright 2012, American Chemical Society.

As shown in Fig. 17a and b, an interesting type of 1D based hierarchical structures is the snowflake–like dendrites (up and bottom surfaces parallel to {0001} plane) synthesized by hydrothermal reactions,[138,139] which can be transformed into Fe, γ–Fe_2O_3, and Fe_3O_4 via H_2 reduction for microwave absorption.[206] In addition, CNT template directed synthesis of CNT@β–FeOOH and the subsequent transformation into CNT@Fe_2O_3 via calcination is an typical example for 1D based hierarchical structures prepared by precursor based methods.[136]

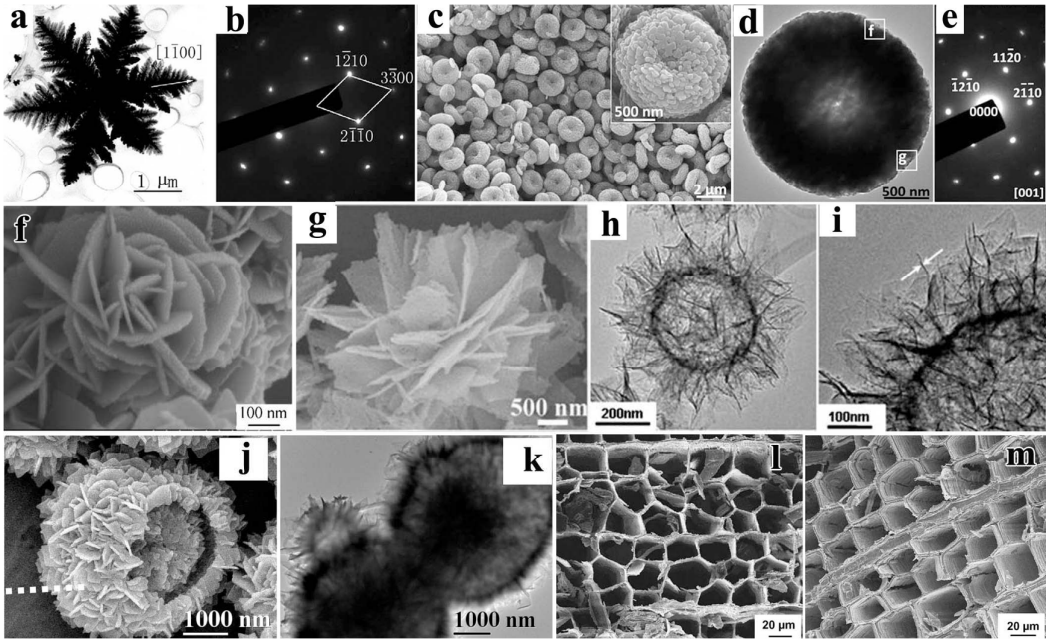

Fig. 17 (a) A TEM image and its corresponding (b) SAED pattern of a snowflake–like dendrite. Reproduce with permission.[138] Copyright 2006, Elsevier. (c) SEM, (d) TEM images, and the corresponding (e) SAED pattern of α–Fe_2O_3 2D hollow micro–platelets obtained after solvothermal reaction with 3 mM NH_4F. Reproduce with permission.[147] Copyright 2014, The Royal Society of Chemistry. (f) A SEM image of Fe_3O_4 nanosheet–flowers synthesized by aqueous solution method at 80°C for 16 h. Reproduce with permission.[207] Copyright 2012, The Royal Society of Chemistry. (g) A SEM image of flower–like α–Fe_2O_3 nanostructure based on FeOOH precursor. Reproduce with permission.[137] Copyright 2011, American Chemical

Society. (h and i) TEM images of hierarchical hollow spheres of α–Fe_2O_3 composed of ultrathin nanosheets based on FeOOH precursor. Reproduce with permission.[148] Copyright 2013, The Royal Society of Chemistry. (j) SEM and (k) TEM images of hollow core / shell hierarchical nanostructures (Fe–EG precursor). Reproduce with permission.[208] Copyright 2008, American Chemical Society. SEM images of cross–section of softwood–templated Fe_2O_3 bulk samples heated at 800°C. (l) Pine–templated Fe_2O_3 and (m) Fir–templated Fe_2O_3. Reproduce with permission.[209] Copyright 2005, Elsevier.

Solvo / hydrothermal reaction and precursor based method are two typical methods for the syntheses of 2D based hierarchical structures. For instances, 2D hollow microplatelets with different porosities but similar platelet–like shapes can be synthesized by a solvothermal method with different amount of NH_4F (Fig. 17c–e).[147] And Fe_3O_4 nanosheet–flowers synthesized by a simply aqueous solution method (Fig. 17f).[207] For precursor based methods, meso–porous flower–like nanostructures are the most common morphologies that observed on porous hierarchical structures based on precursors such as FeOOH,[137,148] Fe–EG,[208] and so on (Fig. 17g–k). In addition, wood templates can be used for the synthesis of hierarchical iron oxide with controllable porous structures (Fig. 17l and m). Basic units of such nanostructures can be found to be 2D films and 0D nanoparticles.

4. ZnO

4.1 0D nanostructures of ZnO

In all of 0D structures of ZnO, ZnO hollow structures with well–defined structures have attracted more and more attention due to their great potential applications in areas such as catalysis, chemical and biological sensors, protection of biologically active agents, waste removal, and large bimolecular–release systems. Therefore, many efforts have been devoted to fabricate ZnO with hollow structure in recent years. Many ZnO hollow structures have been successfully prepared.

The researches mainly focused on template–assisted process, which usually employed polystyrene spheres, carbon spheres, spherobacteria and so on as template for the growth of ZnO hollow structures. In the course of fabrication, ZnO nanoshells or precursors were first deposited onto the surfaces of template spheres to form core–shell composite spheres. Soon after, the template particles were removed by dissolution in an appropriate solvent or by calcination at elevated temperature. Finally, ZnO hollow spheres could be obtained.

Zeng *et al.*[210] developed a three–tiered organization of ZnO nano–building blocks into hollow spherical conformations using cetyl–trimethyl–ammonium–bromide (CTAB) as template (Fig. 18). [210] CTAB surfactant can form colloidal vesicles in polar media, which act as a soft template for the self–assembly of ZnO multipod units, whereas ZnO nanorods are synthesized with the assistance of EDA chelating agent.

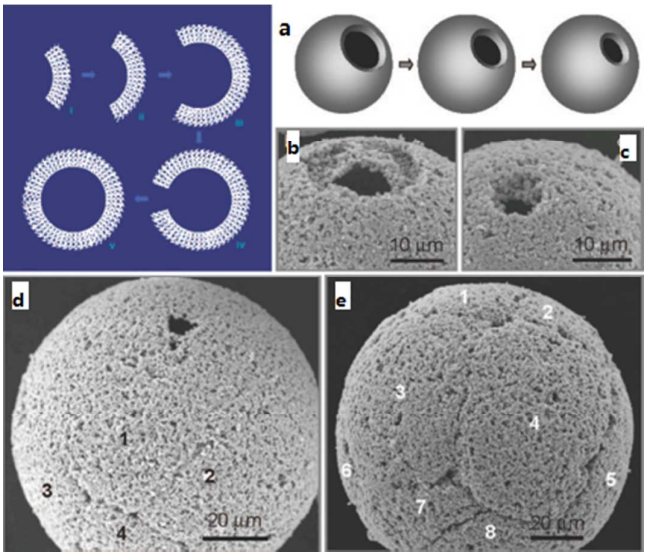

Fig. 18 (a) Self–assembling process of ZnO microspheres using CTAB as template; (b, c) FESEM images of the openings of microspheres; (d, e) SEM images of domains (marked with numbers) of assembled nanobuilding units. Reproduce with permission.[210] Copyright 2007, American Chemical Society.

Wu *et al.*[211] presented a novel process for the synthesis of ZnO hollow spheres. In the approach, when $Zn(Ac)_2 \cdot 2H_2O$ was put into the ethanol solution with sulfonated polystyrene core–shell spheres, zinc ions would adhere to the surfaces of template spheres via electrostatic interaction. As the NaOH solution was added into the solution, they would react with zinc ions to form ZnO crystal nucleus, which was followed by the formation of ZnO nanoshells. Therewith, neither additional dissolution nor calcination was employed to remove the PS core–shell spheres, template cores could be directly "dissolved" in the same solution, and form ZnO hollow spheres in the end (Fig. 19).[211] The size of hollow spheres could be controlled by the size of the template spheres, and the wall thickness could be tailored by the concentration of $Zn(Ac)_2 \cdot 2H_2O$.

Fig. 19 Illustration of the forming process of the ZnO hollow spheres using PS as template. Reproduce with permission.[211] Copyright 2008, American Chemical Society.

Lv *et al.*[212] also synthesized hollow spheres of ZnO using the PS core–shell spheres as the template spheres. In this process, inorganic precursors were adsorbed into the sulfonated PS templates with negatively charge. The sulfonation process could facilitate the adhesion of Zn^{2+} on the surfaces of PS. Afterwards, the PS template would be removed by calcination, and the hollow spheres of ZnO formed.

Wang *et al.*[213] employed trisodium citrate assisted rapid alkaline precipitation techniques to fabricate well–defined ZnO hollow spheres. The shell of ZnO hollow sphere with partial open gaps was composed of a mass of ZnO nanospheres, which were pure hexagonal phase. Trisodium citrate was demonstrated to play an essential role in the formation of hollow spheres. And the annealed ZnO with hollow sphere architecture showed excellent gas response.

Wu *et al.*[214] reported on the preparation of ZnO hollow sphere templated by carbon microspheres. The prepared ZnO hollow spheres had a diameter of 200–400 nm and a shell thickness of about 25 nm. Song *et al.*[215] prepared ZnO hollow spheres by the glucose–mediated, one–pot hydrothermal synthesis of Zn–coated carbon spheres, and then calcined it at 500°C. Finally, the hollow ZnO microspheres with diameters of 1–2 mm were gradually transformed into solid microspheres.

The traditional template–assisted technology always employ inorganic template, which shows time–consuming, expensive and environment–unfriendly. To overcome these problems, biological templates begin to be applied to fabricate ZnO hollow spheres.

For instance, Zhang *et al.*[216] successfully prepared ZnO hollow spheres in a hydrothermal process by applied streptococcus thermophilus as green and economical biotemplate, which was based on the interaction between the reactants and the inherent functional groups on the cell walls, followed by calcination (Fig. 20).[216] They considered that the formation of as–obtained ZnO hollow spheres involves a two–step encapsulation process, which has an influence on the pore structure of the

products.

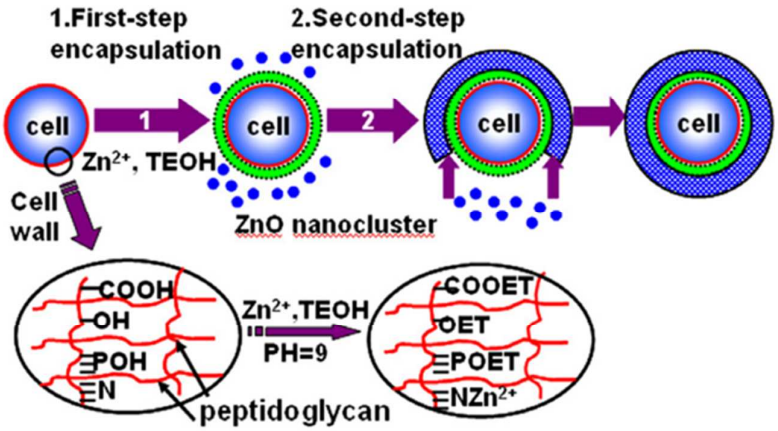

Fig. 20 Diagram of the formation mechanism of bacteria / ZnO core–shell spheres via a two–step encapsulation process. (TEOH represents triethanolamine, $N(CH_2CH_2OH)_3$). Reproduce with permission.[216] Copyright 2007, Elsevier.

The techniques discussed above require additional template, which need to be removed later, to construct sphere structures. Recently, many efforts have been devoted to research template–free approaches, which could avoid these complex processes. Nevertheless, great challenges still remain to prevent the incorporation of impurities and to control the size.

Xie *et al.*[217] extended the methods of coordination chemistry to fabricate hollow spheres of inorganic materials, which has been successfully put forward to synthesize ZnO submicrometer hollow spheres. In this approach, no additional template materials are needed to obtain submicrometer hollow sphere structures. It is noteworthy that the 1D rigid chain of the coordination polymer and the amount of NH_4OH are crucial to the formation of ZnO hollow spheres. A possible mechanism has also been proposed.

Gao *et al.*[218] reported the conversion of $Zn(NH_3)_4^{2+}$ under hydrothermal conditions, which resulted in the formation of ZnO hollow spheres with inner diameter of 100 nm and an outer diameter of 600 nm. The hollow spheres were composed of ZnO nanorods (Fig. 21).[218] And it was demonstrate that the pH value of initial mixture and the volume ratio of the ethanol with the solution have an important part in the formation of hollow spheres. Meanwhile, the results of characterization showed that the ZnO hollow spheres obtain presented excellent room–temperature photoluminescent properties with UV emission at 390 nm.

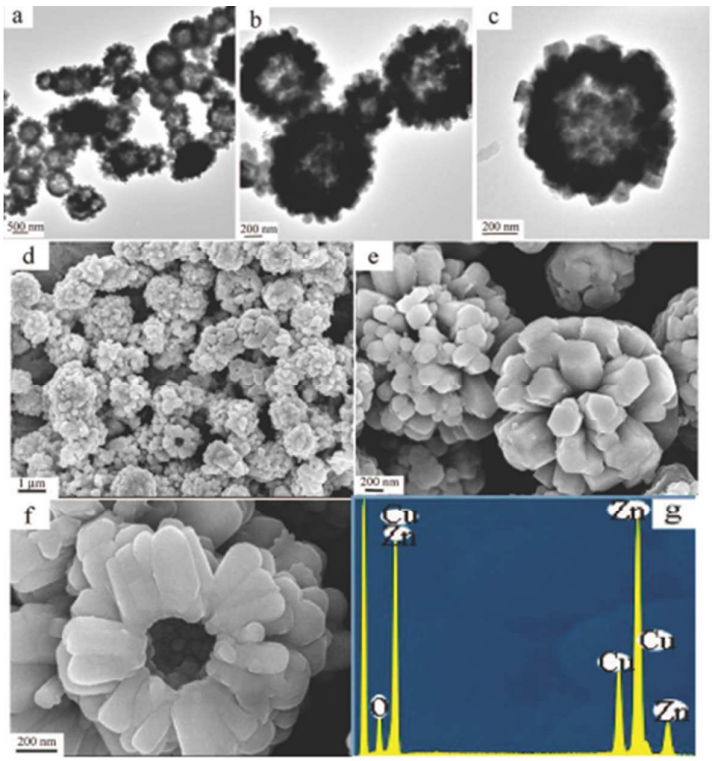

Fig. 21 Morphology of the hollow spheres composed of ZnO nanorods. (a) TEM image of the samples. (b, c) Typical magnified TEM images of hollow spheres. (d, e) SEM image of the samples. (f) Typical magnified SEM image of a hollow sphere. (g) The EDS spectrum of hollow spheres. Reproduce with permission.[218] Copyright 2008, American Chemical Society.

4.2 1–Dimension (1D) nanostructures of ZnO

In 2001, Kong *et al.*[219] and Yang *et al.*[220] synthesized single–crystalline ZnO nanowires using high–temperature VLS growth methods, respectively. In the process, ZnO nanowires have been prepared by the formation of Zn vapor at a high temperature. The growth process of the ZnO nanowires involved two stages: the nucleation of eutectic alloy droplets and the growth of nanowires through supersaturated liquid droplets. Wang *et al.*[221] reported an effective process to fabricate large–area and patterned ZnO nanorods (Fig. 22).[221] They combined the self–assembly–based mask technique with the surface epitaxial process to synthesize hexagonal arrays of ZnO nanorods. In the beginning of the experiment, submicron spheres and gold particles were deposited onto substrate successively to form gold catalyst array with hexagonal pattern. The catalyst could guide the VLS growth of ZnO on the substrate.

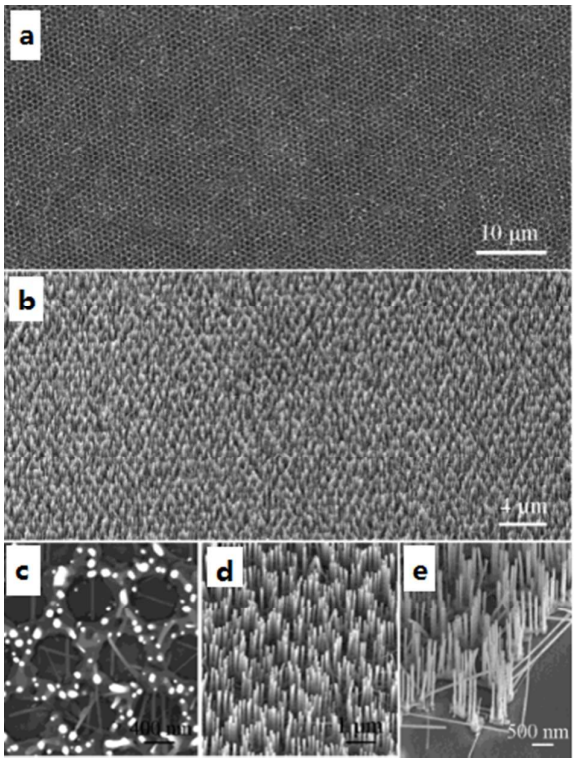

Fig. 22 (a) Low magnification top−view SEM image of aligned ZnO nanorods grown onto a honeycomb catalyst pattern (b) Side view of the aligned ZnO nanorods (c, d) Top and a 30° view of aligned ZnO nanorods. (e) Aligned ZnO nanorods at the edge of the growth pattern. Reproduce with permission.[221] Copyright 2004, American Chemical Society.

From what have been discussed above, it can be concluded that 1D ZnO nanostructures have been successfully fabricated via VLS process. Furthermore, in VLS process, Au, Sn, Co and NiO are always introduced into the preparation process of 1D ZnO nanostructures as catalysts, which initiates and guides the growth of 1D nanostructures. Subsequently, the techniques based on CVD without catalysis were achieved, which involved low−temperature CVD, MOCVD, MOVPE and template−assisted growth.

In general, the CVD processes were always carried out at rather high temperature so as to form Zn vapor, which increased the cost of equipment and complexity of operation. In 2002, Wu *et al.*[222,223] presented low−temperature CVD technology to synthesized high−quality and well−oriented ZnO nanorods on different substrates. In addition, they achieved diameter−controlled growth of the nanorods. In the process of preparation, zinc acetylacetonate hydrate was used to be zinc source and the

temperature was controlled to be at 130–140°C

Since the pioneering work of the discovery of carbon nanotubes by Iijima, numerous works have contributed to the synthesis and characterization of the nanotubular structures. In 2003, Yu et al reported on the fabrication of ZnO nanotubes via vapor phase growth. ZnO and Zn powders were well mixed in a quartz boat, which was placed in an alumina tube. The synthesis of ZnO nanotubes began with the thermal evaporation of the ZnO–Zn powder mixture under a wet oxidation condition. The ZnO nanotubes obtained had hollow core, and possessed 8–20 nm in thickness of crystalline wall.

In addition to nanowires, nanorods and nanotubes of ZnO, a variety of ZnO nanostructures consisted of ZnO nanobelts have been fabricated under controlled conditions based on CVD methods.

Wang *et al.*[224] achieved ZnO ultralong nanobelts by simply evaporating the commercial ZnO powders at high temperatures with no catalyst. In the experiments, thermal evaporation of ZnO powders was carried out at 1400°C for 2 hours, the products formed on the surface of the alumina substrate exhibited white woollike. SEM and TEM observations indicated that the products involved abundant nanobelts with uniform width in the range of 50 to 300 nm, and the typical width–to–thickness ratio of the nanobelt was in the range of 5 to 10. HRTEM and electron diffraction show that these nanobelts were formed through two growth directions. The one, growing along [0001], was free from dislocations; while the one along $[01\bar{1}0]$ possessed a single stacking fault (Fig. 23).[224]

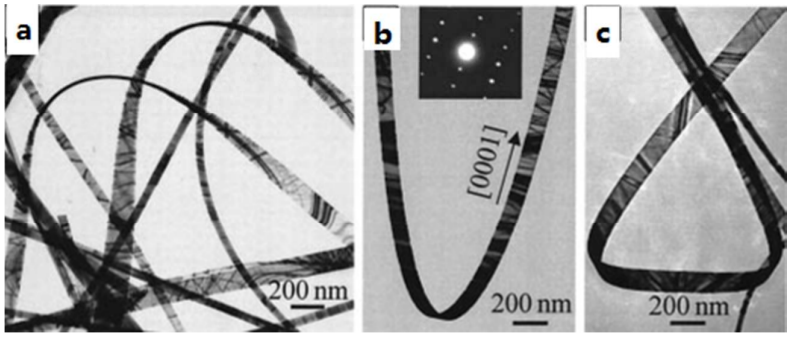

Fig. 23 TEM and HRTEM images of ZnO nanobelts. Reproduce with permission.[224] Copyright 2001, AAAS.

Structurally, the crystal structure of ZnO can be described as a mass of planes consisting of tetrahedrally coordinated Zn^{2+} and O^{2-} ions, stacking along the c axis alternatingly. The as–produced oppositely charged polar surfaces involve negatively

charged O^{2-} $(000\bar{1})$ and positively charged Zn^{2+} (0001) polar surfaces, which lead to the divergence of surface energy for polar surfaces. Compared with the polar surfaces, the commonly observed nonpolar planes of $(01\bar{1}0)$ and $(2\bar{1}\bar{1}0)$ have lower surface energy, which give rise to anisotropic growth of ZnO. So for 1D ZnO nanostructures, the most common morphologies are the nanostructures, which restraint large area (0001) polar surfaces to minimize the surface energy. In general, during the course of growth of ZnO nanobelts, the highest growth rate is along the c axis and the large facets are usually $\{01\bar{1}0\}$ and $\{2\bar{1}\bar{1}0\}$.

Wang *et al.*[225–228] synthesized the novel nanostructures based on ZnO nanobelts, which grow along the a–axis and whose surfaces are dominated by the polared ±(0001) facets, by a VS process. In the products, the positive and negative ionic charges on the polared ±(0001) surfaces would give rise to a spontaneous polarization across the nanobelts thickness. For the sake of minimizing the energy contributed by polar charges, surface area, and elastic deformation, nanohelixes (Fig. 24),[228] nanorings and nanospirals would be formed via a spontaneous self–coiling process of single–crystal nanobelts.

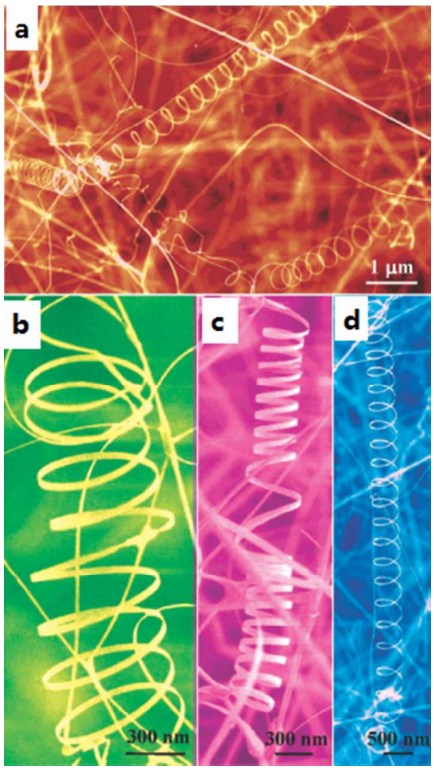

Fig. 24 SEM images of the as–synthesized ZnO nanobelts, showing helical nanostructure. Reproduce with permission.[228] Copyright 2003, American Chemical Society.

The VLS process has been widely applied to fabricate ZnO nanorods or nanowires. In this process, metal nanoparticles are used as catalysts to grow ZnO nanorods. However, a very high growth temperature was essential to form Zn vapor, which dissolved into metal droplets. Meanwhile, metal nanoparticles are easy to be incorporated into the final product. It is well known that even low impurities concentrations have an impact on physical properties of device based on ZnO. These are the drawbacks of VLS growth technique.

In 2002, Park *et al.*[229] introduced MOVPE, which required no metal catalysts, to grow ZnO nanorods. In the course of synthesis, diethylzinc and oxygen were used as the reactants, and argon was employed as carrier gas. The growth temperature was controlled in the range of 400–500°C. The ZnO nanorods grown on Al_2O_3 substrates showed length distributions and uniform thickness, which benefited many device applications. The results demonstrated MOVPE to be the effective approach to fabricate ZnO nanorods at a low temperature without metal catalyst.

Subsequently, Liu *et al.*[230] grew vertically well–aligned ZnO nanorods on different substrates by plasma–enhanced chemical vapor deposition (PECVD) without any catalyst. The method was divided into two–step: nucleation and growth. In this process, diethylzinc and oxygen gas were employed as sources for zinc and oxygen, respectively. The ZnO nanorods obtained possessed highly uniform length and diameter. In addition, they proposed a possible growth mechanism for the growth of ZnO nanorods, which suggested that lattice matching, electric field enhancement and the amount of defects of nuclei might play an important role on the self–alignment of nanorods.

According to the CVD techniques mentioned in the literatures, although they have advantages of high–quality products and simplicity, the high–temperatures are also essential, which is economically prohibitive.

Subsequently, researchers introduced the MOCVD approach, which made use of organometallic zinc precursors, into the synthesis of 1D ZnO nanostructures to reduce the deposition temperature. But this approach remains constrained by the expensive substrates needed for oriented growth, and the size and cost of the equipment.

In consideration of the requirement for the applications in solar cells, sensors, and other promising areas, the fabrication of 1D ZnO nanostructures should be the low–temperature, large–scale, and versatile synthetic process. During the past years, solution–phase growth has attracted much interest due to their low growth

temperatures, low demand for equipment and well potential for yield. This synthesis technique is large−scale production on any substrates regardless crystalline or amorphous.

Vayssieres *et al.*[231,232] grew highly oriented ZnO microtubes and nanorods on solid supports by a hydrothermal process at low temperature(Fig. 25).[231] The results demonstrated the solution synthesis to be a potential process for 1D ZnO nanostructures. Zeng *et al.*[233] developed the hydrothermal synthesis to prepare monodispersed ZnO nanorods with high crystallinity in the diameter regime of 50 nm.

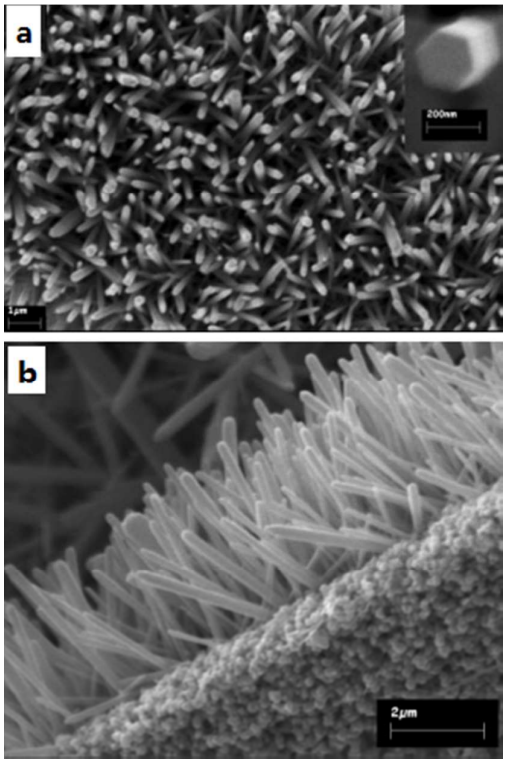

Fig. 25 FE−SEM images of ZnO arrays synthesized by hydrothermal process at low temperature. (a) on Si wafer (b) on ZnO thin film. Reproduce with permission.[231] Copyright 2003, Wiley−VCH.

In 2002, Liu *et al.*[234] prepared helical ZnO rods and columns by a two−step process: controlled nucleation and growth (Fig. 26).[234] The achievement presented a new approach to control orientations and shapes of nanostructure for practical applications. Soon afterwards, Yang *et al.*[235] presented a similar process to grow well−aligned ZnO nanowire arrays on arbitrary substrates by mild solution process. Before the hydrothermal growth of ZnO nanowires on substrate, homogeneous ZnO nanocrystals were dispersed onto the substrate to form a seed layer. Chang et al. made

use of the two–step process to grow well–aligned crystalline ZnO nanotubes on a variety of substrates.

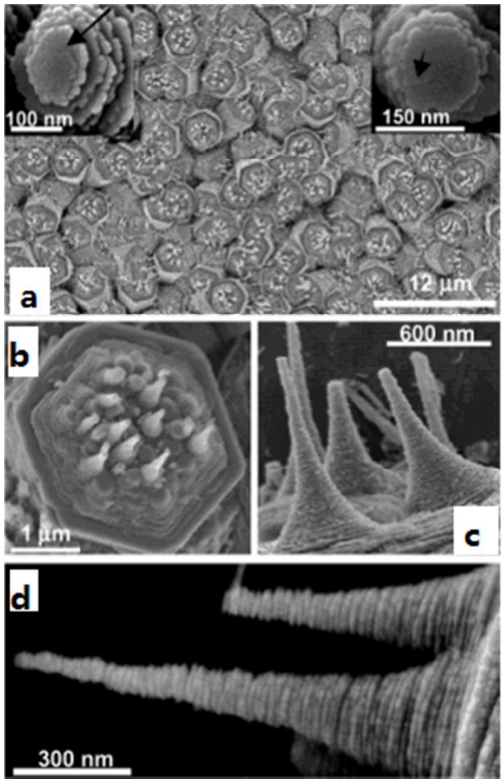

Fig. 26 SEM images of helical ZnO nanorods on oriented ZnO crystals. (a) Large arrays of well–aligned helical ZnO nanorods on top of base ZnO rods. (b) Precisely aligned ZnO nanorods on the (002) surface of one ZnO crystal. (c) Tilted high–magnification SEM image of arrays of helical nanorods on one (002) surface. (d) High–magnification SEM image of two long helical ZnO nanorods. Reproduce with permission.[234] Copyright 2002, American Chemical Society.

In order to improve the hydrothermal process, many efforts have been devoted to this field. Xu *et al.*[236] introduced microemulsions into the solution–phase growth of ZnO nanorods firstly, then employed dodecyl benzene sulfonic acid sodium salt as the modifying and protecting agent. In the course of reaction, $Zn(OH)_2$ precursors were formed after the in situ reduction of Zn salt, which originated from microemulsions. The ZnO nanorods obtained exhibited well–proportioned and perfect crystallized. The experiment presented a novel chemical route of solution–phase, which realized easily controlled and mild conditions. Oh *et al.*[237] introduced sonochemical route into the hydrothermal synthesis of ZnO nanorods arrays and to fabricate a resistive–type gas sensor. Vertically aligned ZnO nanorod arrays were successfully grown on alumina substrate under ultrasound–assisted conditions.

Anodic aluminum oxide (AAO) is the chemically and thermally stable template, which possess ordered porous structures and provide channels with nanoscale diameter for the growth of ZnO. It has been demonstrated that AAO template–assisted growth is an effective method to fabricate ordered nanowire arrays of ZnO.

In 2000, Li *et al.*[238] synthesized highly ordered ZnO nanowire arrays by a three–step process: electrochemical generation of an alumina template with nanochannels, which were highly ordered; electrodepositing metal Zn in the template; oxidizing the metal Zn to form nanowire arrays. The nanowires obtained with the diameters ranging from 15 to 90 nm were uniformly assembled into the ordered nanochannels of the template. In 2003, Lee *et al.*[239] reported the fabrication of ZnO nanowire arrays in AAO templates (Fig. 27)[239] by vapor deposition. The arrays obtained with narrow diameter distribution, high aspect ratio and high wire density, exhibited ordered and homogeneous.

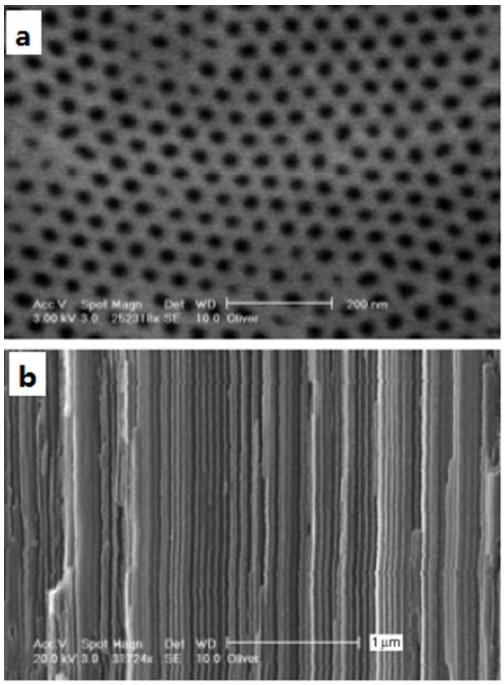

Fig. 27 SEM images of AAO template (a) plan–view (b) side–view. Reproduce with permission.[239] Copyright 2003, Wiley–VCH.

5. TiO_2

Over the past 10 years, more than forty thousand papers concerning TiO_2 have been published, which make it to be one of the most investigated semiconductor materials in materials science. TiO_2 was applied for many devices which exploit solar energy due to the strong oxidizing power of photogenerated holes, low cost, and well

stability. The dye–sensitized solar cells based on TiO_2 can convert sunlight into electricity more efficiently. Hydrogen, which may be the fuel of the future, can be produced by splitting water under the help of photogenerated electron–hole pairs of TiO_2. In addition, TiO_2, as photocatalyst, can degrade organic pollutants into environmentally friendly species, such as carbon dioxide and water.

For these applications, the specific surface area of the material have much influence on the overall efficiency, which lead to the widespread use of nanoparticulated forms of TiO_2. However, due to the existence of defects, grain boundaries and surface states, the electron diffusion coefficients of TiO_2 nanoparticles are comparably slow.[240,241]

In order to considerably overcome the bottleneck, one–dimensional nanostructures of TiO_2, such as nanotubes,[242,243] nanorods[244,245] and nanowires,[246] are developed to substitute nanoparticles for the application. It is well known that the specific surface area and electronic behaviors can be effectively improved by reducing the dimension of the materials to the nanoscale, which making the system more excellent. These 1D nanostructures are able to significantly accelerate electron transport behavior, and also possess large specific surface area. Herein, we mainly focus on the approaches for the synthesis of TiO_2 nanotubes.

Up to now, many approaches have been applied to synthesize 1D TiO_2.[247–251] These approaches can be mainly classified to three groups, namely, template method, electrochemical synthesis and hydrothermal approaches.

5.1 Template method

During the last decade, the methods for synthesis of nanostructured materials using template have been rapidly developed.[252]

The method makes use of the material with desired morphology as a template to guide the formation of products, which as a result possess a similar morphology with the template. By means of this general approach, a large number of traditional or advanced materials with a variety of controlled shapes have been obtained through adjusting shape parameters of template.

It should be noticed that much efforts for the fabrication of TiO_2 nanotubes attempted to use porous alumina as a template.[253–255]

Back in 2001, Chu *et al.*[253] successfully introduced porous Al_2O_3 template into sol–gel technology to fabricate TiO_2 nanotubes arrays, which possess large surface areas and anatase structure with (101) preferential orientation, standing on glass

substrates (Fig. 28).[253] In the process of preparation, highly pure Al film was first deposited on a glass substrate followed anodized process in a phosphoric acid solution to obtain porous Al_2O_3 structures. The results of characterization showed that the TiO_2 nanotubules arrays obtained exhibited high transmittance and strong absorbance for visible and ultraviolet light, respectively.

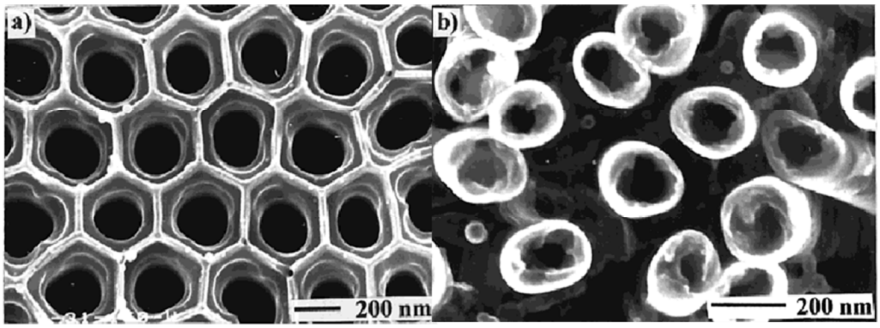

Fig. 28 FESEM images of (a) a bottom view of anodic alumina film after pore widening and before sol–gel coating (b) TiO_2 nanotubes arrays standing on a glass substrate after removal of anodic alumina. Reproduce with permission.[253] Copyright 2002, American Chemical Society.

According the molecules, the templates applied for the preparation of TiO_2 nanotubes can be divided into several groups. Among these groups, self–assembled organic surfactant templates have been widely used due to a large variety of organic molecules.[256–360]

In 2000, Hanabusa *et al.*[256] reported the preparation of TiO_2 nanotubes using an amphiphilic compound, trans–(1R,2R)–1,2–Cyclohexanedi (11–aminocarbonylundecylpyridinium) hexafluorophosphate, as a self–assembled template. The process contained the sol–gel polymerization of $Ti[OCH(CH_3)_2]_4$ and the self–assembly of the amphiphilic compound. Finally, TiO_2 nanotubes could be obtained by the electrostatic interaction between the TiO_2 species and the compound under basic conditions (Fig. 29).[256] Subsequently, in 2003, Peng *et al.*[257] obtained TiO_2 microtubes with high specific surface areas by means of surfactant–mediated template in a laurylamine hydrochloride / tetra–n–butyl–orthotitanatesystem. The microtubules obtained possessed well–developed cylindrical nanochannels and mesoporous walls, whose thickness were 0.2–2 μm. In the same year, Rao *et al.*[258] employed tripodal cholamide–based hydrogel as a template to synthesize TiO_2 nanotubes. The diameters of the nanotubes can be controlled through adopting the suitable hydrogelator or modifying the conditions of gelation.

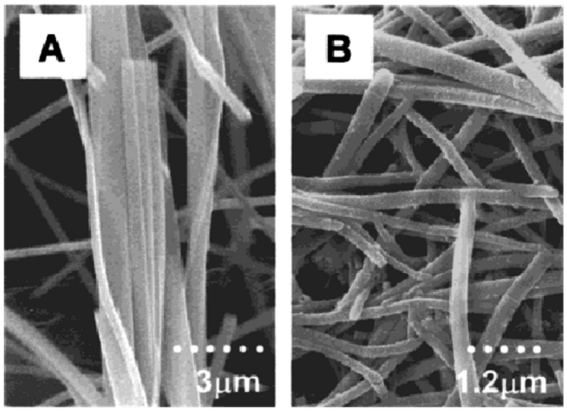

Fig. 29 SEM images of the TiO_2 nanotubes obtained under (a) acidic and (b) basic conditions. Reproduce with permission.[256] Copyright 2000, American Chemical Society.

From what have been discussed above, it can be concluded that the method for the synthesis of TiO_2 nanotubes using templates in general involves three steps as follows: the hydrolysis of titanium–containing compounds in the presence of templating agents, the polymerization of TiO_2 or deposition of TiO_2 onto the surface of the templates, and selective removal of the templates.

However, in most cases, the template method has an obvious disadvantage that the template using in process need to be removed in the end of synthesis, which increases the preparation cost and makes the process more complex.

5.2 The hydrothermal approach

In 1998, Kasuga et al.[261] attempted to fabricate nanotubes composed of TiO_2 with a large specific surface area by treating fine TiO_2–based powders in a NaOH aqueous solution with appropriate concentration at temperatures in the range 110–150°C. In this process, no sacrificial template was involved. The outer diameter and the length of TiO_2 nanotubes obtained in the work are about 8 nm and 100 nm, respectively. This opens up a new route to synthesize TiO_2 nanotubes using hydrothermal approaches.

Soon afterwards, much effort was devoted to transform a variety of TiO_2 polymorphs to the TiO_2 nanotubes under hydrothermal conditions. It has been demonstrated that all polymorphs of TiO_2 (anatase, rutile, brookite or amorphous) can be transformed to TiO_2 nanotubes under hydrothermal conditions.

In 1999, Kasuga et al.[262,263] succeed in transforming anatase–phase and rutile–phase TiO_2 to nanotubes. In the process, the raw materials were treated successively by NaOH aqueous solution, HCl aqueous solution and distilled water. Meanwhile, the formation mechanism of obtained TiO_2 nanotubes was also discussed.

Kasuga et al. considered that during the alkali treatment, an amorphous product would be formed, and after treatment with distilled water and HCl aqueous solution, TiO_2 nanotubes were obtained. In 2005, Gao et al.[264] reported the fabrication of TiO_2 nanotubes from rutile TiO_2 powder by means of simple hydrothermal reaction (Fig. 30).[264] In such process, the raw TiO_2 powder first reacted with NaOH solution to form layered sodium TiO_2 with hollow–tube morphology. Subsequently, the structure can be transformed to layered hydrogen TiO_2 retaining same morphology through treatment with dilute HCl. Meanwhile, the effect of experimental parameters (such as time, temperature) on TiO_2 obtained was explored and a possible mechanism for the reaction was also proposed.

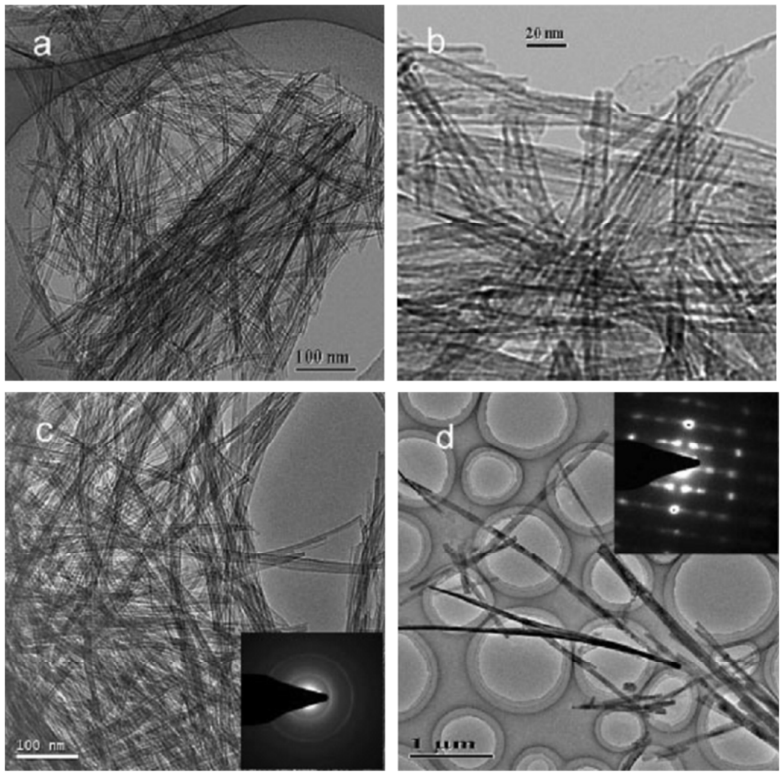

Fig. 30 TEM images of TiO_2 nanotubes and nanorods prepared by treating rutile with 10 M NaOH for 48 h at: a)100°C; b) 125°C; c) 150°C; d) 180°C. Reproduce with permission.[264] Copyright 2005, Elsevier.

5.3 Electrochemical synthesis

The products prepared by above methods often showed single tubes and loose agglomerates of tubes in the solution, which possess a wide distribution of tube lengths. For the application of electron devices, TiO_2 nanotubes in the form of layers are often attached to the electrode surface. However, the layers prepared by above methods often involve nanotubes with arbitrary orientation, which cannot make the

best of many advantages of 1D nanostructures. To overcome this problem, the electrochemical anodization approach is developed to fabricate the array of TiO_2 nanotubes with uniform orientation and perpendicular to the substrate. Through electrochemical anodization method, almost any shape of substrate can be coated with dense nanotubes, which is in favor of fine electrically connection and easy to handle

In 2001, Grimes and co–workers[265] fabricated well–aligned TiO_2 nanotubes arrays with a barrier layer at the bottom, the top of the nanotube was open while the bottom were closed, by anodizing pure Ti sheets in a H_2O–HF electrolyte under variable conditions. The diameters of the nanotubes range from 25 to 65 nm and increase with anodizing voltage, while the length of the nanotube was independent of anodization time. In contrast to the products achieved by other methods, the nanotubes obtained here were perpendicular to the surface of the electrode with the same orientation forming a continuous film (Fig. 31). [265] Finally, a possible growth mechanism was also proposed.

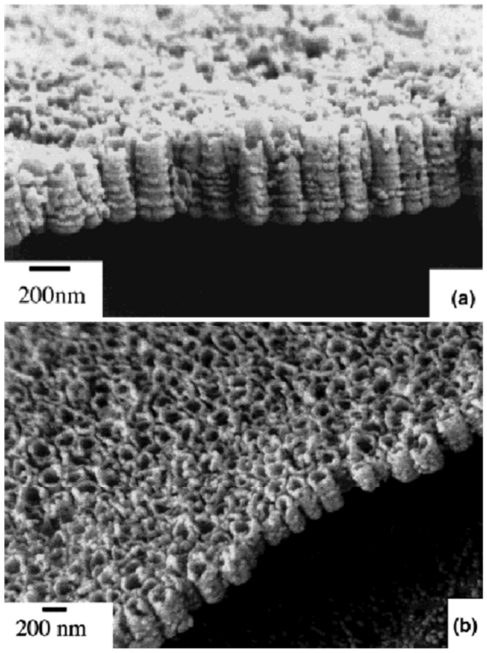

Fig. 31 FE–SEM cross–sectional images of TiO_2 nanotubes arrays. Reproduce with permission.[265] Copyright 2001, Materials Research Society.

A number of papers describing electrolytes for the preparation of TiO_2 nanotubes by anodization of titanium have been published.

In 2005, Schmuki et al.[266] obtained layers composed of TiO_2 nanotubes with high–aspect–ratio porous through anodic oxidation in $(NH_4)_2SO_4$ electrolytes containing NH_4F by potential sweeps. The nanotubes obtained possess diameter in the

range of 90–110 nm and porosity in the order of 37–42%. It was demonstrated that the sweep rate had an impact influence on the thickness and morphology of the structures. In addition, they proposed a possible mechanism for the growth of the structure. They believed that a thin layer composed of titanium oxide–hydroxide would appear in the initial periods of anodization, followed the formation of porous structure underneath the initial layer. Subsequently, the porous structure would grow randomly and self–organize.

In the same year, Schmuki et al.[267] yet prepared the self–organized TiO_2 nanotubes using phosphate electrolytes with small amounts of fluoride ions. The work explored the influence of the electrochemical conditions, such as applied potential, anodizing time, and sweep rate, on the pore diameter and length of TiO_2 nanotubes. The results showed that by tailoring the electrochemical parameters, the highly self–organized TiO_2 nanotubes with diameters in the range of 40 nm to 100 nm and length from 100 nm to 4 μm were obtained.

Subsequently, Schmuki *et al.*[268] reported the preparation of TiO_2 nanotube layers by means of electrochemical anodization of Ti in water–free electrolytes (CH_3COOH / NH_4F). The results of the work indicated that the morphology of TiO_2 nanotube layers obtained was strongly dependent on the applied potential. At low potentials, nanotubes as–synthesized possessed a diameter of 20 nm and a length of about 100 nm. In addition, bridging rings forming on the sidewall of the layers promoted the formation of connection between ordered TiO_2 nanotubes. Yet, at higher potentials, due to the appearance of local breakdown on the layers, some parts of them resembled coral reefs

6. VO_2

There is much interest in vanadium oxides owing to their broad range of applications in areas such as electrodes for lithium batteries,[269] catalysis,[270] electrochromic / –optical devices,[271] sensors.[272] Vanadium oxide compounds exhibit a rich phase diagram due to the multiple valence states. Vanadium pentoxide (V_2O_5) is the most stable member of these compounds since it possesses the maximal oxidation state. As a Li^+ intercalation host, V_2O_5 has further advantages due to its layered structure[1]. In addition, V_2O_5 (Eg = 2.8eV) is susceptible to photoactivation with wavelengths less than 443 nm and has been used as asemiconductor–type photocatalyst.[273]

Nanomaterials offer unusual mechanical, electrical, and optical properties and the overall behaviors of such materials exhibit combinations of bulk and surface

properties. For example, the nanostructure of vanadium oxide can considerably improve the capacities of molecules for sensing as well as for energy–storage devices in comparison to bulk.V_2O_5 nanorods with nanometer–sized diameters (*e.g.*, 70nm) deliver dramatically higher specific discharge capacities at low temperature than V_2O_5 nanorods with micrometer–sized diameters.[274] A variety of vanadium oxide nanostructures have been synthesized, such as nanoparticles,[275] nanoneedles, nanowires, nanorods,[333,276] nanorolls,[277] nanoribbons.[278,279] Many chemical and physical methods had been reported for the synthesis of nanostructured vanadium oxide. Those methods are classified into two categories:[280] (1) dry processes including chemical vapor deposition (CVD),[281] flame spray pyrolysis,[275] pulsed laser deposition (PLD),[339] and thermal treatment.[282] (2) wet processes such as hydrothermal treatment,[283] sol–gel synthesis,[284,285] self–assembly,[286] and templating methods.[286–288] The wet process, that is solution–based method or liquid phase method, is well–known for their advantages in tailoring the size and morphology of the nanostructures.In addition, they can combine with each other to produces the most desirable nanostructures with remarkable, selectivity, and variety.

Petr Nova´k *et al.*[275] had successfully synthesized crystalline, spherical–like V_2O_5 nanoparticles (30–60 nm) by a one–step and scalable flame spray pyrolysis (FSP) and optimized the process conditions to obtain nanoparticles with improved electrochemical performance. Aldo *et al.*[282] had easily prepared highly stable and crystalline V_2O_5 nanoparticles with an average diameter of 15 nm by thermal treatment of a bariandite–like vanadium oxide, $V_{10}O_{24}•9H_2O$. Reshef[280] and his team dedicated to the synthesis of hollow and closed V_2O_5 nanoparticles (NIF–V_2O_5) with a structure analogous to that of fullerene–like (IF) by PLA.

The tubular form of V_2O_5 is especially attractive because it possesses three different contact regions: inner and outer surface as well as the tube ends. Spahr *et al.*[277] reported the synthesis and electrochemical properties of vanadium oxide nanorolls. In their reaction procedure, the sol–gel reaction contacting with hydrothermal treatment of vanadium oxide precursor was conducted in the presence of hexadecylamine that acted as structure–directing template. TEM images of the resultant nanorolls indicated the multishell structure of the tube walls with an average layer thickness was about 3 nm. The free inner diameter of the tubes range between 25 and 35 nm and the total tube diameters are between 50 and 70 nm (Fig. 32).[277]

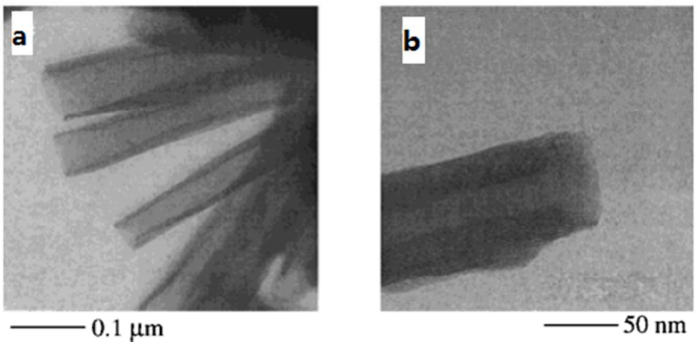

Fig. 32 High–resolution TEM images of the vanadium oxide nanotubes, indicating the multishell structure of the tube walls with an average layer thickness of about 3 nm. The free inner diameter of the tubes range between 25 and 35 nm and the total tube diameters are between 50 and 70 nm.Reproduce with permission.[277] Copyright 1998, Wiley–VCH.

Martin[289] and co–workers used a sol–gel–based template method to synthesize V_2O_5 nanorod arrays by depositing vanadium oxide (TIVO) into the pores of polycarbonate filtration membranes followed by removal of membranes at high temperature. In the latest work, they prepared V_2O_5 nanorods with different diameters and compared their electrochemical properties.[274] Single–crystal vanadium pentoxide (V_2O_5) nanorod arrays were first reported by Cao's group.[276] They utilized a template–based electrodeposition method by depositing V_2O_5 into pores of polycarbonate templates with the assistance of electric field from different solutions or sol. Uniformly sized vanadium oxide nanorods with a length of about 10 um with diameters ranging from 100 to 200 nm were grown over a large area with near unidirectional alignment. In the case of nanorods made from the V_2O_5 sol by electrophoretic deposition, the formation of single–crystal nanorods is explained by homoepitaxial aggregation of crystalline nanoparticles.[290]

Nanoribbons, with a rectangular cross section, have been synthesized, and their morphology is distinctly different from that of nanowires and nanotubes. Such nanostructure was mostly synthesized by hydrothermal treatment with different vanadium precursors. Li *et al.*[337] obtained the nanoribbons by a simple hydrothermal method with the assistance of organic surfactant. The ribbons are tens of micrometers, typically 60–100nm wide and 10–20nm thick. Xie *et al.*[291] successfully synthesized uniform V_2O_5•$0.9H_2O$ nanobelts with high aspect ratios on a large scale by a simple hydrothermal growth method using NH_4VO_3 as the raw material in the presence of sulfuric acid. The possible mechanism for the formation of the nanobelts was

presented. Based on the layered structure of vanadium pentoxide and the experimental results of the hydrolysis and condensation of NH_4VO_3, the H_3O^+ intercalating and splitting process was proposed to elucidate the formation of the nanostructure. $[VO(OH)_3]$ units which were formed at the initial stage, each coordinated with two water molecules, were condensed and polymerized to form the layered framework of $V_2O_5 \cdot xH_2O$.Then,the interlayer spaces in the layered structure of $V_2O_5 \cdot xH_2O$ were occupied by H_3O^+ions, and thus the interactions between the layers were weakened and the layered $V_2O_5 \cdot xH_2O$ gradually split to form nanobelts.

7. NiO

NiO have received a great deal of attention in industry and academia since its potential applications in fuel cell electrodes, thermistors, high–power ultra–capacitors and optical switching devices. NiO is considered a proto–typical p–type, wide band gap (3.6–4.0 eV) semiconductor.[292–294] Nanostructure NiO may results in various interesting properties compared to their bulk properties which may bring breakthrough in its traditional applications. Many ways are developed to get the dimension NiO material. This part reviews several current studies that center on produce low dimension NiO material. Various methods have been used and developed for synthesizing NiO powders in nanoscale dimensions.

7.1 0D nanostructures of NiO

0D nanostructures of NiO have attracted more and more attention due to their great potential applications in areas such as catalysis, chemical and biological sensors, and electrodes. Therefore, many efforts have been devoted to fabricate NiO nanoparticle in recent years. The researches mainly focused on microwave–hydrothermal process, which is an easy route of obtaining various morphologies of NiO nanoparticle.

Vijayakumar *et al.*[295] reported they synthesized the nano flakes nickel oxide successfully using microwave heating method. In their work, nickel nitrate hexahydrate cetyltrimethyl was added to the ammonium bromide. Then, the pH of the solution was increased to 10 by drop of ammonia. After the microwave radiation, they collected the precipitate. Finally the as prepared nanoparticles are converted into NiO nanopowder by calcination. In the process the formation mechanism of the NiO nano flakes includes the followi ng: nucleation, growth, and oriented attachment. Microwave accelerates the nucleation rate and also enhances the growth process.

Zhu *et al.*[296] reported they synthesized the flower–like NiO. They also use the nickel nitrate hexahydrate cetyltrimethyl, the ammonium bromide, and ammonia but

with different ratio. Through the hydro–thermal system they got the flower–like $Ni(OH)_2$. To obtain the NiO architectures, the as–prepared $Ni(OH)_2$ was calcined in air for 4 h.

Ren *et.al.*[297] got the similar nanostructure of NiO, but his way was much simple. In the experiment nickel nitrate hexahydrate cetyltrimethyl dissolved in the anhydrous ethanol, then the precursor solution was subjected to microwave heating maintained at 150^{o}C. After calcine, they also got the flower–like NiO.

Chemical deposition is also an efficient way to produce the NiO particle with different nanostructure. To obtain the uniform nanostructure by chemical deposition, a suitable temperature is needed to control the reaction speed. Zhang *et al.*[298] got the three–dimensional mesoporous NiO nanostructures by a simple ethylene glycol (EG)–mediated self–assembly route and subsequent calcination process. They point out that role of acetate was found to be very critical in this synthesis method. The acetate will precipitate to become the nuclei with EG. Xia *et al.*[299] reported hierarchically structured NiO nanoflowers were facile synthesized by incorporating a convenient solution process with a subsequent thermal treating process.

7.2 1D nanostructures of NiO

1D nanofibers have gained intensive attention due to their excellent magnetic, optical, electric, and chemical properties.[300] Compared with general ferromagnetic materials, one–dimensional nanostructured magnetic materials have greater value of spontaneous magnetization and coercivity due to their low–symmetry structure.[301]Among various methods of making one–dimensional nanostructure magnetic materials, electrospinning is a simple, versatile and convenient approach with the characteristic of easy control and low cost. A high voltage applied between the needle and the acceptor. Under the power of static field, the sol–gel will ejected from the needle tubing forming the nanowire. The voltages, viscosity of the sol–gel, speed of syringe pump, the humidity are the key factor which will affect the nanostructure of the nanowire. Luo *et al.*[302] reported they have fabricated the NiO nanowire by electrospinning. First $Ni(AC)_2{\cdot}4H_2O$ and the appropriate amount of $Fe(NO_3)_3{\cdot}9H_2O$ with different atomicratios weremade. Then they added the PVP powder slowly into the solution.The precursor sol solution was loaded into a plastic syringe. A high voltage was applied between the cooper plate collector and the syringe needle. Then the PVP / $Ni(CH_3COO)_2$ composite nanofibers were collected on thecooper during electrospining processes. NiO nanofibers were finally obtained by

calcination at 650°C.

The precursor is a key factor in electrospinning process. The volatility and the content of the precursor will affect the feature of the nanowire during the electrospinning process. According to the work of Wang *et al.*[303], they reported that N,N−dimethylformamide solution containing 10 wt.% polyacryloni−trile (PAN) was prepared, and then nickel nitrate hexahydrate was added into this solution. Applied with 10kv voltage and the 600°C calcination they got the porous NiO fiber.

Electrospinning is an efficient way to produce the 1D NiO nanowire. However, it cannot provide large amount of NiO nanofibers, which means to obtain enough NiO nanofibers, large energy may be wasted. Compared with the electrospinning methods, microwave heating has unique effects and significant merits such as rapid vol−umetric heating, high reaction rate, short reaction time, and energy saving. Song *et al.*[04] got polycrystalline NiO nanorods using microwave−assisted method. First, the microwave−assisted method has been successfully used for fast synthesis of rod−shaped $CH_3COO–Ni–OC_2H_4OH$. Then they got the pure polycrystalline NiO rod after calcination.

7.3 1−1 Dimension nanostructures of NiO

Electrospinning and hydrothermal are two simple but efficient way to produce nanostructure material. Combine this two method together may provide an efficient way to design the complex nanostructure of the material with large surface area and unique performance. Lin *et al.*[305] controlled the growth of ZnO nanorod arrays on NiO nanowires (NWs) to construct nanocomposites by electrospining and hydrothermal methods (Fig. 33)[305]. The results indicated that the UV photosensors based on the nanocomposites exhibited excellent performance.

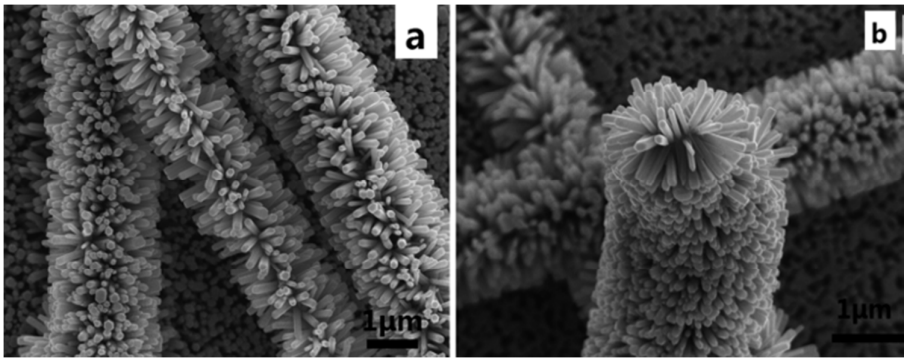

Fig. 33 SEM images of nanocomposites composed of ZnO nanorods and NiO nanowires. Reproduce with permission.[305] Copyright 2014, American Chemical

Society.

8. The Application of transition–Metal Oxide Nanostructures

Over the past decade, metal–oxide materials have been studied extensively as an important class of materials with useful functionalities and unique properties for optical, electronic, and magnetic applications. In this section, these applications will be discussed briefly.

8.1 Photovoltaic application

Metal oxide semiconductors, which are stable and environment friendly materials, are used in photovoltaics either as photoelectrode in dye–sensitized solar cells (DSSCs) or to build metal oxide p–n junctions. Binary metal oxides such as TiO_2,[306–308] ZnO,[309–314] Fe_2O_3,[315,316] ZrO_2,[317] Nb_2O_5,[318,319] Al_2O_3,[320] and ternary compounds such as $SrTiO_3$[321–325] and Zn_2SnO_4[326–329]have been tested for their use as photoelectrodes in DSSCs (Fig. 34). TiO_2, ZnO, and Nb_2O_5 are the best candidates as photoelectrode due to high chemical and thermal stability, hole blocking property, and suitable electron selectivity.

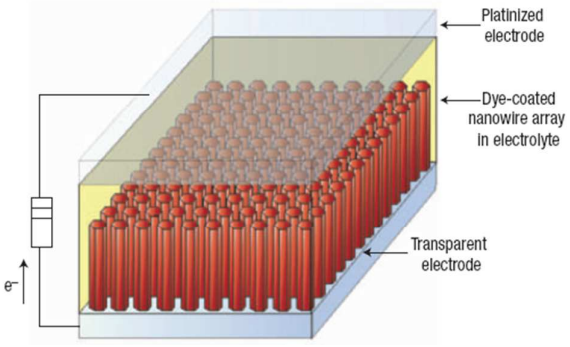

Fig. 34 Schematic diagram of the nanowire dye–sensitized solar cell based on a ZnO wire array. Reproduce with permission.[312] Copyright 2014, American Chemical Society.

8.2 Lithium ion batteries

Lithium–ion batteries are emerging as the technology of choice for portable electronics, electrodes for Lithium–ion batteries made of metal oxide nanoparticles (such as SnO_2, TiO_2, Fe_2O_3, Co_3O_4 and complex metal oxides) provide high specific capacity, superior rate capability, and improved cycling performance (Fig. 35).[330–335] Lithium–ion batteries are commonly used for electronics, electric vehicles, and other applications. Transition metal oxides, which possess significantly higher capacities than that of the current commercial anode material (graphite), hold great promise

toward a high–energy density anode.

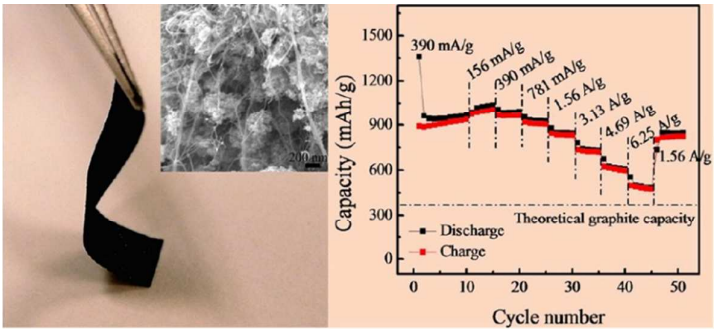

Fig. 35 Photograph of a flexible Fe_3O_4–carbon composite electrode and the correspondingareal–normalized capacity of the composite electrode at different current densities calculated based onelectrode area and mass loading (inset is the SEM image of a fractured electrode showing an intimateentanglement between the composite particles and the CNT networks). Reproduce with permission.[333] Copyright 2012, American Chemical Society.

8.3 Photocatalysis

In the main classic photocatalytic areas (pollution degradation, water splitting and organic synthesis), TiO_2 has been the most investigated photocatalytic material, photocatalytic reactions on TiO_2 have over the last 30 years attracted tremendous scientific and technological interest (Fig. 36).[338,339] In addition to the TiO_2 photocatalyst, other metal oxides, such as SnO_2, ZnO, WO_3, Fe_2O_3, Cu_2O and $SrTiO_3$ have been studied to determine their photocatalytic oxidation properties.[336–347] It is widely recognized that a photocatalyst with high photocatalytic activity requires both high crystallinity and large surface area to reduce recombination of the photo–generated electron–holes and to increase the density of active surface sites, as well as to enhance the light harvesting. The high–ordered mesoporous tungsten oxide (m–WO_3) hybridized with reduced graphene oxide has been successfully fabricated for the photocatalytic O_2 evolution from water under visible light irradiation.[342] It was found that CdS nanorods / reduced graphene oxide composites possessed excellent photocatalytic properties under visible light for the degradation of MO with a rate constant was about three times higher than that of blank CdS nanorods.[344]

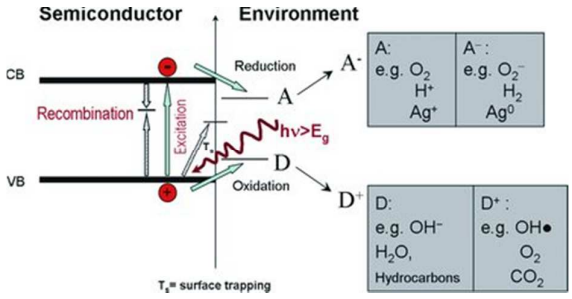

Fig. 36 Scheme of photo–induced processes at a TiO_2 semiconductor / electrolyte interface. Reproduce with permission.[338] Copyright 2012, Wiley–VCH.

8.4 Gas–sensing

Semiconducting metal oxides such as WO_3 (Fig. 37a), SnO_2 (Fig. 37b), TiO_2, and ZnO are used for gas sensing applications due to the sensitivity of their electrical conductivity to the ambient gas composition, which arises from charge transfer interactions with reactive gases such as O_2, NOx, CO, hydrocarbons and volatile organic compounds (Fig. 37c and d).[348–350] For gas sensing materials, considerable effort has been made to achieve better sensitivity and higher selectivity towards low concentrations of pollutant gases under low operating temperatures. SnO_2 nanostructures have attracted most attention for the detection of a range of harmful gases due to their good chemical and long term thermal stability under the operating conditions of sensors.[351–355]

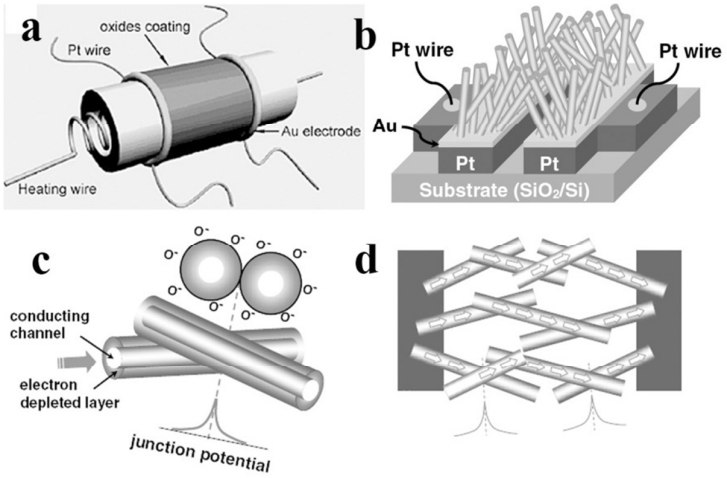

Fig. 37 (a) The schematic illustration for tube–based gas sensors. Reproduce with permission.[349] Copyright 2011, Elsevier. The schematic illustration for (b) plate–based gas sensors, and (c and d) the gas sensing mechanism of the network–structured gas sensor. Reproduce with permission.[350] Copyright 2008, IOP

Publishing Ltd.

8.5 Biomedical application

Magnetic metal–oxide materials which have been functionalized with biological agents have many potential and exciting applications in the biomedical field. For example, the superparamagnetic Fe_3O_4[356–363] are chemically and magnetically stable and biocompatible, and they can serve as potent nanoprobes for magnetic fluid hyperthermia (MFH), magnetic resonance imaging (MRI, Fig. 9b), and biosensors. Ferrite MFe_2O_4 (M = Mn, Co, Ni, Zn, *etc.*) have also been studied as carriers for targeted drug delivery and therapy.[364–366]

9. Summary and Outlook

This article provides a relatively comprehensive review of achievements on the growth control of metal oxide nanostructures with various morphologies synthesized by different approaches. However it cannot be the full coverage of all the achievements reported due to a large number of research works. The research for fabrication of metal oxide nanostructures has been well–developed, meanwhile the morphologies of the nanostructures have been well–controlled through various methods. The fundamental effort have made tremendous achievements and pave the way for the future applications in devices based on metal oxide nanostructures, such as nano laser, field–effect transistor, solar cell, sensors and so on. The achievements inspire more enthusiasm of researchers to overcome the challenges that remains.

Acknowledgements

This work was supported by the NSF of China (51272121, 51221291, 51328203 and 51025205).

References

1 T. Kida, T. Doi and K. Shimanoe, *Chem. Mater.*, 2010, **22**, 2662.

2 T. R. Gordon, M. Cargnello, T. Paik, F. Mangolini, R. T. Weber, P. Fornasiero and C. B. Murray, *J. Am. Chem. Soc.*, 2012, **134**, 6751.

3 K. Chen, A. T. Bell and E. Iglesia, *J. Catal.*, 2002, **209**, 35.

4 V. V. Sysoev, B. K. Button, K. Wepsiec, S. Dmitriev and A. Kolmakov, *Nano Lett.*, 2006, **6**, 1584.

5 M. Gutowski, J. E. Jaffe, C. L. Liu, M. Stoker, R. I. Hegde, R. S. Rai and P. J. Tobin, *Appl. Phys. Lett.*, 2002, **80**, 1897.

6 J. Robertson, *Rep. Prog. Phys.*, 2006, **69**, 327.

7 A. V. Emeline, G. V. Kataeva, A. V. Panasuk, V. K. Ryabchuk, N. V. Sheremetyeva and N. Serpone, *J. Phys. Chem. B*, 2005, **109**, 5175.

8 M. Kröger, S. Hamwi, J. Meyer, T. Riedl, W. Kowalsky and A. Kahn, *Org. Electron.*, 2009, **10**, 932.

9 G. Mavrou, S. Galata, P. Tsipas, A. Sotiropoulos, Y. Panayiotatos, A. Dimoulas, E. K. Evangelou, J. W. Seo and C. Dieker, *J. Appl. Phys.*, 2008, **103**, 014506.

10 M. J. Lee, S. Han, S. H. Jeon, B. H. Park, B. S. Kang, S. E. Ahn, K. H. Kim, C. B. Lee, C. J. Kim, I. K. Yoo, D. H. Seo, X. S. Li, J. B. Park, J. H. Lee and Y. Park, *Nano Lett.*, 2009, **9**, 1476.

11 E. Redel, S. Petrov, D. Omer, J. Moir, C. Huai, P. Mirtchev and G. A. Ozin, *Small*, 2012, **8,** 68.

12 E. Redel, C. Huai, S. Petrov, D. Omer, P. O'Brien, M. G. Helander, J. Mlynarski and G. A. Ozin, *Small*, 2012, **8,** 3806.

13 M. Pan, W.E. Fenwick, M. Strassburg, N. Li, H. Kang, M.H. Kane, A. Asghar, S. Gupta, R. Varatharajan, J. Nause, N. El–Zein, P. Fabiano, T. Steiner and I. Ferguson, *J. Cryst. Growth*, 2006, **287**, 688.

14 G. Malandrino, S. T. Finocchiaro, R. L. Nigro, C. Bongiorno, C. Spinella and I. L. Fragala`, *Chem. Mater.* 2004, **16**, 5559.

15 R. S. Wagner and W. C. Ellis, *Appl. Phys. Lett.*, 1964, **4**, 89.

16 R. S. Wagner, W. C. Ellis, K. A. Jackson and S. M. Arnold, *J. Appl. Phys.*, 1964, **35**, 2993.

17 S. Y. Bae, H. W. Seo and J. Park, *J. Phys. Chem. B*, 2004, **108**, 5206.

18 X. Liu, C. Li, S. Han, J. Han and C. Zhou, *Appl. Phys. Lett.*, 2003, **82**, 1950.

19 L. Dai, X. L. Chen, J. K. Jian, M. He, T. Zhou and B. Q. Hu, *Appl. Phys. A*, 2002,

75, 687.

20 Z. R. Dai, J. L. Gole, J. D. Stout and Z. L. Wang, *J. Phys. Chem. B*, 2002, **106**, 1274.

21 J. M. Wu, H. C. Shih, W. T. Wu, Y. K. Tseng and I. C. Chen, *J. Cryst. Growth*, 2005, **281**, 384.

22 A. Umar, S. H. Kim, Y. S. Lee, K. S. Nahm and Y. B. Hahn, *J. Cryst. Growth*, 2005, **282**, 131.

23 Q. Zhao, X. Xu, H. Zhang, J. Xu and D. Yu, *Appl. Phys. A*, 2004, **79**, 1721.

24 M. J. Zheng, L. D. Zhang, G. H. Li and W. Z. Shen, *Chem. Phys. Lett.*, 2002, **363**, 123.

25 Q. Kuang, X. Wang, Z. Jiang, Z. Xie and L. Zheng, *Acc. Chem. Res.*, 2014, **47**, 308.

26 R. S. Devan, R. A. Patil, J.–H. Lin and Y.–R. Ma, *Adv. Funct. Mater.*, 2012, **22,** 3326.

27 Y. Hou, F. Zuo, A. P. Dagg, J. Liu and P. Feng, *Adv. Mater.*, 2014, **26,** 5043.

28 M. Qamar, M. Gondal, K. Hayat, Z. Yamani and K. Al–Hooshani, *J. Hazard. Mater.*, 2009, **170,** 584.

29 B. M. Klepser and B. M. Bartlett, *J. Am. Chem. Soc.*, 2014,**136**,1694.

30 H. Zhang, M. Yao, L. Bai, W. Xiang, H. Jin, J. Li and F. Yuan, *CrystEngComm*, 2013, **15,** 1432.

31 M. Yao, Q. Li, G. Hou, C. Lu, B. Cheng, K. Wu, G. Xu, F. Yuan, F. Ding, Y. Chen, *ACS Appl. Mater. Interfaces*, 2015, *7*, 2856–2866..

32 S. Bai, K. Zhang, L. Wang, J. Sun, R. Luo, D. Li and A. Chen, *J. Mater. Chem. A*, 2014, **2,** 7927.

33 T. Stoycheva, F. E. Annanouch, I. Gràcia, E. Llobet, C. Blackman, X. Correig and S. Vallejos, *Sens. Actuators, B–*, 2014, **198,** 210.

34 T. Kida, A. Nishiyama, Z. Hua, K. Suematsu, M. Yuasa and K. Shimanoe, *Langmuir*, 2014, **30,** 2571.

35 K. Huang, Q. Pan, F. Yang, S. Ni, X. Wei and D. He, *J. Phys. D: Appl. Phys.*, 2008, **41**, 155417.

36 M. Shibuya and M. Miyauchi, *Chem. Phys. Lett.*, 2009, **473,** 126.

37 D. Wang, J. Li, X. A. Cao, G. S. Pang and S. H. Feng, *Chem. Commun.*, 2010, **46,** 7718.

38 F. Liu, L. Li, F. Mo, J. Chen, S. Deng and N. Xu, *Cryst. Growth Des.*, 2010, **10,**

5193.

39 J. Zhang, J.–P. Tu, X.–H. Xia, X.–L. Wang and C.–D. Gu, *J. Mater. Chem.*, 2011, **21,** 5492.

40 F. Zheng, H. Lu, M. Guo and M. Zhang, *CrystEngComm*, 2013, **15,** 5828.

41 C. Y. Ng, K. Abdul Razak and Z. Lockman, *J. Alloys Compd.*, 2014, **588,** 585.

42 S. R. Bathe and P. S. Patil, *Sol. Energy Mater. Sol. Cells*, 2007, **91,** 1097.

43 Y.–R. Ma, C.–M. Lin, C.–L. Yeh and R.–T. Huang, *J. Vac. Sci. Technol., B*, 2005, **23,** 2141.

44 F. Galléa, Z. Li and Z. Zhang, *Appl. Phys. Lett.*, 2006, **89,** 193111.

45 M. Remškar, J. Kovac, M. Viršek, M. Mrak, A. Jesih and A. Seabaugh, *Adv. Funct. Mater.*, 2007, **17,** 1974.

46 M. Zumer, V. Nemanicˇ, B. Zajec, M. Wang, J. Wang, Y. Liu and L.–M. Peng, *J. Phys. Chem. C*, 2008, **112,** 5250.

47 B. J.–W. Liu, J. Zheng, J.–L. Wang, J. Xu, H.–H. Li and S.–H. Yu, *Nano Lett.*, 2013,**13,**3589.

48 G. Gu, B. Zheng, W. Q. Han, S. Roth and J. Liu, *Nano Lett.*, 2002, **2,** 849.

49 C. Guo, S. Yin, M. Yan, M. Kobayashi, M. Kakihana and T. Sato, *Inorg. Chem.*, 2012, **51,** 4763.

50 W. Hu, Y. Zhu, W. Hsu, B. Chang, M. Terrones, N. Grobert, H. Terrones, J. Hare, H. Kroto and D. Walton, *Appl. Phys. A*, 2000, **70,** 231.

51 R. Hu, H. Wu and K. Hong, *J. Cryst. Growth*, 2007, **306,** 395.

52 H. Zheng, J. Z. Ou, M. S. Strano, R. B. Kaner, A. Mitchell and K. Kalantar-zadeh, *Adv. Funct. Mater.*, 2011, **21,** 2175.

53 P. Roussel, P. Labbe and D. Groult, *Acta Crystallogr. Sect. B: Struct. Sci.*, 2000, **56,** 377.

54 A. Phuruangrat, D. J. Ham, S. J. Hong, S. Thongtem and J. S. Lee, *J. Mater. Chem.*, 2010, **20,** 1683.

55 S. Rajagopal, D. Nataraj, D. Mangalaraj, Y. Djaoued, J. Robichaud and O. Y. Khyzhun, *Nanoscale Res. Lett.*, 2009, **4,** 1335.

56 Z. Gu, H. Li, T. Zhai, W. Yang, Y. Xia, Y. Ma and J. Yao, *J. Solid State Chem.*, 2007, **180,**98.

57 Z. J. Gu, Y. Ma, W. S. Yang, G. J. Zhang and J. N. Yao, *Chem. Commun.*, 2005, **28,** 3597.

58 J. Su, X. Feng, J. D. Sloppy, L. Guo and C. A. Grimes, *Nano Lett.*, 2011, **11,**203.

59 X. Han, X. Han, L. Li and C. Wang, *New J. Chem.*, 2012, **36,** 2205.

60 Z.–G. Zhao, Z.–F. Liu and M. Miyauchi, *Chem. Commun.*, 2010, **46,**3321.

61 Y. Guo, N. Murata, K. Ono and T. Okazaki, *J. Nanopart. Res.*, 2005, **7,** 101.

62 C. Klinke, J. B. Hannon, L. Gignac, K. Reuter and P. Avouris, *J. Phys. Chem. B*, 2005,**109,** 17787.

63 Y. Li, Y. Bando, D. Golberg and K. Kurashima, *Chem. Phys. Lett.*, 2003, **367,** 214.

64 A. J. Naik, M. E. Warwick, S. J. Moniz, C. S. Blackman, I. P. Parkin and R. Binions, *J. Mater. Chem. A*, 2013, **1,** 1827.

65 Z.–G. Zhao and M. Miyauchi, *Angew. Chem. Int. Ed.*, 2008, **47,** 7051.

66 D. Chen, L. Gao, A. Yasumori, K. Kuroda and Y. Sugahara, *Small*, 2008, **4,** 1813.

67 D. Chen, X. Hou, H. Wen, Y. Wang, H. Wang, X. Li, R. Zhang, H. Lu, H. Xu and S. Guan, *Nanotechnology*, 2010, **21,** 035501.

68 J. Ma, J. Zhang, S. Wang, T. Wang, J. Lian, X. Duan and W. Zheng, *J. Phys. Chem. C*, 2011,**115,** 18157.

69 H. Zhang, G. Duan, Y. Li, X. Xu, Z. Dai and W. Cai, *Cryst. Growth Des.*, 2012, **12,** 2646.

70 X.–L. Li, T.–J. Lou, X.–M. Sun and Y.–D. Li, *Inorg. Chem.*, 2004, **43,** 5442.

71 Z. Gu, T. Zhai, B. Gao, X. Sheng, Y. Wang, H. Fu, Y. Ma and J. Yao, *J. Phys. Chem. B*, 2006, **110,**23829.

72 X. Zhao, T. L. Y. Cheung, X. Zhang, D. H. L. Ng and J. Yu, *J. Am. Ceram. Soc.*, 2006, **89,** 2960.

73 D. Chen and J. H. Ye, *Adv. Funct. Mater.*, 2008, **18,** 1922.

74 L. Brus, *J. Phys. Chem.*, 1986, **90,** 2555.

75 S. Cong, Y. Tian, Q. Li, Z. Zhao and F. Geng, *Adv. Mater.*, 2014,**26**, 4260.

76 H. Watanabe, K. Fujikata, Y. Oaki and H. Imai, *Chem. Commun.*, 2013, **49,** 8477.

77 J. Polleux, A. Gurlo, N. Barsan, U. Weimar, M. Antonietti and M. Niederberger, *Angew. Chem. Int. Ed.*, 2006, **45,** 261.

78 J. Polleux, N. Pinna, M. Antonietti and M. Niederberger, *J. Am. Chem. Soc.*, 2005, **127,** 15595.

79 Z. Tang, N. A. Kotov and M. Giersig, *Science*, 2002, **297,** 237.

80 M. Daniel, B. Desbat, J. Lassegues, B. Gerand and M. Figlarz, *J. Solid State Chem.*, 1987, **67,** 235.

81 L. Wang, A. Teleki, S. Pratsinis and P. Gouma, *Chem. Mater.*, 2008, **20,**4794.

82 K. Kalantar–zadeh, A. Vijayaraghavan, M.–H. Ham, H. Zheng, M. Breedon and M.

S. Strano, *Chem. Mater.*, 2010, **22,** 5660.

83 E. K. Salje, S. Rehmann, F. Pobell, D. Morris, K. S. Knight, T. Herrmannsdörfer and M. T. Dove, *J. Phys.: Condens. Matter*, 1997,**9,** 6563.

84 T. Vogt, P. M. Woodward and B. A. Hunter, *J. Solid State Chem.*, 1999, **144,** 209.

85 J. Wang, E. Khoo, P. S. Lee and J. Ma, *J. Phys. Chem. C*, 2008, **112,** 14306.

86 B. C. Satishkumar, A. Govindaraj, M. Nath and C. N. R. Rao, *J. Mater. Chem.*, 2000, **10,**2115.

87 K. Zhu, H. He, S. Xie, X. Zhang, W. Zhou, S. Jin and B. Yue, *Chem. Phys. Lett.*, 2003, **377,**317.

88 J. Li, X. Liu, Q. Han, X. Yao and X. Wang, *J. Mater. Chem. A*, 2013, **1,**1246.

89 S.–J. Choi, I. Lee, B.–H. Jang, D.–Y. Youn, W.–H. Ryu, C. O. Park and I.–D. Kim, *Anal. Chem.*, 2012, **85,** 1792.

90 X. Y. Xue, B. He, S. Yuan, L. L. Xing, Z. H. Chen and C. H. Ma, 2011, Nanotechnology, 22, 395702.

91 J. Shi, G. Hu, Y. Sun, M. Geng, J. Wu, Y. Liu, M. Ge, J. Tao,M. Cao, N. Dai, *Sens. Actuators, B*, 2011, 156, 820.

92 L. Li, Y. Zhang, X. Fang, T. Zhai, M. Liao, X. Sun, Y. Koide, Y. Bando and D. Golberg, *J. Mater. Chem.*, 2011, **21,** 6525.

93 J. Chen, Y. Dai, J. Luo, Z. Li, S. Deng, J. She and N. Xu, *Appl. Phys. Lett.*, 2007, **90,** 253105.

94 S. Vallejos, P. Umek and C. Blackman, *J. Nanosci. Nanotechno.*, 2011, **11,** 8214.

95 X. Zhang, L. Gong, K. Liu, Y. Cao, X. Xiao, W. Sun, X. Hu, Y. Gao, J. Chen and J. Zhou, *Adv. Mater.*, 2010, **22,**5292.

96 Y. Zhang, Y. Chen, H. Liu, Y. Zhou, R. Li, M. Cai and X. Sun, *J. Phys. Chem. C*, 2009,**113,**1746.

97 J. Zhou, L. Gong, S. Z. Deng, J. Chen, J. C. She, N. S. Xu, R. Yang and Z. L. Wang, *Appl. Phys. Lett.*, 2005,**87,** 223108.

98 A. P. E. York, J. Sloan and M. L. H. Green, *Chem. Commun.*, 1999, **3,** 269.

99 X. W. Lou and H. C. Zeng, *Inorg. Chem.*, 2003,**42,**6169.

100G. Xi, S. Ouyang, P. Li, J. Ye, Q. Ma, N. Su, H. Bai and C. Wang, *Angew. Chem. Int. Ed.*, 2012, **51,** 2395.

101 Z. Xiao, L. Zhang, X. Tian and X. Fang, *Nanotechnology*, 2005, **16,** 2647.

102 G. Dawson, W. Zhou and R. Blackley, *PCCP*, 2011, **13,**20923.

103 X. Gao, X. Su, C. Yang, F. Xiao, J. Wang, X. Cao, S. Wang and L. Zhang, *Sens.*

Actuators, B, 2013, **181,**537.

104 Y. Oaki and H. Imai, *Adv. Mater.*, 2006, **18,**1807.

105 Y. Q. Zhu, W. Hu, W. K. Hsu, M. Terrones, N. Grobert, J. P. Hare, H. W. Kroto, D. R. M. Walton and H. Terrones, *Chem. Phys. Lett.*, 1999, **309,** 327.

106 Z. L. Li, F. Liu, N. S. Xu, J. Chen and S. Z. Deng, *J. Cryst. Growth*, 2010, **312,** 520.

107 Y. M. Zhao, Y. H. Li, I. Ahmad, D. G. McCartney, Y. Q. Zhu and W. B. Hu, *Appl. Phys. Lett.*, 2006, **89,** 133116.

108 J. Zhou, Y. Ding, S. Z. Deng, L. Gong, N. S. Xu and Z. L. Wang, *Adv. Mater.*, 2005, **17,** 2107.

109 R. H. Coridan, K. A. Arpin, B. S. Brunschwig, P. V. Braun and N. S. Lewis, *Nano Lett.*, 2014, **14,** 2310.

110 M. D'Arienzo, L. Armelao, C. M. Mari, S. Polizzi, R. Ruffo, R. Scotti and F. Morazzoni, *J. Am. Chem. Soc.*, 2011,**133,**5296.

111 J. Z. Ou, S. Balendhran, M. R. Field, D. G. McCulloch, A. S. Zoolfakar, R. A. Rani, S. Zhuiykov, A. P. O'Mullane and K. Kalantar–zadeh, *Nanoscale*, 2012, **4,** 5980.

112 C. Ng, C. Ye, Y. H. Ng and R. Amal, *Cryst. Growth Des.*, 2010,**10,** 3794.

113 A. Yella, U. K. Gautam, E. Mugnaioli, M. Panthofer, Y. Bando, D. Golberg, U. Kolb and W. Tremel, *CrystEngComm*, 2011, **13,** 4074.

114M. Shibuya and M. Miyauchi, *Adv. Mater.*, 2009, **21,**1373.

115 J. Yin, H. Cao, J. Zhang, M. Qu and Z. Zhou, *Cryst. Growth Des.*, 2012, **13,**759.

116 A. Z. Sadek, H. Zheng, M. Breedon, V. Bansal, S. K. Bhargava, K. Latham, J. Zhu, L. Yu, Z. Hu, P. G. Spizzirri, W. Wlodarski and K. Kalantar–zadeh, *Langmuir*, 2009,**25,** 9545.

117J. Zhang, X. L. Wang, X. H. Xia, C. D. Gu and J. P. Tu, *Sol. Energy Mater. Sol. Cells*, 2011, **95,**2107.

118 J. Tucek, R. Zboril, A. Namai and S. –I. Ohkoshi, *Chem. Mater.*, 2010, **22,** 6483.

119 R. Zboril, M. Mashlan and D. Petridis, *Chem. Mater.*, 2002,**14,** 969.

120 L. Machala, J. Tucek and R. Zboril, *Chem. Mater.*, 2011, **23,** 3255.

121 T. Ninjbadgar, S. Yamamoto and M. Takano, *Solid State Sci.*, 2005, **7,**33.

122 S. Sakurai, A. Namai, K. Hashimoto and S.–i. Ohkoshi, *J. Am. Chem. Soc.*, 2009, **131,** 18299.

123 B. H. Kim, N. Lee, H. Kim, K. An, Y. I. Park, Y. Choi, K. Shin, Y. Lee, S. G. Kwon and H. B. Na, *J. Am. Chem. Soc.*, 2011, **133,** 12624.

124 J. Ouyang, J. Pei, Q. Kuang, Z. Xie and L. Zheng, *ACS Appl. Mater. Interfaces*, 2014, **6,** 12505.

125 X. Wang, Z. Zhao, J. Qu, Z. Wang and J. Qiu, *Cryst. Growth Des.*, 2010, **10,** 2863.

126 P. Basnet, G. K. Larsen, R. P. Jadeja, Y.–C. Hung and Y. Zhao, *ACS Appl. Mater. Interfaces*, 2013,**5,**2085.

127 C.–J. Jia, L.–D. Sun, Z.–G. Yan, Y.–C. Pang, L.–P. You and C.–H. Yan, *J. Phys. Chem. C*, 2007, **111,** 13022.

128 X. Wen, S. Wang, Y. Ding, Z. L. Wang and S. Yang, *J. Phys. Chem. B*, 2004, **109,** 215.

129 A. Hu, X. Chen, Y. Tang, Q. Tang, L. Yang and S. Zhang, *Electrochem. Commun.*, 2013, **28,**139.

130 W. Cheng, J. He, T. Yao, Z. Sun, Y. Jiang, Q. Liu, S. Jiang, F. Hu, Z. Xie, B. He, W. Yan and S. Wei, *J. Am. Chem. Soc.*, 2014, **136,**10393.

131 L. Chen, X. Yang, J. Chen, J. Liu, H. Wu, H. Zhan, C. Liang and M. Wu, *Inorg. Chem.*, 2010, **49,** 8411.

132 X. Hu, J. C. Yu, J. Gong, Q. Li and G. Li, *Adv. Mater.*, 2007, **19,** 2324.

133 W.–D. Zhang, H.–M. Xiao, L.–P. Zhu and S.–Y. Fu, *J. Alloys Compd.*, 2009,**477,** 736.

134 H. Peng, B. Liuyang, Y. Lingjie, L. Jinlin, Y. Fangli and C. Yunfa, *Nanoscale Res. Lett.*, 2009, **4,** 1047.

135 M. Hu, A. A. Belik, M. Imura, K. Mibu, Y. Tsujimoto and Y. Yamauchi, *Chem. Mater.*, 2012,**24,** 2698.

136 Z. Wang, D. Luan, S. Madhavi, Y. Hu and X. W. D. Lou, *Energ. Environ. Sci.*, 2012, **5,** 5252.

137 L. Wang, T. Fei, Z. Lou and T. Zhang, *ACS Appl. Mater. Interfaces*, 2011, **3,** 4689.

138 C. Jia, Y. Cheng, F. Bao, D. Chen and Y. Wang, *J. Cryst. Growth*, 2006, **294,** 353.

139 X. Hu, J. C. Yu and J. Gong, *J. Phys. Chem. C*, 2007, **111,** 11180.

140 M. Marelli, A. Naldoni, A. Minguzzi, M. Allieta, T. Virgili, G. Scavia, S. Recchia, R. Psaro and V. Dal Santo, *ACS Appl. Mater. Interfaces*, 2014, **6**, 11997.

141 L. Li and N. Koshizaki, *J. Mater. Chem.*, 2010, **20,** 2972.

142 F. Lu, Q. Wu, X. Yang, L. Chen, J. Cai, C. Liang, M. Wu and P. Shen, *PCCP*, 2013,**15,**9768.

143 X. Wang, W. Tian, D. Liu, C. Zhi, Y. Bando and D. Golberg, *Nano Energy*, 2013, **2,**257.

144 Q. Q. Xiong, J. P. Tu, Y. Lu, J. Chen, Y. X. Yu, Y. Q. Qiao, X. L. Wang and C. D. Gu, *J. Phys. Chem. C*, 2012, **116,** 6495.

145 T. Zhu, J. S. Chen andX. W. Lou,*J. Phys. Chem. C*, 2011, 115, 9814.

146 M. V. Reddy, T. Yu, C. H. Sow, Z. X. Shen, C. T. Lim, G. V. Subba Rao and B. V. R. Chowdari, *Adv. Funct. Mater.*, 2007, **17,** 2792.

147 H. Liang, W. Chen, X. Jiang, X. Xu, B. Xu and Z. Wang, *J. Mater. Chem. A*, 2014, **2,** 4340.

148 J. Zhu, Z. Yin, D. Yang, T. Sun, H. Yu, H. E. Hoster, H. H. Hng, H. Zhang and Q. Yan, *Energ. Environ. Sci.*, 2013, **6,** 987.

149 C. Wu, P. Yin, X. Zhu, C. OuYang and Y. Xie, *J. Phys. Chem. B*, 2006, **110,** 17806.

150 X. Yang, X. Wang, X. Liu, Y. Zhang, W. Song, C. Shu, L. Jiang and C. Wang, *J. Mater. Chem. A*, 2013, **1,** 8332.

151 J. Kim, J. E. Lee, S. H. Lee, J. H. Yu, J. H. Lee, T. G. Park and T. Hyeon, *Adv. Mater.*, 2008, **20,** 478.

152 N. Lee and T. Hyeon, *Chem. Soc. Rev.*, 2012, **41,** 2575.

153 F. M. Kievit and M. Zhang, *Acc. Chem. Res.*, 2011, **44,** 853.

154 K. Cheng, S. Peng, C. Xu and S. Sun, *J. Am. Chem. Soc.*, 2009, **131,** 10637.

155 J. Park, K. An, Y. Hwang, J.–G. Park, H.–J. Noh, J.–Y. Kim, J.–H. Park, N.–M. Hwang and T. Hyeon, *Nat.Mater.*, 2004, **3,** 891.

156 Y. Tian, B. Yu, X. Li and K. Li, *J. Mater. Chem.*, 2011, **21,** 2476.

157 R. Buonsanti, V. Grillo, E. Carlino, C. Giannini, F. Gozzo, M. Garcia–Hernandez, M. A. Garcia, R. Cingolani and P. D. Cozzoli, *J. Am. Chem. Soc.*, 2010, **132,** 2437.

158 H. O. Pierson, *Handbook of chemical vapor deposition: principles, technology and applications*, William Andrew, 1999.

159 A. S. Teja and P.–Y. Koh, *Prog. Cryst. Growth Charact. Mater.*, 2009, **55,**22.

160 S. Vangelista, R. Mantovan, S. Cocco, A. Lamperti, O. Salicio and M. Fanciulli, *Thin Solid Films*, 2012,**520,**4617.

161 R. Mantovan, A. Lamperti, M. Georgieva, G. Tallarida and M. Fanciulli, *J. Phys. D: Appl. Phys.*, 2010, **43,**065002.

162 U. Cvelbar, Z. Chen, M. K. Sunkara and M. Mozetič, *Small*, 2008, **4,** 1610.

163 Y. M. Zhao, Y.–H. Li, R. Z. Ma, M. J. Roe, D. G. McCartney and Y. Q. Zhu,

Small, 2006,**2,** 422.

164 L. Zhao, H. Zhang, J. Tang, S. Song and F. Cao, *Mater. Lett.*, 2009, **63,** 307.

165 R. Zheng, H. Gu, B. Xu, K. K. Fung, X. Zhang and S. P. Ringer, *Adv. Mater.*, 2006,**18,** 2418.

166 D. Kim, N. Lee, M. Park, B. H. Kim, K. An and T. Hyeon, *J. Am. Chem. Soc.*, 2008,**131,**454.

167 X.–L. Cheng, J.–S. Jiang, D.–M. Jiang and Z.–J. Zhao, *J. Phys. Chem. C*, 2014, **118,** 12588.

168 Z. L. Wang, *Adv. Mater.*, 1998,**10,**13.

169 T.–K. Van, H. G. Cha, C. K. Nguyen, S.–W. Kim, M.–H. Jung and Y. S. Kang, *Cryst. Growth Des.*, 2012,**12,** 862.

170 J. Zhu, K. Y. S. Ng and D. Deng, *Cryst. Growth Des.*, 2014, **14,** 2811.

171 K. Tai, K. Sun, B. Huang and S. J. Dillon, *Nanotechnology*, 2014,**25,**145603.

172 J. R. Morber, Y. Ding, M. S. Haluska, Y. Li, J. P. Liu, Z. L. Wang and R. L. Snyder, *J. Phys. Chem. B*, 2006, **110,** 21672.

173 X. Wen, S. Wang, Y. Ding, Z. L. Wang and S. Yang, *J. Phys. Chem. B*, 2005, **109,**215.

174 A. Nasibulin, S. Rackauskas, H. Jiang, Y. Tian, P. Mudimela, S. Shandakov, L. Nasibulina, S. Jani and E. Kauppinen, *Nano Res.*, 2009, **2,**373.

175 J. Bachmann, J. Jing, M. Knez, S. Barth, H. Shen, S. Mathur, U. Gösele and K. Nielsch, *J. Am. Chem. Soc.*, 2007, **129,** 9554.

176 Y. Sui, R. Skomski, K. D. Sorge and D. J. Sellmyer, *Appl. Phys. Lett.*, 2004, **84,**1525.

177 J. Chen, L. Xu, W. Li and X. Gou, *Adv. Mater.*, 2005,**17,** 582.

178 P. Yang, A. Zhang, X. Cheng, G. Zhou and M. Lü, *J. Colloid Interface Sci.*, 2010, **351,** 77.

179 J. Yeo, S. Hong, W. Manorotkul, Y. D. Suh, J. Lee, J. Kwon and S. H. Ko, *J. Phys. Chem. C*, 2014,**118,** 15448.

180 S. Mollah, S. Henley and S. Silva, *Nanotechnology*, 2008, **19,** 205604.

181 S. K. Mohapatra, S. E. John, S. Banerjee and M. Misra, *Chem. Mater.*, 2009, **21,** 3048.

182 R. Li and J. Liu, *Electrochim. Acta*, 2014, **120,** 52.

183 W. Zhang, S. Jia, Q. Wu, J. Ran, S. Wu and Y. Liu, *Mater. Lett.*, 2011,**65,** 1973.

184 L. Lu, Z. Ai, J. Li, Z. Zheng, Q. Li and L. Zhang, *Cryst. Growth Des.*, 2007, **7,**

459.

185 W. Wu, X. Xiao, S. Zhang, J. Zhou, L. Fan, F. Ren and C. Jiang, *J. Phys. Chem. C*, 2010, **114,** 16092.

186 H. U. Lee, S. C. Lee, Y.–C. Lee, S. Vrtnik, C. Kim, S. Lee, Y. B. Lee, B. Nam, J. W. Lee and S. Y. Park, *J. Hazard. Mater.*, 2013,**262,** 130.

187 F. Mou, J. Guan, Z. Xiao, Z. Sun, W. Shi and X.–A. Fan, *J. Mater. Chem.*, 2011, **21,**5414.

188 S. Cavaliere–Jaricot, A. Brioude and P. Miele, *Langmuir*, 2009,**25,** 2551.

189 Y. Ren, C. Zhu, S. Zhang, C. Li, Y. Chen, P. Gao, P. Yang and Q. Ouyang, *Nanoscale*, 2013, **5,** 12296.

190 R. Yuan, X. Fu, X. Wang, P. Liu, L. Wu, Y. Xu, X. Wang and Z. Wang, *Chem. Mater.*, 2006, **18,**4700.

191 Z. Sun, H. Yuan, Z. Liu, B. Han and X. Zhang, *Adv. Mater.*, 2005,**17,** 2993.

192 J.–H. Lim, S.–G. Min, L. Malkinski and J. B. Wiley, *Nanoscale*, 2014,**6,** 5289.

193 J. Wang, Y. Ma and K. Watanabe, *Chem. Mater.*, 2007, **20,** 20.

194 F. Mou, J.–G. Guan, W. Shi, Z. Sun and S. Wang, *Langmuir*, 2010, **26,** 15580.

195 J. Qu, Y. Yu, C.–Y. Cao and W.–G. Song, *Chem. Eur. J.*, 2013,**19,** 11172.

196 Z. Zhou, Z. Zhao, H. Zhang, Z. Wang, X. Chen, R. Wang, Z. Chen and J. Gao, *ACS Nano*, 2014, **8,** 7976.

197 Y. Wang, C. Wang, L. Yuan, R. Cai, X. Liu, C. Li and G. Zhou, *J. Phys. Chem. C*, 2014, **118,** 5796.

198 F. Cao, Y. Liu, W. Hu and Q. Chen, *J. Phys. Chem. C*, 2008, **112,** 2337.

199 L.–P. Zhu, H.–M. Xiao and S.–Y. Fu, *Cryst. Growth Des.*, 2007, **7,**177.

200 M. Muruganandham, R. Amutha, M. Sathish, T. S. Singh, R. P. S. Suri and M. Sillanpää, *J. Phys. Chem. C*, 2011,**115,**18164.

201 P. Hu, L. Yu, A. Zuo, C. Guo and F. Yuan, *J. Phys. Chem. C*, 2008, **113,**900.

202 Y. Liu, Y. Wang, S. Zhou, S. Lou, L. Yuan, T. Gao, X. Wu, X. Shi and K. Wang, *ACS Appl. Mater. Interfaces*, 2012, **4,**4913.

203 H.–L. Xu, H. Bi and R.–B. Yang, *J. Appl. Phys.*, 2012, **111**, 07A522.

204 L. Zhang, H. B. Wu, S. Madhavi, H. H. Hng and X. W. Lou, *J. Am. Chem. Soc.*, 2012, **134,** 17388.

205 M. Hu, S. Furukawa, R. Ohtani, H. Sukegawa, Y. Nemoto, J. Reboul, S. Kitagawa and Y. Yamauchi, *Angew. Chem. Int. Ed.*, 2012, **51,** 984.

206 G. Sun, B. Dong, M. Cao, B. Wei and C. Hu, *Chem. Mater.*, 2011, **23,** 1587.

207 L. Han, Y. Chen and Y. Wei, *CrystEngComm*, 2012, **14,** 4692.

208 S.–W. Cao and Y.–J. Zhu, *J. Phys. Chem. C*, 2008, **112,** 12149.

209 Z. Liu, T. Fan, W. Zhang and D. Zhang, *Micropor. Mesopor. Mat.*, 2005, **85,** 82.

210 B. Liu and H. C. Zeng, *Chem. Mater.*, 2007, **19**, 5824.

211 Z. Deng, M. Chen, G. Gu and L. Wu, *J. Phys. Chem. B*, 2008, **112**, 16.

212 X. F. Li, K. L. Lv, K. J. Deng, J. F. Tang, R. Su, J. Sun and L. Q. Chen, *Mater. Sci. Eng. B*, 2009, **158**, 40.

213 L. Ge, X. Y. Jing, J. Wang, J. Wang, S. Jamil, Q. Liu, F. Liu and M. Zhang, *J. Mater. Chem.*, 2011, **21**, 10750.

214 J. Zhang, S. Wang, Y. Wang, M. Xu, H. Xia, S. Zhang, W. Huang, X. Guo and S. Wu, *Sens. Actuators, B –*, 2009, **139**, 411.

215 P. Song, Q. Wang and Z. X. Yang, *Mater. Lett.*, 2012, **86**, 168.

216 H. Zhou, T. X. Fan and D. Zhang, *Micropor. Mesopor. Mat.*, 2007, **100**, 322.

217 Z. Li, Y. Xie, Y. Xiong and R. Zhang, *New J. Chem.*, 2003, **27**, 1518.

218 Z. T. Chen and L. Gao, *Cryst. Growth Des.*, 2008, **8**, 460.

219 Y. C. Kong, D. P. Yu, B. Zhang, W. Fang and S. Q. Feng, *Appl. Phys. Lett.*, 2001, **78**, 407.

220 M. H. Huang, Y. Wu, H. Feick, N. Tran, E. Weber and P. Yang, *Adv. Mater.*, 2001, **13**, 113.

221 X. Wang, C. J. Summers and Z. L. Wang, *Nano Lett.*, 2004, **4**, 423.

222 J. J. Wu and S. C. Liu, *Adv. Mater.*, 2002, **14**, 215.

223 J. J. Wu and S. C. Liu, *J. Phys. Chem. B*, 2002, **106**, 9546.

224 Z. W. Pan, Z. R. Dai and Z. L. Wang, *Science*, 2001, **291**, 1947.

225 X. Y. Kong, Y. Ding, R. Yang and Z. L. Wang, *Science*, 2004, **303**, 1348.

226 P. X. Gao, Y. Ding, W. Mai, W. L. Hughes, C. Lao, Z. L. Wang, *Science*, 2005, **309**, 1700.

227 X. Y. Kong and Z. L. Wang, *Appl. Phys. Lett.*, 2004, **84**, 975.

228 X. Y. Kong and Z. L. Wang, *Nano Lett.*, 2003, **3**, 1625.

229 W. I. Park, D. H. Kim, S. W. Jung and G. C. Yi, *Appl. Phys. Lett.*, 2002, **80**, 4232.

230 X. Liu, X. H. Wu, H. Cao and R. P. H. Chang, *J. Appl. Phys.*, 2004, **95**, 3141.

231 L. Vayssieres, *Adv. Mater.*, 2003, **15**, 464.

232 L. Vayssieres, K. Keis, A. Hagfeldt and S. E. Lindquist, *Chem. Mater.*, 2001, **13**, 4395.

233 B. Liu and H. C. Zeng, *J. Am. Chem. Soc.*, 2003, **125**, 4430.

234 Z. R. Tian, J. A. Voigt, J. Liu, B. Mckenzie and M. J. Mcdermott, *J. Am. Chem. Soc.*, 2002, **124**, 12954.

235 L. E. Greene, M. Law, J. Goldberger, F. Kim, J. C. Johnson, Y. Zhang, R. J. Saykally and P. Yang, *Angew. Chem. Int. Ed.*, 2003, **42**, 3031.

236 L. Guo, Y. L. Ji and H. B. Xu, *J. Am. Chem. Soc.*, 2002, **124**, 14864.

237 E. Oh, H. Y. Choi, S.–H. Jung, S. Cho, J. C. Kim, K.–H. Lee, S.–W. Kang, J. Kim, J.–Y. Yun and S.–H. Jeong, *Sens. Actuators, B–*, 2009, **141**, 239.

238 Y. Li, G. W. Meng and L. D. Zhang, *Appl. Phys. Lett.*, 2000, **76**, 2011.

239 C. H. Liu, J. A. Zapien, Y. Yao, X. M. Meng, C. S. Lee, S. S. Fan, Y. Lifshitz and S. T. Lee, *Adv. Mater.*, 2003, **15**, 838.

240 S. Nakade, Y. Saito, W. Kubo, T. Kitamura, Y. Wada and S. Yanagida, *J. Phys. Chem. B*, 2003, **107,** 8607.

241 L. M. Peter, *J. Phys. Chem. C*, 2007, **111,** 6601.

242 J. R. Jennings, A. Ghicov, L. M. Peter, P. Schmuki and A. B. Walker, *J. Am. Chem. Soc.*, 2008, **130**, 13364.

243 D. Kim, A. Ghicov, S. P. Albu and P. Schmuki, *J. Am. Chem. Soc.*, 2008, **130,** 16454.

244 S. H. Kang, S. –H. Choi, M. –S. Kang, J. –Y. Kim, H. –S. Kim, T. Hyeon and Y. –E. Sung, *Adv. Mater.*, 2008, **20,** 54.

245 Y. Ohsaki, N. Masaki, T. Kitamura, Y. Wada, T. Okamoto, T. Sekino, K. Niihara and S. Yanagida, *PCCP*, 2005, **7,** 4157.

246 K. Zhu, T. B. Vinzant, N. R. Neale and A. J. Frank, *Nano Lett.*, 2007, **7,** 3739.

247 E. Redel, V. S. K. Chakravadhanula, Y. Lan, C. Natzeck and S. Heissler, Nanotechnology, 2015, 26, 051001.

248 D. B. Zhang, L. M. Qi, J. M. Ma and H. M. Cheng, *J. Mater. Chem.*, 2002, **12,** 3677–3680.

249 H. Imai, Y. Takei, K. Shimizu, M. Matsuda and H. Hirashima, *J. Mater. Chem.*, 1999, **9,** 2971–2972.

250 M. S. Sander, M. J. Cote, W. Gu, B. M. Kile and C. P. Tripp, *Adv. Mater.*, 2004, **22,** 2052.

251 Y. Xia, P. D. Yang, Y. G. Sun, Y. Y. Wu, B. Mayers, B. Gates, Y. D. Yin, F. Kim and H. Q. Yan, *Adv. Mater.*, 2003, **5,** 353.

252 J. C. Hulteen and C. R. Martin, *J. Mater. Chem.*, 1997, **7,** 1075.

253 S. Z. Chu, K. J. Wada, S. Inoue and S. Todoroki, *Chem. Mater.*, 2002, **14,** 267.

254 S. M. Liu, L. M. Gan, L. H. Liu, W. D. Zhang and H. C. Zeng, *Chem. Mater.*, 2002, **14,** 1392.

255 A. Michailowski, D. AlMawlawi, G. S. Cheng and M. Moskovits, *Chem, Phys. Lett.*, 2001, **349,** 1–5.

256 S. Kobayashi, K. Hanabusa, N. Hamasaki, M. Kimura and H. Shirai, *Chem. Mater.*, 2000, **12,** 1523–1525.

257 T. Y. Peng, A. Hasegawa, J. R. Qiu and K. Hirao, *Chem. Mater.*, 2003, **15,** 2011–2016.

258 G. Gundiah, S. Mukhopadhyay, U. G. Tumkurkar, A. Govindaraj, U. Maitra and C. N. R. Rao, *J. Mater. Chem.*, 2003, **13,** 2118–2122

259 S. Fujikawa and T. Kunitake, *Langmuir,* 2003, **19,** 6545–6552.

260 C. Hippea, M. Warka, E. Lorkb and G. Schulz–EkloV, *Micropor. Mesopor. Mat.*, 1999, **31,** 235–239.

261 T. Kasuga, M. Hiramatsu, A. Hoson, T. Sekino and K. Niihara, *Langmuir*, 1998, **14,** 3161–3163.

262 T. Kasuga, M. Hiramatsu, A. Hoson, T. Sekino and K. Niihara, *Adv. Mater.*, 1999, **11,** 1307– 1311.

263 Y. Lan, X. P. Gao, H. Y. Zhu, Z. F. Zheng, T. Y. Yan, F. Wu, S. P. Ringer and D. Y. Song, *Adv. Funct. Mater.*, 2005, **15,** 1310–1318.

264 X. D. Meng, D. Z. Wang, J. H. Liu, and S. Y. Zhang, *Mater. Res. Bull.*, 2004, **39,** 2163–2170.

265 D. W. Gong, C. A. Grimes and O. K. Varghese, *J. Mater. Res.*, 2001, **16,** 3331–3334.

266 L. V. Taveira, J. M. Macák, H. Tsuchiya, L. F. P. Dick and P. Schmuki, *J. Electrochem. Soc.*, 2005, **152,** B405–B410.

267 A. Ghicov, H. Tsuchiya, J. M. Macak and P. Schmuki, *Electrochem. Commun.*, 2005, **7,** 505–509.

268 H. Tsuchiya, J. M. Macak, L. Taveira, E. Balaur, A. Ghicov, K. Sirotna and P. Schmuki, *Electrochem. Commun.*, 2005, **7,** 576–580.

269 X. Rui, Z. Lu, H. Yu, D. Yang, H. H. Hng, T. M. Lim and Q. Yan, *Nanoscale*, 2013, **5**, 556.

270 B. Schimmoeller, H. Schulz, S. Pratsinis, A. Bareiss, A. Reitzmann and B. Kraushaarczarnetzki, *J. Catal.*, 2006, **243**, 82.

271 D. Wei, M. R. Scherer, C. Bower, P. Andrew, T. Ryhanen and U. Steiner, *Nano*

Lett., 2012, **12**, 1857.

272 L. Biette, F. Carn, M. Maugey, M. F. Achard, J. Maquet, N. Steunou, J. Livage, H. Serier and R. Backov, *Adv. Mater.*, 2005, **17**, 2970.

273 K. Teramura, T. Tanaka, M. Kani, T. Hosokawa and T. Funabiki, *J. Mol. Catal. A: Chem.*, 2004, **208**, 299.

274 C. R. Sides and C. R. Martin, *Adv. Mater.*, 2005, **17**, 125.

275 S.–H. Ng, T. J. Patey, R. Büchel, F. Krumeich, J.–Z. Wang, H.–K. Liu, S. E. Pratsinis and P. Novák, *PCCP*, 2009, **11**, 3748.

276 K. Takahashi, S. J. Limmer, Y. Wang and G. Z. Cao, *J. Phys. Chem. B*, 2004, **108**, 9795.

277 M. E. Spahr, P. Bitterli, R. Nesper, M. Muller, F. Krumeich and H. U. Nissen, *Angew. Chem. Inte. Ed.*, 1998, **37**, 1263.

278 J.–F. Liu, X. Wang, Q. Peng and Y. Li, *Adv. Mater.*, 2005, **17**, 764.

279 S. Shi, M. Cao, X. Fle and H. Xie, *Cryst. Growth Des.*, 2007, **7**, 1893.

280 R. Levi, M. Bar−Sadan, A. Albu−Yaron, R. Popovitz−Biro, L. Houben, C. Shahar, A. Enyashin, G. Seifert, Y. Prior and R. Tenne, *J. Am. Chem. Soc.*, 2010, **132**, 11214.

281 H. A. Le, S. Chin, E. Park, G. Bae and J. Jurng, *Chem. Vap. Deposition*, 2012, **18**, 6–9.

282 W. G. Menezes, D. M. Reis, T. M. Benedetti, M. M. Oliveira, J. F. Soares, R. M. Torresi and A. J. Zarbin, *J. Colloid Interface Sci.*, 2009, **337**, 586.

283 F. Sediri and N. Gharbi, *J. Phys. Chem. Solids*, 2007, **68**, 1821.

284 B. B. Lakshmi, C. J. Patrissi and C. R. Martin, *Chem. Mater.*, 1997, **9**, 2544.

285 M. Al Zoubi, H. K. Farag and F. Endres, *J. Mater. Sci.*, 2009, **44**, 1363.

286 A. M. Cao, J. S. Hu, H. P. Liang and L. J. Wan, *Angew. Chem. Int. Ed.*, 2005, **44**, 4391.

287 H. B.Wu, A. Pan, H. H.Hng and X. W.D.Lou, *Adv. Funct. Mater.*, 2013, 23, 5669.

288 N. Asim, S. Radiman, M. A. Yarmo and M. S. Banaye Golriz, *Micropor. Mesopor. Mat.*, 2009, **120**, 397.

289 C. J. Patrissi and C. R. Martin, *J. Electrochem. Soc.*, 1999, **146**, 3176.

290 K. Takahashi, S. J. Limmer, Y. Wang and G. Z. Cao, Jpn. J. Appl. Phys., 2005, **44**, 662.

291 B. Li, Y. Xu, G. Rong, M. Jing and Y. Xie, *Nanotechnology*, 2006, **17**, 2560.

292 N. Ozer, C. M. Lampert, *Sol. Energy Mater. Sol. Cells*, 1998, **54**, 147.

293 I. Porqueras, E. Bertran, *Thin Solid Films*, 2003, **398**, 41.

294 F. Iwata, K. Mikage, H. Sakguchi and A. Sasaki, *Solid State Ion.*, 2003, **165**, 7.

295 S. Vijayakumar, S. Nagamuthu and G. Muralidharan. *ACS Appl. Mater. Interfaces*, 2013, **5**, 2188.

296 Z. Zhu, N. Wei, H. Liu and Z. He. *Adv. Powder Technol.*, 2011, **22**, 422.

297 Y. Ren and L. Gao, *J. Am. Ceram. Soc.*, 2010, **93**, 3560.

298 G. Zhang, Y. Chen, B. Qu, L. Hu, L. Mei, D. Lei, Q. Li, L. Chen, Q. Li and T. Wang, *Electrochim. Acta*, 2012, **80**, 140.

299 C. Cao, W. Guo, Z. Cui, W. Song and W. Cai, *J. Mater. Chem.*, 2011, **21**, 3204.

300 S. Manna, A. K. Deb, J. Jagannath and S. K. De, *J. Phys. Chem. C*, 2008, **112**, 10659.

301 W. S. Yan, W. X. Weng, G. B. Zhang, Z. H. Sun, Q. H. Liu, Z.Y. Pan, Y. X. Guo, P. S. Xu, S. Q. Wei, Y. P. Zhang and S. S. Yan, *Appl. Phys. Lett.*, 2008, **92**, 052508.

302 Y. D. Luo, Y. H. Lin, Y. N. Feng, Y. J. Zhang, Y. Song, Y. Shen and C. W. Nan, *J. Appl. Phys.*, 2012, **112**, 116101.

303 B. Wang, J. L. Cheng, Y. P. Wu, D. Wang, D. N. He, *Electrochem. Comm.*, 2012, **23**, 5.

304 X. Song and L. Gao, *J. Am. Ceram. Soc.*, 2008, **91**, 3465.

305 T. Guo, Y. D. Luo, Y. J. Zhang, Y. H. Lin and C. W. Nan, *Cryst. Growth Des.*, 2014, **14**, 2329.

306 Q. P. Lu, Z. D. Lu, Y. Z. Lu, L. F. Lv, Y. Ning, H. X. Yu, Y. B. Hou and Y. D. Yin, *Nano Lett.*, 2013, **13**, 5698.

307 Meng, J. Ren and E. Kaxiras, *Nano Lett.*, 2008, **8**, 3266.

308 G. Kim, J. Walker, L. A. Samuelson and J. Kumar, Nano Lett., 2003, **3**, 523.

309 Xu, X. Yang, H. K. Wang, X. Chen, C. Y. Luan, Z. X. Xu, Z. Z. Lu, V. A. L. Roy, W. J. Zhang and C. S. Lee, *Nano Lett.*, 2011, **11**, 4138.

310 J. Cole, X. Wang, R. J. Knuesel and H. O. Jacobs, *Nano Lett.*, 2008, **8**, 1477.

311 J. Schrier, D. O. Demchenko and L. W. Wang, *Nano Lett.*, 2007, **7**, 2377.

312M. Law, L. E. Greene, J. C. Johnson, R.Saykally andP.Yang,*Nat. Mater.*, 2005, 4, 455.

313 S. Shoaee, J. Briscoe, J. R. Durrant and S. Dunn, *Adv. Mater.*, 2014, **26**, 263.

314 Y. Q. Bie, Z. M. Liao, P. W. Wang, Y. B. Zhou, X. B. Han, Y. Ye, Q. Zhao, X. S. Wu, L. Dai, J. Xu, L. W. Sang, J. J. Deng, K. Laurent, Y. Leprince−Wang and D. P. Yu, *Adv. Mater.*, 2010, **22**, 4284.

315 S. Agarwala, Z. H. Lim, E. Nicholson and G. W. Ho, *Nanoscale*, 2012, **4**, 194.

316 H. Du, Y. Cao, Y. B. Bai, P. Zhang, X. M. Qian, D. J. Wang, T. J. Li and X. Y. Tang, *J. Phys. Chem. B*, 1998, **102**, 2329.

317 E. M. Jin, J. Y. Park, X. G. Zhao, I. H. Lee, S. M. Jeong and H. B. Gu, *Mater. Lett.*, 2014, **126**, 281.

318 H. N. Kim and J. H. Moon, *ACS Appl. Mater. Interfaces*, 2012, **4**, 5821.

319 H. L. Luo, W. J. Song, P. G. Hoertz, K. Hanson, R. Ghosh, S. Rangan, M. K. Brennaman, J. J. Concepcion, R. A. Binstead, R. A. Bartynski, R. Lopez and T. J. Meyer, *Chem. Mater.*, 2013, **25**, 122.

320 B. C. O'Regan, S. Scully, A. C. Mayer, E. Palomares and J. Durrant, *J. Phys. Chem. B*, 2005, **109,** 4616.

321 H. Ni, S. L. Da, K. Zhao, Y. C. Kong, H. K. Wong and S. Q. Zhao, *J. Appl. Phys.*, 2012, **112**, 023101.

322 A. D. Wei, J. R. Sun, W. M. Lu and B. G. Shen, *Appl. Phys. Lett.*, 2009, **95**, 052502.

323 J. R. Sun, S. Y. Zhang, B. G. Shen and H. K. Wong, *Appl. Phys. Lett.*, 2005, **86**, 053503.

324 T. L. Qu, Y. G. Zhao, D. Xie, J. P. Shi, Q. P. Chen and T. L. Ren, *Appl. Phys. Lett.*, 2011, **98**, 173507.

325 C. Luo, K. X. Jin, C. L. Chen and T. Wu, *Appl. Phys. Lett.*, 2013, **103**, 212401.

326 X. S. Liu, J. Q. Wang, E. J. Liang and W. F. Zhang, *Appl. Surf. Sci.*, 2013, **280**, 556.

327 Q. L. Dai, J. J. Chen, L. Y. Lu, J. K. Tang and W. Y. Wang, *Nano Lett.*, 2012, **12**, 4187.

328 D. W. Kim, S. S. Shin, I. S. Cho, S. Lee, D. H. Kim, C. W. Lee, H. S. Jung and K. S. Hong, *Nanoscale*, 2012, **4**, 557.

329 X. Y. Liu, H. W. Zheng, Z. L. Zhang, X. S. Liu, R. Q. Wan and W. F. Zhang, *J. Mater. Chem.*, 2011, **21**, 4108.

330 N. Spinner, L. C. Zhang and W. E. Mustain, *J. Mater. Chem. A*, 2014, **2**, 1627.

331 H. B. Wu, J. S. Chen, H. H. Hng and X. W. Lou, *Nanoscale*, 2012, **4**, 2526.

332 Z. Y. Wang, L. Zhou and X. W. Lou, *Adv. Mater.*, 2012, **24**, 1903.

333 X. L. Jia, Z. Chen, X. Cui, Y. T. Peng, X. L. Wang, G. Wang, F. Wei and Y. F. Lu, *Acs Nano*, 2012, **6**, 9911.

334 P. He, H. J. Yu, D. Li and H. S. Zhou, *J. Mater. Chem.*, 2012, **22**, 3680.

335 Z. C. Yang, J. G. Shen and L. A. Archer, *J. Mater. Chem.*, 2011, **21**, 11092.

336 J. S. Zhou, H. H. Song, X. H. Chen, L. J. Zhi, S. Y. Yang, J. P. Huo and W. T. Yang, *Chem. Mater.*, 2009, **21**, 2935.

337 P. Poizot, S. Laruelle, S. Grugeon, L. Dupont and J. M. Tarascon, *Nature*, 2000, **407**, 496.

338 I. Paramasivam, H. Jha, N. Liu and P. Schmuki, *Small*, 2012, **8**, 3073.

339 I. Justicia, P. Ordejon, G. Canto, J. L. Mozos, J. Fraxedas, G. A. Battiston, R. Gerbasi and A. Figueras, *Adv. Mater.*, 2002, **14**, 1399.

340 A. Kafizas, N. Noor, P. Carmichael, D. O. Scanlon, C. J. Carmalt and I. P. Parkin, *Adv. Funct. Mater.*, 2014, **24**, 1758.

341 J. Pal, M. Ganguly, C. Mondal, A. Roy, Y. Negishi and T. Pal, *J. Phys. Chem. C*, 2013, **117**, 24640.

342 H. Huang, Z. K. Yue, G. Li, X. M. Wang, J. Huang, Y. K. Du and P. Yang, *J. Mater. Chem. A*, 2013, **1**, 15110.

343 Y. Dong, J. Li, L. Shi, J. Xu, X. B. Wang, Z. G. Guo and W. M. Liu, *J. Mater. Chem. A*, 2013, **1**, 644.

344 X. Q. An, X. L. Yu, J. C. Yu and G. J. Zhang, *J. Mater. Chem. A*, 2013, **1**, 5158.

345 D. S. Bohle and C. J. Spina, *J. Am. Chem. Soc.*, 2009, **131**, 4397.

346 J. N. Kondo, M. Uchida, K. Nakajima, D. L. Lu, M. Hara and K. Domen, *Chem. Mater.*, 2004, **16**, 4304.

347 M. Miyauchi, A. Nakajima, T. Watanabe and K. Hashimoto, *Chem. Mater.*, 2002, **14**, 2812.

348 A. Rothschild and Y. Komem, *J. Appl. Phys.*, 2004, **95**, 6374.

349 J. Shia, G. Hu, Y. Sun, M. Geng, J. Wu, Y. Liu, M. Ge, J. Tao,M. Cao, N. Dai *Sens. Actuators, B*, 2008, 820.

350 Y. J. Choi, I. S. Hwang, J. G. Park, K. J. Choi, J. H. Park and J. H. Lee, *Nanotechnology*, 2008, 19, 095508.

351 Z. Y. Zhang, R. J. Zou, G. S. Song, L. Yu, Z. G. Chen and J. Q. Hu, *J. Mater. Chem.*, 2011, **21**, 17360.

352 L. Renard, O. Babot, H. Saadaoui, H. Fuess, J. Brotz, A. Gurlo, E. Arveux, A. Klein and T. Toupance, Nanoscale, 2012, **4**, 6806.

353 G. X. Ma, R. J. Zou, L. Jiang, Z. Y. Zhang, Y. F. Xue, L. Yu, G. S. Song, W. Y. Li and J. Q. Hu, Crystengcomm, 2012, **14**, 2172.

354 A. Kolmakov, D. O. Klenov, Y. Lilach, S. Stemmer and M. Moskovits, *Nano Lett.*, 2005, **5**, 667.

355 A. S. Zuruzi, N. C. MacDonald, M. Moskovits and A. Kolmakov, *Angew. Chem. Int. Ed.*, 2007, **46**, 4298.

356 Y. Zhao, L. N. Lin, Y. Lu, H. L. Gao, S. F. Chen, P. Yang and S. H. Yu, *Adv. Healthc. Mater.*, 2012, **1**, 327.

357 F. Y. Cheng, C. H. Su, Y. S. Yang, C. S. Yeh, C. Y. Tsai, C. L. Wu, M. T. Wu and D. B. Shieh, *Biomaterials*, 2005, **26**, 729.

358 B. Das, M. Mandal, A. Upadhyay, P. Chattopadhyay and N. Karak, *Biomed. Mater.*, 2013, **8**.

359 W. Wang, M. Zou and K. Z. Chen, *Chem. Commun.*, 2010, **46**, 5100.

360 D. K. Nagesha, B. D. Plouffe, M. Phan, L. H. Lewis, S. Sridhar and S. K. Murthy, *J. Appl. Phys.*, 2009, **105**.

361 A. Tomitaka, K. Ueda, T. Yamada and Y. Takemura, *J. Magn. Magn. Mater.*, 2012, **324**, 3437.

362 E. Umut, F. Pineider, P. Arosio, C. Sangregorio, M. Corti, F. Tabak, A. Lascialfari and P. Ghigna, *J. Magn. Magn. Mater.*, 2012, **324**, 2373.

363 C. Tudisco, F. Bertani, M. T. Cambria, F. Sinatra, E. Fantechi, C. Innocenti, C. Sangregorio, E. Dalcanale and G. G. Condorelli, *Nanoscale*, 2013, **5**, 11438.

364 V. Georgiadou, C. Kokotidou, B. Le Droumaguet, B. Carbonnier, T. Choli–Papadopoulou and C. Dendrinou–Samara, *Dalton T.*, 2014, **43**, 6377.

365 A. M. Al–Saie, M. Bououdina, A. Jaffar, S. Arekat, J. M. Melnyczuk, Y. T. Thai and C. S. Brazel, *J. Alloy. Compd.*, 2011, **509**, S393.

366 M. R. Phadatare, V. M. Khot, A. B. Salunkhe, N. D. Thorat and S. H. Pawar, *J. Magn. Magn. Mater.*, 2012, **324**, 770.